ISSN 0038-531X

Russian Original Vol. 57, No. 4, October, 1984

April, 1985

SATEAZ 57(4) 673-750 (1984)

SOVIET ATOMIC ENERGY

АТОМНАЯ ЭНЕРГИЯ
(ATOMNAYA ÉNERGIYA)

TRANSLATED FROM RUSSIAN

c/b CONSULTANTS BUREAU, NEW YORK

SOVIET ATOMIC ENERGY

Soviet Atomic Energy is abstracted or indexed in *Chemical Abstracts, Chemical Titles, Pollution Abstracts, Science Research Abstracts, Parts A and B, Safety Science Abstracts Journal, Current Contents, Energy Research Abstracts,* and *Engineering Index.*

Mailed in the USA by Publications Expediting, Inc., 200 Meacham Avenue, Elmont, NY 11003.

POSTMASTER: Send address changes to *Soviet Atomic Energy,* Plenum Publishing Corporation, 233 Spring Street, New York, NY 10013.

Soviet Atomic Energy is a translation of *Atomnaya Énergiya,* a publication of the Academy of Sciences of the USSR.

An agreement with the Copyright Agency of the USSR (VAAP) makes available both advance copies of the Russian journal and original glossy photographs and artwork. This serves to decrease the necessary time lag between publication of the original and publication of the translation and helps to improve the quality of the latter. The translation began with the first issue of the Russian journal.

Consultants Bureau journals appear about six months after the publication of the original Russian issue. For bibliographic accuracy, the English issue published by Consultants Bureau carries the same number and date as the original Russian from which it was translated. For example, a Russian issue published in December will appear in a Consultants Bureau English translation about the following June, but the translation issue will carry the December date. When ordering any volume or particular issue of a Consultants Bureau journal, please specify the date and, where applicable, the volume and issue numbers of the original Russian. The material you will receive will be a translation of that Russian volume or issue.

Subscription (2 volumes per year)
Vols. 56 & 57: $560 (domestic), $621 (foreign) Single Issue: $100
Vols. 58 & 59: $645 (domestic), $715 (foreign) Single Article: $8.50

CONSULTANTS BUREAU, NEW YORK AND LONDON

c/b
233 Spring Street
New York, New York 10013

Published monthly. Second-class postage paid at Jamaica, New York 11431.

SOVIET ATOMIC ENERGY

A translation of *Atomnaya Énergiya*

April, 1985

Volume 57, Number 4 **October, 1984**

CONTENTS

Engl./Russ.

The Russian press date (podpisano k pechati) of this issue was Publication therefore did not occur prior to this date, but must be assumed to have taken place reasonably soon thereafter.

POWER STARTUP OF THE IBR-2 REACTOR AND THE FIRST PHYSICS INVESTIGATIONS IN ITS BEAMS

V. D. Anan'ev, V. A. Arkhipov, A. I. Babaev,
Yu. M. Bulkin, B. N. Bunin, V. S. Dmitriev,
N. A. Dollezhal', L. V. Edunov, A. D. Zhirnov,
V. L. Lomidze, V. I. Dushchikov, Yu. I. Mityaev,
Yu. M. Ostanevich, Yu. N. Pepelyshev, V. S. Smirnov,
I. M. Frank, N. A. Khryastov, Yu. M. Cherkashov,
E. P. Shabalin, and Yu. S. Yazvitskii

UDC 621.039.514.23

The powerful pulsed, periodic-action neutron source — IBR-2 [1] — was constructed in the Neutron Physics Laboratory (NPL) of the Joint Institute of Nuclear Research (JINR) at Dubna. The reactor was designed for research in the field of nuclear physics, the physics of condensed media, molecular biology, the physics of elementary particles (fundamental properties of the neutron), and also for solving various applied problems by means of neutrons.

Reactors of the IBR type have been developed in the NPL for a long time. It is well known that modern scientific research on reactors requires a high neutron-flux density. It is not by chance, therefore, that from the large number of research reactors a group of so-called high-flux reactors is distinguished, with a maximum thermal neutron flux of 10^{15} $cm^{-2} \cdot sec^{-1}$ (in the Soviet Union SM-2 and the PIK under construction, in the USA — BHFR, and in France HFR-ILL). These reactors have a high thermal capacity (50-100 MW), with a maximum acceptable specific power of the fuel. For many technical and economic reasons, it is difficult to reckon on a significant increase of the neutron flux of stationary reactors. For a wide class of research, further advancement is possible by the use of pulsed periodic-action sources, in conjunction with the time-of-flight method. The first reactor of this type with a low initial power — the IBR-1 — was constructed at Dubna by the initiative of D. I. Blokhintsev. Later, it was redesigned as the IBR-30, which has operated successfully up to the present time. In its parameters and design, the IBR-2 differs considerably from its forerunner, the IBR-30.

Experience has shown that on a facility of this type problems can be fruitfully solved which are considered to be traditional for stationary reactors: for example, neutron diffraction investigations and investigations using the method of small-angle scattering. All the more, this is related to the study of elastic and inelastic scattering of slow neutrons and neutron spectroscopic investigations of nuclei. The use of a pulsed fast reactor in conjunction with the time-of-flight method considerably extends the range of slow-neutron energies available for experiments.

The pulsed neutron flux of a reactor of the IBR type should be compared with the steady flux in a normal reactor. With their equivalence, the reproducibility of the experimental equipment, positioned in the beams extracted from the reactor, is found to be approximately identical. Thus, the IBR-30 with an average power of 20 kW is equivalent in its potentialities to research reactors of megawatt power. This was taken into account in the IBR-2 project. With an average power of several megawatts, the pulsed neutron flux of such a reactor should attain 10^{16} $cm^{-2} \cdot sec^{-1}$; i.e., it significantly exceeds the flux of stationary reactors. In this case, the low average power, by comparison with the power of high-flux reactors, eliminates many technological difficulties, in the first place the rapid burnup of nuclear fuel.

Experience in the use of the IBR has allowed the advantages of pulsed sources to be better understood, not only for research in the field of neutron spectroscopy of nuclei, but also in the field of the physics of condensed media. Hence the origination of a number of designs for powerful pulsed sources on the basis of an accelerator and which, at the present time, are being built in many countries.

Translated from Atomnaya Énergiya, Vol. 57, No. 4, pp. 227-234, October, 1984. Original article submitted March 13, 1984.

0038-531X/84/5704-0673$08.50

[illegible] of the IBR-2 has been given in previous publications, for example, in [1]. Therefore, we shall recall here only briefly the main structural solutions. The core of the IBR-2 is charged with plutonium dioxide fuel with a total mass of ~90 kg. The fuel elements are cooled by sodium with an inlet temperature of 300°C. The cooling system is dual circuit, dual loop, with a sodium flow rate of 100 m^3/h. The reactor is surrounded by water neutron moderators (Fig. 1), which are "scanned" by 14 horizontal channels. Two moderators — "comb-shaped" — have an extended luminescent surface, the shape of which allows the thermal neutron leakage flux to be increased by a factor of 2 to 3.

The power pulse is shaped by a reactivity modulator (RM), made in the form of two coaxially positioned movable neutron reflectors — the main axial movable reflector (MMR), and the supplementary movable reflector (SMR) (see Fig. 1). The frequency of rotation of the MMR is 1500 min^{-1}. The pulse frequency is varied discretely by means of the SMR, at rest or rotating with a low speed [2]. In the latter case, the pulse is developed only at the instant of time when both reflectors are close to the core. The most important results of the power startup of the IBR-2 are given below, and experiments are described which are being conducted in its beams.

Pulsed Characteristics of the Reactor. In 1982, the IBR-2 was brought on an average power of 2 MW with a rotation frequency of the MNR of 1500 min^{-1} and a pulse frequency of 25 Hz, which corresponds to a reactor pulsed power of 270 MW. The basic frequency regime of the reactor, 5 Hz at a power of 2 MW, was achieved in 1984: The peak reactor power attained 1350 MW. The values of the principal parameters of the IBR-2, obtained at the present time, are as follows (the error of the neutron flux estimate amounts to 20%):

Average thermal power	2 MW
Power per pulse	1460 MW
Duration of power pulse	215 μsec
Background power	0.1 MW
Duration of thermal neutron pulse in plane moderator	230 μsec
Thermal neutron flux density:	
average with respect to time at the surface of the plane moderator	$5 \cdot 10^{12}$ $cm^{-2} \cdot sec^{-1}$
same, peak value	$4 \cdot 10^{15}$ $cm^{-2} \cdot sec^{-1}$
at the surface of the comb-shaped moderator	$1 \cdot 10^{16}$ $cm^{-2} \cdot sec^{-1}$

The power startup of the IBR-2 was conducted with a modified reactivity modulator, which differed from the RM described in [3], in the construction of the SMR. This was done in order to shorten the power pulse duration of the reactor Θ. As is well known, Θ is determined in the following way:

$$\Theta \sim (\tau/\alpha v^2)^{1/3}, \quad (1)$$

where α is the coefficient of the parabola describing the change of reactivity during movement of the MMR close to the position corresponding to the maximum reactivity of the reactor, τ is the average lifetime of the prompt neutrons in the reactor, and v is the velocity of the MMR relative to the core. During the physics startup, it was ascertained that the value of α, which was in essence the characteristic of the MMR, depends markedly on the geometry of the SMR.

Replacement of the original version of the SMR made of beryllium by steel in the form of a trident (it is shown in the front plane of Fig. 1) allowed α to be increased by a factor of 3. It follows from Table 1 that, taking account of the reduction of τ in consequence of the additional screening of the core from the external moderators, this gives a fourfold reduction of the ratio τ/α, which is equivalent to a reduction of the pulse duration by a factor of 1.6, i.e., down to 140 μsec instead of the former 220 μsec. However, this advantage was lost in view of the change to a reduced frequency of rotation of the MMR from 3000 to 1500 min^{-1}; at the present time $\Theta = 215 \pm 3$ μsec. A reduction of Θ can be achieved by the use of a RM of two lattices, rotating contrary to one another [4]. It has been established experimentally that this modulator provides a power pulse duration of ~130 μsec, with a rotation frequency of the rotors of 1500 min^{-1} [5].

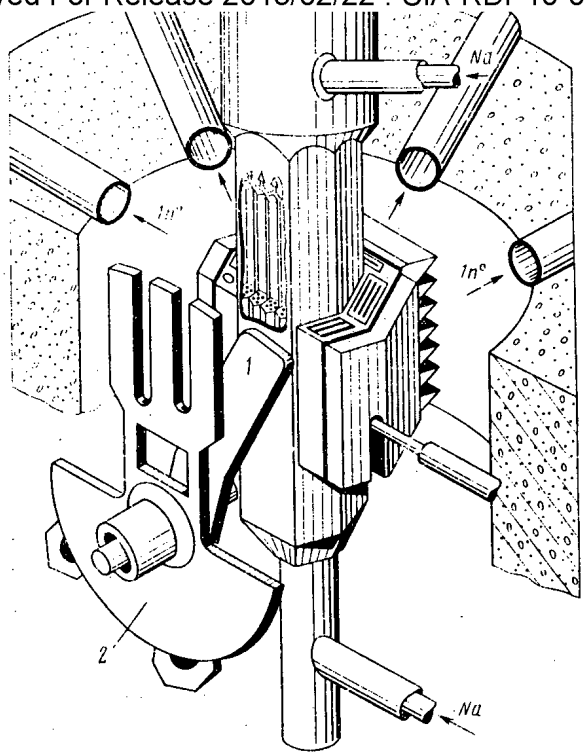

Fig. 1. Schematic diagram of the IBR-2 reactor: 1) axial movable reflector (MMR); 2) supplementary movable reflector (SMR).

TABLE 1. Power Pulse Duration for Two RM Versions in the IBR-2

RM version	α, $10^{-4}\times$ $\times$ deg^{-1}	τ, nsec	Θ, μsec	
			τ=1500 min^{-1}	τ=3000 min^{-1}
SMR with beryllium block	1,0±0,02	80±10	360 *	220±5
SMR in the form of a steel trident	3,00±0,06	63±4	215±3	140 *

*Numerical estimate.

The measured shape of the IBR-2 power pulse is close to Gaussian and for the accepted RM version is almost independent of the operating frequency regime of the reactor. The ratio of the pulse amplitude to the power background, i.e., the power released between the main pulses, is equal to $1.3\cdot10^4$. Figure 2 shows the measured reactor power distribution during a single pulse repetition interval in the 5-Hz regime. The four additional pulse satellites are due to the passage of the MMR by the core at the instant when the SMR is not located in the immediate vicinity of the reactor.

The thermal neutron pulse is formed as a result of moderation of the fast neutrons in the water moderator surrounding the core. The thermal neutron pulse duration is estimated approximately by the formula

$$\Delta t = \sqrt{\Theta^2 + \Delta t_0^2}, \qquad (2)$$

where Δt_0 is the thermal neutron pulse duration, originating from the instantaneous fast neutron burst, i.e., when $\Theta = 0$. The amplitude of the thermal neutron flux Φ can be determined in terms of the ratio of the flux, averaged over time, to the pulse duration Δt. The parameters of the IBR-2 as a source of slow neutrons have been given previously. Data about the thermal neutron flux for the IBR-2 are based on the experimental value of the flux density $\bar{\Phi}$

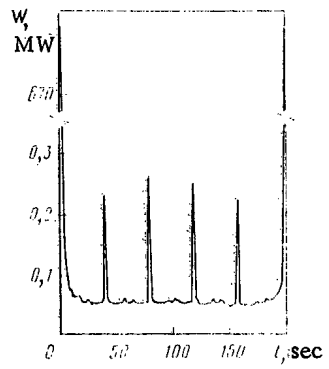

Fig. 2

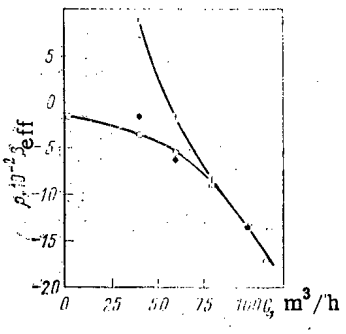

Fig. 3

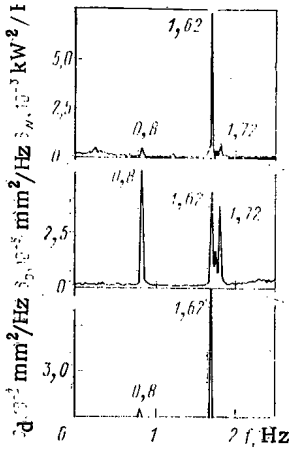

Fig. 4

Fig. 2. Power distribution for a single pulse repetition interval in the 5-Hz regime, with an average reactor power of 1 MW.

Fig. 3. Dependence of the reactivity ρ on the sodium flowrate G for a different reactor power W. ○) W = 0; ●) W = 100 kW; +) W = 1 MW.

Fig. 4. Spectra of the amplitude fluctuations of the power pulses S_W, transverse vibrations of the MMR, S_o, and the SMR, S_d, measured in the 5-Hz regime, at an average reactor power of 1 MW and with a sodium flowrate of 80 m^3/h.

at the surface of the plane moderator, averaged with respect to time, and which was found to be a factor of 2 higher than the calculated value and equal to $2.5 \cdot 10^{12}$ $cm^{-2} \cdot sec^{-1}$ at 1-MW average power.

Power Fluctuations and Other Reactor Parameters. The sensitivity of the periodic-action pulsed reactor to external reactivity perturbations is determined not by the fraction of delayed neutrons β_{eff}, as in a normal reactor, but by the so-called pulsed fraction of delayed neutrons β_p, which once again is a factor of 10 less than β_{eff} [1]. Thus, for IBR-2, $\beta_p = 1.6 \cdot 10^{-4}$ k_{eff} in the 5-Hz regime and $2 \cdot 10^{-4}$ k_{eff} in the 25-Hz regime. Therefore, the question concerning the fluctuations of a pulsed reactor requires increased attention. With a relatively high average reactor power, when stochastic fluctuations can be neglected, the principal contribution to the random deviations of the pulse amplitude from the average value is made by the vibrations of the RM and fluctuations of the coolant parameters. Fluctuations of the parameters of other technological systems are small: their total contribution to the reactivity does not exceed $2 \cdot 10^{-6}$ k_{eff}.

The measured power fluctuations of the IBR-2 are considerably lower than the maximum acceptable. In all the reactor operating regimes investigated, the relative standard deviation of energy of the power pulses was found to be within the limits of 1.5-6%. The power fluctuations increase with increase of the sodium flowrate and the average reactor power.

The fluctuations of the sodium flowrate do not exceed 0.5% and are concentrated mainly in the region of lower frequencies (less than 1.6 Hz). Variations of the sodium temperature at the reactor inlet are similar to the variations of white noise, with a standard deviation of 0.1°C for a power of 1 MW, and lead to reactivity fluctuations of $\sim 2 \cdot 10^{-6}$ k_{eff}. Approximately the same reactivity fluctuations are caused by variations of the sodium flowrate, and the value of the fluctuations is almost independent of the reactor power, with a flow rate close to nominal, G_o = 100 m^3/h. In particular, therefore, the angle of slope of the ρ(G) curves for $G \sim G_o$ is almost identical for a different reactor power (Fig. 3).

Fluctuations due to the reactivity modulator of the IBR-2 were studied most thoroughly, and still continue to be studied during operation of the reactor. Figure 4 shows the power spectrum of the reactor and the spectra of the transverse mechanical vibrations of the MMR and the SMR, measured in 1983 in the 5-Hz regime at a power of 1 MW. All three spectra have a clearly defined resonance structure. The resonance peaks shown in the figure are characterized by a frequency measured in hertz, and are explained in the following way: The resonance of 0.8 Hz is due to vibrations of the SMR with a frequency of ~84 Hz; the resonance of

 d
insignificant wobbles in the transfer units of the kinematic scheme of the RM, occurring with a frequency of 16.4 Hz. Under the resonance peak of 1.72 Hz, the frequency of the natural vibrations of the MMR blades is masked, equal to ~51 Hz.

No significant variations of the statistical parameters of the RM rotor vibrations and fluctuations of the reactor power during the time of power startup were observed, although the fast neutron fluence at the MMR blades attained $3.6 \cdot 10^{20}$ cm^{-2}. According to the data of subsequent measurements, the transverse vibrations of the blades of the movable reflectors on the average (standard deviations) amount to 0.006 mm for the MMR and 0.04 mm for the SMR. The corresponding reactivity fluctuations should be equal to $3 \cdot 10^{-6}$ k_{eff} and $4 \cdot 10^{-6}$ k_{eff}; however, the total contribution of the MMR and SMR to the reactivity, according to an estimate by measurements of the power noise, amount to ~$2 \cdot 10^{-6}$ k_{eff}. This is because the vibrations of the rotors of the MMR and SMR are correlated, as on meeting the latter are displaced to different sides (they converge).

In the 5-Hz regime, both movable reflectors are rotating, and the angle φ between the and SMR at the instant of their meeting can vary with time and thereby directly affects the reactivity and the pulse duration Θ, as the parameter α depends on the relative disposition of the reflectors. In operating conditions, the angle φ fluctuates with a frequency of 0.62 Hz and a standard deviation of ~0.16°. These fluctuations have almost no effect on the reactivity. The fluctuations of Θ also are small and amount to 0-3 μsec, depending on the actual value of the average angle of desynchronization, which is close to $\varphi = 0$ (Fig. 5).

Effects of Reactivity and Stability of the Reactor. When studying the powerful effects of reactivity, no direct measurements of the transfer functions of the reactor were carried out. The transient power processes after the reactivity jump were investigated mainly in different operating regimes of the reactor. It was established that with a sodium flowrate of more than 40 m^3/h, the IBR-2 is stable at all power levels. The typical nature of the change of power of the IBR-2, in consequence of reactivity perturbations, for a small time of observation is shown in Fig. 6, in which the effect of a rapid and quite profound negative feedback is seen clearly. With a longer time of observation, measured in hours, the effect of a very slow positive feedback is appreciable.

The fast component of the power coefficient of reactivity (PCR), with a time constant of ~10 sec, is negative and equal to approximately $-1.4 \cdot 10^{-3}$ k_{eff}/MW [6]. The value of this component of the PCR, due mainly to expansion of the fuel elements, coincides approximately with the design calculations and plays the principal role in ensuring the safety and stability of the reactor. The presence of a slow positive component of the PCR, with a time constant ~90 min, proved to be unexpected and which, in absolute value almost coincides with the negative component. It is explained by the slow displacements of the stationary reflectors as a result of their heating up. Moreover, a negative component of the PCR is observed, with a time constant of several days, the representation of which can be obtained from Fig. 7. The nature of the latter component most likely is related somehow with heating up of the reactor shields.

As mentioned, with a coolant flowrate of more than 40 m^3/h, the IBR-2 is stable. With lower sodium flow rates, self-excited power fluctuations are possible with a period of ~1 min and which have the nature of autooscillations. However, the amplitude and frequency of these oscillations depend on the power in such a way that their onset is possible only at low power (less than 400 kW). In these narrow ranges of flow rate and power, the fast component of the PCR is separated into two components, one of which is positive and inversely proportional to the sodium flow rate and also the reactor power. The similar nature of the positive feedback was discovered earlier in the BR-5 [7], the core design of which was the prototype for the IBR-2.

In the course of the startup experiments, other reactivity effects also were studied. The isothermal reactivity coefficient was found to be equal to -10^{-2} β_{eff}/°C ($\beta_{eff} = 2.165 \cdot 10^{-3}$ k_{eff}). As it follows from Fig. 3, the hydrodynamic effect is negative and is due to movement of the fuel element assembly under the action of the coolant flow. The barometric reactivity effect, which could originate because of the presence of gas bubbles in the coolant, was not found in the IBR-2.

The effect of drinage of water from the external moderators leads to an increase of reactivity of the reactor. The total effect of water drainage for all moderators is equal to

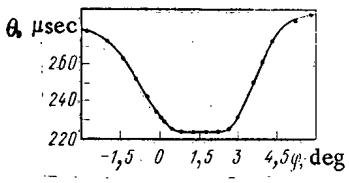

Fig. 5

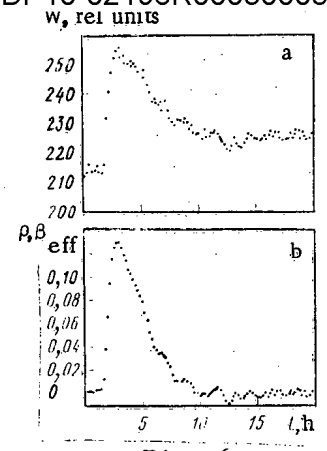

Fig. 6

Fig. 5. Dependence of the power pulse duration Θ on the angle of desynchronization Φ of the MMR and SMR.

Fig. 6. Variations of power W and total reactivity ρ, caused by the injection of reactivity $0.28\beta_{eff}$ for 1.5 sec.

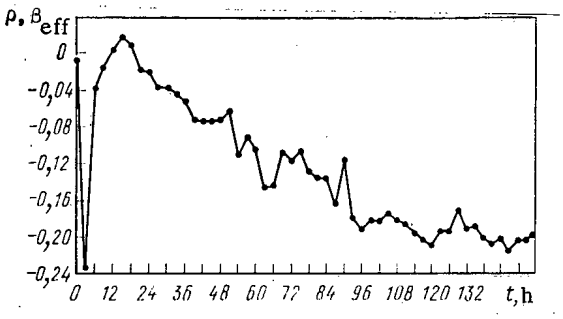

Fig. 7. Variation with time of the reactivity margin ρ of the IBR-2, after bringing the reactor to a power of 1 MW at the time t = 3 h.

$1\beta_{eff}$ and is explained by the entry into the core of fast and resonance neutrons from the thermal and radiation shields of the reactor. In the presence of water, these neutrons are moderated and are delayed in the absorbing screens separating the core from the moderators.

Operation of the Reactor Systems. At the time of writing this paper, the IBR-2 has functioned for 250 MW•days; the maximum nuclear fuel burnup amounted to 0.5%. This small operating experience, however, allows the reliability of the reactor systems to be discussed. In the first place, it should be noted that in the sodium cooling system of the core, there was not a single failure or breakdown. In the period of the power startup and operation of the IBR-2, particular attention was paid to the operation of the cooling system in emergency situations. In the design, in the case of de-energizing of the structure, connection of the circulatory pumps to a safe autonomous feed source is provided for. Afrer dumping the emergency shield, during the first 1 to 2 min forced cooling of the core is implemented with a reduced flowrate, and then because of the natural sodium circulation, with a flowrate of 2 to 5 m^3/h. Testing of this cooling scheme showed that cooling of the core in any cases whatsoever takes place satisfactorily, and the nonsteady temperature stresses in the reactor vessel and the pipelines in transitions regimes, remain within the limits of the permissible values.

The moving reflector, which is one of the most important systems of the IBR-2, is provided with sensors which constantly follow the oscillations of the rotors, the level of vibrations of the bearings, and the technological parameters of the principal structural units. In addition to this regular monitoring, a periodic analysis is carried out of the state of the moving reflector by statistical methods, which are characterized by a high sensitivity and by a large volume of data obtained. After more than a 2-yr period of operation of the reactor

System in the IBR-2 and Their Causes

Cause	1981	1982	1983	1984*
Control and safety system:				
failure in electronic equipment	1	1	1	1
failures of control and meas. equip.	—	5	—	—
pickups in electronic equipment	—	13	17	7
Defects in the electrical systems	—	3	3	—
Breakdowns of power supply	—	5	6	1
Personnel errors	—	3	2	—
Cause ambiguous	—	2	—	2
Average duration of operation of reactor between activations of the scram system, h	16	42	83	178

*On July 1, 1984.

TABLE 3. Utilization Time of the IBR-2 in the Power Startup Period, h

Year	Total on power	In the 5-Hz regime	In the 25-Hz regime	On physics experimentation
1981	132	34	98	—
1982	1554	755	799	608
1983	2588	2564	24	2315
1984*	2027	2027	—	1925
Total:	6301	5380	921	4848

*Up to June 1, 1984.

TABLE 4. Comparison of Average Thermal Neutron Fluxes at the Sample, for the IBR-2 and HFR-ILL (Grenoble) Reactors

IBR-2, W = 2 MW		HFR-ILL, W = 56 MW	
type of spectrometer	$\bar{\Phi}$, $cm^{-2} \cdot sec^{-1}$	type of spectrometer	$\bar{\Phi}$, $cm^{-2} \cdot sec^{-1}$
Diffractometers:		Diffractometers:	
DN-2, DN-3	$2 \cdot 10^7$	D2, D8,	$5 \cdot 10^7$
NSVR	$4 \cdot 10^6$	D1, D5, D10	$(6-8)\,10^6$
Small-angle scattering:		D15	
SAS	$3 \cdot 10^7$—$4 \cdot 10^6$	Small-angle scattering:	
Inelastic scattering:		D11	$5 \cdot 10^6$—$5 \cdot 10^5$
KORA	$3 \cdot 10^7$	D17	$1 \cdot 10^6$
KDSOG	$1 \cdot 10^7$	Inelastic scattering:	
		IN8	$(8-1{,}5)\,10^7$
		IN3, IN11	$(2-1)\,10^7$
		IN2, IN4, IN5 etc.	10^4—10^6

at a power of 1-2 MW, no significant deviations in the functioning of the moving reflector have been observed.

The control and safety system of the reactor functions reliably. The fast-response scram system, tested at different power levels, is found to be within the limits of the design requirements. However, in consequence of the complexities of this system, there were breaks in its operation, mainly associated with inadequate interference protection (Table 2). The causes of the failures, leading to activation of the scram system, were gradually recognized and eliminated.

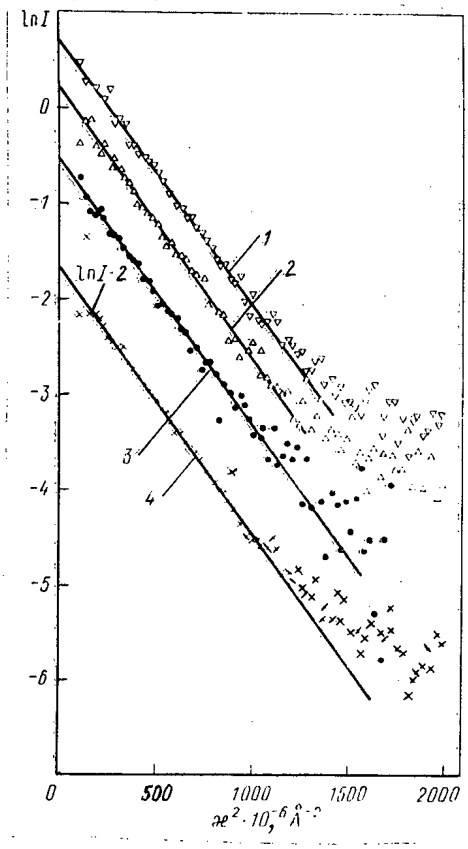

Fig. 8

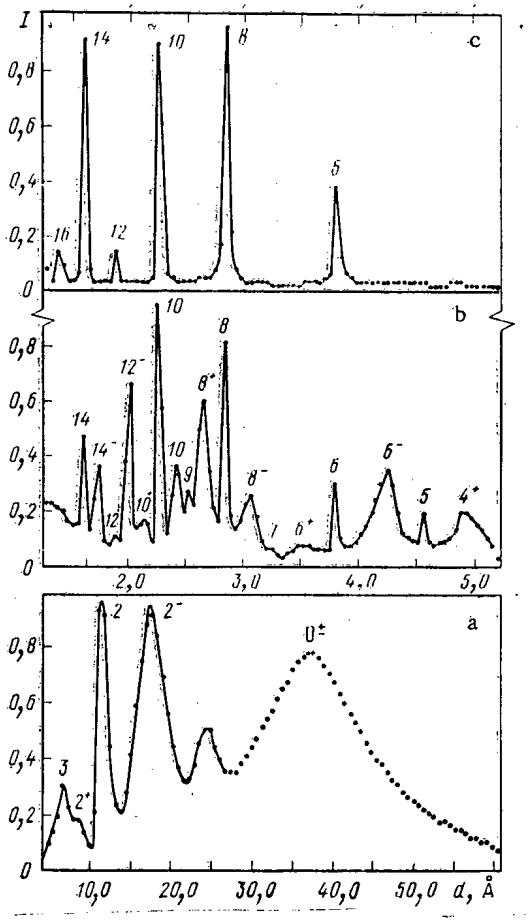

Fig. 9

Fig. 8. Intensity of small-angle diffusive scattering of neutrons as a function of the square of the transmitted pulse (in inverse Angstrom units) for a solution of 70S ribosomes of bacteria *E. coli*. Curves 1-4 and the different experimental points correspond to a different isotopic (with respect to hydrogen) composition of the solvent.

Fig. 9. Diffraction spectrum from a plane (00*l*) single crystal of $BaCo_2Ti_2Fe_8O_{19}$ (hexaferrite type M) at room and helium temperatures: d is the interplane distance, Å; I is the relative intensity of the neutrons scattered at an angle 2α; a) 2α = 9.6°, T = 4.2°K; b) 2α = 150°, T = 4.2°K; c) 2α = 150°, T = 300°K.

The radiation environment both in the reactor building and in surrounding locations satisfies the standard requirements for radiation safety with a large margin.

Physics Investigations in the Beams. In the power startup period of the IBR-2, in addition to the startup experiments, work on the utilization of the neutron beams was carried out in parallel: the study of their characteristics, construction of physics facilities and scientific investigations on them, and improvement of the monitoring of the radiation environment in the beams (Table 3).

The physics facilities were located in two experimental halls with an area of 30 × 60 m each. For the scientific investigations in the beams of the IBR-2, a number of spectrometers were installed for elastic and inelastic neutron scattering. At the present time, of the 14 horizontal beams of the IBR-2, eight (nine facilities) are being operated; four beams are at the utilization stage (extracted beams have been obtained and adjustment work is being carried out). In the future, it is planned to extract four beams beyond the limits of the experimental hall for the purpose of obtaining flight bases of more than 30 m.

The detailed characteristics of the IBR-2 spectrometers have been given in a number of publications [8, 9]. A definite idea of the experimental possibilities of the IBR-2 can be obtained by comparing the average neutron fluxes at the sample being investigated in the IBR-2

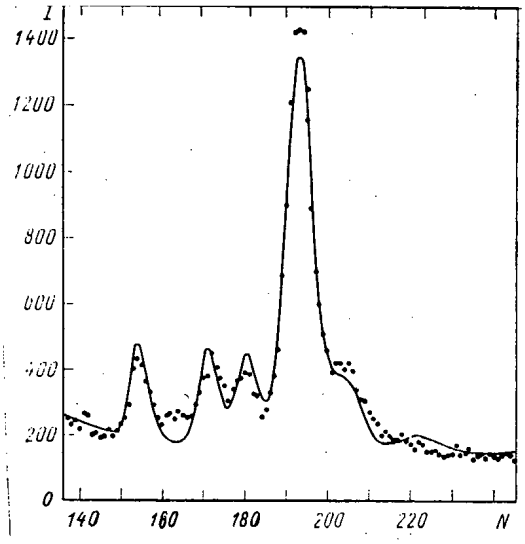

Fig. 10. Spectrum of the inelastic paramagnetic scattering of neutrons from the intermetallic compound $PrAl_3$ at 80°K; E is the imparted energy, MeV; N is the channel number of the analyzer with a width of 128 μsec; I is the count in the channel.

conditions and a high-flux stationary reactor. The comparison of the fluxes is shown in Table 4, where data for the spectrometers in the HFR-ILL high-flux reactor are taken from [10]. It follows from Table 4 that, despite the 30-fold difference in the average powers of the reactors being compared, fully comparable average monoenergetic neutron fluxes are being achieved at the point of location of the sample. It should be borne in mind, that the experimental facilities on the IBR-2 are still not completely optimized. This apparent disparity is explained by the fact that for one and the same requirements on the angular divergence of the neutrons and also on the degree of their monochromatization, on the stationary reactor monochromatization is accomplished by extracting from the beam only neutrons of a specified wavelength, as a result of which the remaining neutrons in this case are not used. On the pulsed reactor, the neutrons are monochromatized according to time of flight without any losses whatsoever, and all or almost all neutrons are used efficiently.

At the present time, the following tasks are being carried out in the neutron beams:

on the physics of amorphous systems: structural investigations of vitreous metals and phase transitions in supercooled (vitreous) liquid crystals;

in the field of molecular biology and structure of solutions: investigations of the structure of ribosomes, orientation of purple membranes in an electric field, hydration of membranes, effects of contraction of immunoglobulins, the structure of hydrated polymer coatings in aqueous solutions, and the structure of solutions of strong electrolytes;

in the field of inelastic neutron scattering: investigations of the dynamics of hydrogen in nickel, the dynamics of adsorbed gases on the surfaces of zeolites and the electronic structure of rare-earth alloys;

in the field of applied research: study of the effects of the biological action of a pulsed irradiation regime, and the conduct of the element analysis of ecological and geological samples.

We shall present some of the results obtained on the IBR-2 spectrometers.

The method of small-angle diffusion scattering of cold neutrons is being used successfully on the IBR-2 for the investigation of large protein structures, conducted jointly with the Protein Institute of the Academy of Sciences of the USSR. Ribosomes of bacteria were grown in a deuterated medium, compensating the density of the coherent scattering amplitudes of the protein and ribonucleic components. When varying the isotopic composition of the solvent, the radius of inertia (characteristic dimension of ribosomes) is unchanged (the slopes of curves 1-4 in Fig. 8 are identical). This demonstrates the neutron-optical uniformity of the ribosomes investigated. Samples with a total volume of 0.6 ml with a ribosome concentration of 2.4-4.8 mg/ml were used in the experiment.

study of the magnetic structure of ferrites (Fig. 9), the magnetic single crystal had also a very small volume (4 mm^3); the duration of the measurements amounted to a total of 1 h. At T = 4.2°K, in addition to the nuclear echoes (the order of which is denoted by figures in Fig. 9), their magnetic satellites are observed (signs + and −) which, naturally, disappear at room temperature. An analysis of the spectrum showed that the magnetic structure of ferrite has a spiral nature with a spiral period of ~40 Å. The work was carried out jointly with the Institute of High-Pressure Physics of the Academy of Sciences of the SSSR.

In the study of the compound $PrAl_3$ (Fig.10), the A. A. Baikov Institute of Metallurgy, Academy of Sciences of the SSSR, and the University of Leipzig (GDR) participated. The measured spectrum of the inelastic scattering of neutrons made it possible to select the parameters of the crystalline electric field, describing the experiment in the best way.

It can be seen from the examples given, that the investigations in the IBR-2 have already developed quite extensively. The future utilization of its capabilities will allow work on qualitatively new experiments to be started, in which the specific properties of the pulsed reactor will be used to a large degree: the high neutron flux in the pulse. Investigations of the kinetics of phase transitions in extremely high magnetic fields, achieved by means of pulsed magnets, investigations of the properties of nonequilibrium perturbations in solids and high-speed processes in biological items (muscle contraction, transportation in membranes under the action of light or electrical stimulators), are related to these experiments. These trends, almost unattainable for normal research reactors, reflect the new fields of application of neutrons in scientific research. The experiments conducted in the IBR-2 to search for the axion [11] — a new neutral particle, predicted in certain versions of the theory of electrically weak interaction — can serve as an illustration of the uses of the pulsed source. Axions could be generated in the absorption of neutrons by hydrogen or boron in the reactor shield, they could pass through the shield almost without capture, and could be recorded by the characteristic decay into two γ-quanta. The pulsed operating regime of the reactor will allow such decays to be discriminated effectively from the time-uniform background of cosmic radiation. The experiments in the IBR-2 have proved to be several times more sensitive than the similar experimental search for the axion in high-powered reactors, and have almost refuted the "standard" model of the axion.

In conclusion of the paper, the authors would wish to stress the exceptionally important role which D. I. Blokhintsev has played in the work of building the IBR-2, prematurely departed from us on the eve of the power startup of the reactor. Much of the creative initiative, energy, and labor was contributed to the power startup of the reactor by the co-workers of the Neutron Physics Laboratory of the JINR, Dubna, the Scientific-Research and Design Institute of Power Technology, and other establishments of the Soviet Union. The authors of the paper express their appreciation to the leading experimentors for having made available the data on the first investigations in the IBR-2 beams.

LITERATURE CITED

1. V. D. Anan'ev et al., Prib. Tekh. Eksp., No. 5, 17 (1977).
2. V. D. Anan'ev et al., At. Energ., 31, No. 4, 352 (1971).
3. V. D. Anan'ev et al., At. Energ., 46, No. 6, 393 (1979).
4. V. L. Lomidze, Ngo Kuang Zui, and E. P. Shabalin, At. Energ., 52, 320 (1982).
5. V. D. Anan'ev et al., Atomkernenergie/Kerntechnik, 43, No. 4, 253 (1983).
6. Yu. N. Pepelyshev, A. K. Popov, and A. D. Rogov, Report R13-83-471 [in Russian], JINR, Dubna (1983).
7. N. V. Krasnoyarov, R. V. Nikol'skii, and I. A. Efrimov, At. Energ., 18, No. 5, 474 (1965).
8. Fourth School on Neutron Physics (Dubna, June 8-18, 1982). D3-4-82-704 [in Russian], JINR, Dubna (1982), pp. 277-291.
9. V. Luschikov, L. Pikelner, Yu. Popov, et al., Selected Topics in Research Programs on the IBR-2/Preprint E3-12740, JINR, Dubna (1979).
10. Neutron Beam Facilities Available for Users, Inst. Laue-Langevin (1981).
11. V. D. Anan'ev, N. A. Kalinina, B. I. Lushchikov, et al., Search for the Axion on the IBR-2 Pulsed Reactor/Preprint R1-83-709 [in Russian], JINR, Dubna (1983).

NUCLEAR DATA REQUIREMENTS FOR FAST REACTORS

V. N. Manokhin and L. N. Usachev*

UDC 539.17:621.039.526

INTRODUCTION

Nuclear data are necessary in many branches of science and technology, primarily in nuclear power engineering. A system of national, regional, and international organizations (committees and centers) has been created for the purpose of consolidating work on the collection, evaluation, establishment, and substantiation of nuclear data requirements.

A system of data centers, each collecting all numerical data on neutron physics within its area and exchanging this information with the other centers, has been in operation successfully for more than 15 years within the framework of the International Atomic Energy Agency (IAEA), under the guidance of the International Committee on Nuclear Data.

A computerized world data bank of neutron data, presently containing experimental data on the cross sections and other nuclear reaction parameters for approximately 400 elements and nuclides (about 3,000,000 numbers), has been created as a result of the activity of these centers. The data bank provides a basis for organizing data banks of estimated nuclear data, which are subsequently used either directly or in group representation for nuclear plant calculations. There are presently a fairly large number of national data banks of estimated general- and special-purpose nuclear data.

Work on data evaluation, the development of existing data banks, and the creation of new ones is in progress in many countries and also within the IAEA framework on the basis of international cooperation. It should be noted that further progress in experimental and theoretical investigations of the atomic nucleus structure and nuclear reactions plays an important role in this work.

Determination and substantiation of nuclear data requirements is an important part of the activity of the International Committee on Nuclear Data, the corresponding national and regional committees, and the system of centers. This has resulted in the publication of the WRENDA international list of requirements, which includes requests for data concerning reactors, the thermonuclear problem, and systems of guarantees.

With regard to fast reactors, nuclear data are necessary for understanding the physical processes underlying the operation of atomic electric power plants, performing the calculations in optimizing the parameters of reactors and atomic power plants as a whole, solving external fuel cycle problems, and deciding on alternative lines of development of nuclear engineering. Nuclear data with the required accuracy are needed, since errors lead to indeterminacy in predicting the reactor parameters. Broad indeterminacies, in turn, lead to large and expensive allowance margins in planning. The data accuracy must be improved still further. On the other hand, extreme refinement of nuclear data also requires considerable investment in experimental technique development, which is the reason for substantiating the required accuracy of nuclear data, i.e., choosing the optimum set of (microscopic and integral) experiments characterized by allowable errors for determining each quantity, which would ensure the necessary accuracy in calculating the reactor parameters at minimum cost.

Many authors [1-14] have considered the problem of indeterminacy of the nuclear data and the requirements imposed on them. This problem has been treated comprehensively in a number of published surveys [9-11]. The problems connected with determining and meeting the nuclear data requirements were discussed at many conferences and meetings, where methods of determining the requirements and the target accuracy of reactor parameters and characteristics were considered, discrepancies between measurements and estimates were analyzed, and the requirements for reactors and other applications in science and technology were formulated.

*Deceased.

Translated from Atomnaya Énergiya, Vol. 57, No. 4, pp. 234-241, October, 1984. Original article submitted May 7, 1984.

0038-531X/84/5704-0683$08.50

are also held within the IAEA framework. The accuracy requirements for nuclear data that have been elaborated in various countries and approved by national and regional committees are included in the WRENDA international list of requirements, which is published by IAEA. The list is revised and re-issued every two years. The list of inquiries provides a fairly complete idea of the need for estimated nuclear data; it can be used as a guide in planning estimates of nuclear data measurements. Approximately 1700 inquiries from 15 countries and international organizations are included in WRENDA-81/82.

The requirements for nuclear data accuracy that have been formulated by different specialists often differ considerably from each other, which can be explained by the different approaches used in determining the requirements. Various authors make different assumptions concerning the target accuracy, the role of integral experiments, the correlative properties of nuclear data errors, etc.

The first step in determining the requirements is the formulation, on the basis of technical and economic considerations, of the target accuracy, i.e., the accuracy requirements in predicting certain plant parameters, the calculation of which requires the knowledge of nuclear data. The next step consists in calculating the coefficient of sensitivity of these parameters to nuclear data variation [15], which provides a basis for determining the requirement for high-accuracy nuclear data and the requirement for nuclear data with lower accuracy. The accuracy requirements for the estimated nuclear data to be used in calculating the reactor characteristics are formulated at this stage (by reactor calculation specialists). The error to be determined is understood as the error of estimated nuclear data, correlated within the assigned energy ranges. The problem of error determination is discussed in detail in [16]. The need for new measurements is established in the process of evaluating the nuclear data and is formulated by data evaluation specialists. In order to elaborate the requirements for the accuracy of estimated nuclear data, it is necessary to have information on the target accuracy and the existing level of errors in these data. Since the number of parameters with demands on their accuracy is greater than the number of parameters whose accuracy must be ensured, it would seem that this is not a single-valued problem. However, the requirement for the minimum cost of the set of measurements and evaluations and also the assumption that the cost of determining each quantity depends on the error (for instance, in proportion to $1/\varepsilon^2$) render this a single-valued problem.

It is also necessary to adopt a certain model with respect to the correlative properties of errors. Many authors have long been emphasizing the importance of considering the correlations between cross sections in determining the necessary accuracy. Surveys of the history of this problem are given in [7, 15, 17] along with the formalism for determining the requirements ensuring accuracy in calculating several reactor parameters by taking into account both microscopic and macroscopic experiments under certain assumptions concerning the correlative properties of the errors. We can conveniently assume that the error is completely correlated within the chosen ranges and that the errors within different ranges are independent of each other. The use of general standards in relative measurements results in the fact that the cross section errors for different nuclides are correlated. The accuracy requirements for estimated nuclear data depend substantially on the assumptions concerning the correlation intervals.

The following should be noted in order to understand the transition from the accuracy of estimated nuclear data, for which the requirements have been formulated, to experimental arrangement requirements. In order to satisfy the requirements imposed on nuclear data, it is necessary to improve the accuracy of individual experiments by analyzing and eliminating errors to the maximum extent possible and also develop new experimental methods. The fact is that systematic errors are revealed only by comparing results obtained by means of different methods. These systematic errors usually pertain to an energy range, rather than to individual experimental points. The requirements formulated in the present article actually pertain to these errors.

In many cases, it is entirely necessary to use integral experiments, since the required accuracy of microscopic data may exceed the accuracy attainable in measuring them, and further refinement could entail appreciably greater measurement expenditures. The significance of integral experiments was discussed by many authors (for instance, [9]).

The rest of this article is devoted to discussions of the target accuracy of reactor parameters, the magnitude of the errors incurred in estimating nuclear data, and the procedure

for elaborating the accuracy requirements with and without consideration of integral experiments.

Target Accuracy

Effective Multiplication Constant (k_{eff}). The fuel characteristics are determined so that the reactor would be critical at the end of a run with the control rods withdrawn. Th- error in calculating the effective multiplication constant or the critical mass, caused by nuclear data inaccuracy, must not exceed 1%. This requirement is based on the possibility of compensating the error in question without modifying the reactor design.

The indeterminacy of k_{eff} is mainly due to the indeterminacy of the nuclear data for the basic fissionable nuclides and structural materials. A 1% accuracy requirement for k_{eff} presupposes stringent requirements for the accuracy of data pertaining to the basic fissionable and raw materials.

Breeding Ratio (br). The volume of uranium production and enrichment and the volume of fuel processing necessary to keep up the supply for the developing power plants with fast reactors are determined by the planned pace of power plant development and the time necessary for doubling the number of breeder reactors. The doubling time, which is inversely proportional to the value of br − 1, must be known with an error of ±10%. The acceptable error in the br value is equal to ±2% (with an allowance for the 10% error of the doubling time and the 1% error of k_{eff}).

Reactivity Variation during a Run. Changes in the reactivity due to fuel depletion and the buildup of actinides and fission products during a run determine the requirements to be imposed on the control elements as well as the fuel reactivity at the end of the run. The target accuracy is ±5%. In order to satisfy these requirements, the total reactivity of fission products must be known with an accuracy of ±10%. The reactivity variation indeterminacy is related to indeterminacies in the capture cross sections of the fission products in the balance of heavy nuclei, caused by their buildup.

Reactivity of the Control Rods. The target accuracy for the reactivity of control rods is ±5%. The prevailing error amounts to ±10%.

Heat Release. For thermophysical calculations of the reactor's ultimate power level, it is necessary to know the irregularity factor — the ratio of the maximum heat release to the mean heat release. This quantity influences directly the top power level, since it is limited by the temperature of the hottest reactor element. On the basis of economic considerations, the required accuracy is ±1%, while the existing error amounts to ±1%. The gamma radiation of fuel elements makes a significant contribution to the heating of control rods and of the blanket. This makes it necessary to state the requirements concerning data on gamma spectra and the cross sections of interaction between gamma radiation and the nuclei.

Radiation Damage Effects. Radiation damage affects directly the economics, design, and safety of nuclear reactors. The maximum irradiation depends on the radiation resistance of the structural materials. Radiation damage causes swelling and creep in the materials along with changes in their characteristics. In order to estimate the swelling and deformation of reactor elements, it is necessary to predict radiation damage doses and dose gradients, the temperature of the materials, the atomic displacement rate, and the rate of helium and hydrogen formation. The neutron flux must be determined so that the observed changes in the properties of materials could be correlated with the irradiation conditions. This entails the need for in-reactor dosimetry. The accuracy requirement for predicting the fluence and the radiation damage dose is ±5%, while the required accuracy in predicting the dose and temperature gradients is ±10%.

The reactivity coefficients determine the reactor kinetics. The most important parameter connected with the nuclear safety of fast reactors is the Doppler reactivity effect, which is primarily due to the broadening of ^{238}U resonances in the 0.5-10-keV range. Fissionable nuclides and the structural materials also provide a substnatial contribution. In order to predict the Doppler effect, it is necessary to know the resonance parameters and the scattering and absorption cross sections, which determine the flux value in the resonance energy range. The accuracy requirement in predicting this effect amounts to 10-15%. The existing accuracy is close to the required one. The sodium reactivity effect is another parameter involving nuclear safety in sodium-cooled fast reactors.

fission scattering in sodium causes neutron moderation and a reduction in neutron leakage. The reactivity effect due to sodium loss depends on the type of fuel and its enrichment. With regard to neutron data, the effect depends on the form of the energy dependence of the fission and capture cross sections as well as the sodium cross sections. The accuracy requirements in predicting the maximum positive sodium effect amount to 10-15%, which can be achieved mainly by improving the calculation method and, to a lesser degree, by improving our knowledge of sodium scattering cross sections. The error in determining the sodium effect is presently ±20%.

Residual Heat Release and the Activity of Irradiated Materials. In designing reactor scram systems and emergency cooling systems, it is necessary to know the residual heat release from fuel elements with an accuracy to 2-5%.

Knowledge of the radioactivity of the spent fuel, the coolant, and the strucutral materials is important for determining the accessibility of equipment and the conditions of handling the reactor parts, designing the shielding for transporting the fuel to be reprocessed, and designing the shielding of regeneration plants. It is necessary to determine the neutron activity of fuel, which is determined by spontaneous fission of curium isotopes and the (α, n) reaction on light (C, O) nuclides, which, in turn, requires the knowledge of the fission and capture cross sections of actinides, which determine their balance in the reactor, and the cross section of the (α, n) reaction. In order to determine the accessibility of the technological equipment, it is necessary to know the sodium activation after exposure, which is due to the (n, 2n) reaction, and the activation of steel components due to the (n, p), (n, α), (n, 2n), and other reactions. The technology of producing fuel elements from plutonium obtained by chemical reprocessing of spent fuel is determined by the built-up activity of ^{236}Pu and ^{238}Pu. It is necessary to know their generation cross sections. The accuracy requirements in predicting the overall activity amount to 20-30%.

Method of Determining the Accuracy Requirements for Microscopic Nuclear Data

A method accounting for the correlative properties of errors based on a simple, but realistic, model [7] has been proposed for determining nuclear data inaccuracies that would allow prediction of reactor quantities with the assigned accuracy. This method allows us to determine quantitatively the required accuracy.

The relative variation of the reactor parameter $\delta C/C$ is expressed linearly in terms of relative variations $(\delta\sigma/\sigma)_{\alpha ij}$ of type α group values of isotope i in group j with the proportionality or sensitivity coefficients $S_{\alpha ij}$,

$$\delta C/C = \sum_{\alpha ij} S_{\alpha ij} (\delta\sigma/\sigma)_{\alpha ij}. \quad (1)$$

The coefficients $S_{\alpha ij}$ are calculated by using the generalized perturbation theory [15, 18].

In order to determine the error in the reactor parameter, an assumption must be made concerning the manner in which the contributions of the many errors included in expression (1) are summed. If we assume that the contributions are random quantities which are not mutually correlated, the variance of the reactor parameter is expressed in terms of the variances of the group microscopic values $d_{\alpha ij}$ as follows:

$$D^2 = \sum_{\alpha ij} S^2_{\alpha ij} d^2_{\alpha ij}. \quad (2)$$

Actually, virtually any nuclear constant may correspond to two or three correlation intervals on the entire energy axis, and, therefore, allowance for the correlation error is important. It has been suggested to subdivide the errors into components with different correlation properties [7, 15]. There are most often three components: the statistical, uncorrelated component; the error component transmitted from the standard when the latter is used (this component is present in the errors of all quantities measured by means of this standard); the assumed error of curve normalization, which is constant within the chosen correlation interval and is caused by a possible systematic error. The $\delta\sigma/\sigma$ value in the form of three components is represented in Eq. (1), and the terms with equal components describing the correlation error are combined so that the new sensitivity coefficients Z_β of the correlation component of error in question constitute sums of the coefficients $S_{\alpha ij}$ over the correlatedness region. Now,

$$\delta C/C = \Sigma Z_\beta \, (\delta\sigma/\sigma)^\beta, \tag{3}$$

where the error components $(\delta\sigma/\sigma)^\beta$ are assumed to be statistically independent, on which basis the passage to expression (4), similar to the passage from Eq. (1) to Eq. (2) is effected:

$$D^2 = \sum_\beta Z_\beta^2 d_\beta^2. \tag{4}$$

With the left-hand side — the reactor parameter error — assigned, it is necessary to determine the set of errors of individual quantities d_β^2.

As stated, this is obviously not a single-valued problem; the contributions provided by the errors of various quantities to the reactor parameter error can be distributed in different ways. However, it is sufficient to impose the condition of cost minimum on the set of experiments, making at the same time the assumption of relative expenditures for measuring various quantities with the accuracy achieved at that time and extrapolating the cost of experiments as a function of the error ε, using, for instance, the relationship $1/\varepsilon^2$, since this has now become a single-valued problem.

The expression for the cost of experiments is written thus,

$$\sum_{\beta=1}^{N} \lambda_\beta / d_\beta^2,$$

where λ_β is the constant characterizing the cost of experiments in determining a quantity with the subscript β [7]. Under the assumption of equal "breakthrough" ability of experimenters, it can be considered that equal expenditures have been incurred in achieving results with the errors d_{β_0}, and, therefore,

$$\lambda_\beta / d_\beta^2 = \text{const}, \ \beta = 1, \ \ldots, \ N.$$

If we keep in mind that the sought errors must be limited from above by the accuracy achieved, the problem of planning an optimum set of microexperiments and evaluations securing the required accuracy in calculating K reactor parameters is reduced to the solution of the following extremum problem:

$$\sum_{\beta=1}^{N} \lambda_\beta / d_\beta^2 \to \min; \tag{5a}$$

$$\sum_{\beta=1}^{N} Z_{\beta l}^2 d_\beta^2 \leqslant D_l^2, \ l = 1, \ \ldots, \ L; \tag{5b}$$

$$0 < d_\beta^2 \leqslant d_{\beta_0}^2. \tag{5c}$$

In the case of a single restraint imposed on the variance of only one reactor parameter, the problem is solved analytically [7]. An algorithm has been developed in [17] for planning an optimum set of microexperiments and evaluations which would ensure the required accuracy for an arbitrary number of reactor parameters; the algorithm has been expanded there to include integral experiments. When data from integral and microscopic measurements are used simultaneously, the accuracy D_ζ in calculating the reactor parameter C_ζ with the sensitivity coefficient $\mathbf{Z}_\zeta$ can be expressed as follows:

$$D_l^2 = \mathbf{Z}_l D \, (N + K) \, \mathbf{Z}_l^T, \tag{6}$$

where

$$D \, (N + K) = \{I - D \, (N) \, F^T [V + FD \, (N) \, F^T]^{-1} F\} \, D \, (N). \tag{7}$$

Here, D (N) is the covariance matrix of only the microscopic experiments, F is the matrix of sensitivity coefficients of the integral experiments used, and V is the experimental error matrix for the integral experiments. The D (N) matrix can be rendered diagonal, where squares of the microscopic data accuracy constitute the diagonal elements.

Consequently, the planning of the set of microscopic experiments in the case of K integral experiments can be reduced to the following extremum problem:

$$\sum_{\beta=1} \lambda_\beta / d_\beta^2 \to \min; \tag{8a}$$

$$\mathbf{Z}_l D(N+K)\mathbf{Z}_l^T \leqslant D_l^2,\ l=1,\ \ldots,\ L; \tag{8b}$$

$$0 < d_\beta^2 \leqslant d_{\beta_0}^2. \tag{8c}$$

The sought accuracy d_β^2 figures in constraint (8c) as an element of the diagonal matrix D (N). Efficient numerical methods have been developed for solving this problem.

Required and Achieved Accuracies for Nuclear Data

According to the WRENDA international list of requirements, the accuracy of nuclear data is characterized only by the standard deviation. The sense of the error, however, is defined only in the inquiries submitted by the USSR. Thus, in L. N. Usachev's inquiries, it is assumed that the error constitutes the sum of components with different correlation properties. The accuracy requirements were established for the most important component of the error correlated over the energy range indicated in the inquiry. This error component determines the accuracy of the integral under the curve over this interval. In inquiries concerning measurements, it is assumed that standards are used — cross sections of the ^{10}B (n, α) reaction (below 100 keV) and the ^{235}U (n, f) reaction. In all inquiries, with the exception of inquiries concerning standards, the accuracy is formulated in relation to measurements with respect to standards, the required accuracy of which has been determined separately.

The required and the achieved accuracies for microscopic nuclear data are considered. Some of the values have been borrowed from survey [9], while the values of data accuracy for actinides and fission products have been taken from [12-14].

Basic Fissionable and Raw Materials [9]. High-accuracy data on fission and capture cross sections, ν values for ^{235}U, ^{238}U, ^{239}Pu and ^{238}U inelastic scattering cross sections are required. This accuracy is determined primarily by the requirements for the prediction of k_{eff} (1%) and of the br value (2%). In the thermal range of neutron energy, the necessary accuracy is ±0.3% for ν and ±1% for σ_f, σ_c, σ_t, and σ_s. The following requirements for fissionable and raw materials, respectively, in the energy range of the fast-reactor spectrum are given below (%):

ν_f . . .	0,3	1
σ_f . . .	2	2
σ_c . . .	4	3
σ_t, σ_s . . .	2	5
σ_{in} . . .	10	5
$\sigma_{n,2n}$ . . .	10	10

For thorium-cycle reactors, the same accuracy values are needed for ^{232}Th and ^{233}U as for ^{238}U and ^{235}U.

Structural Materials. Accuracy requirements for the nuclear data relating to the coolant and the structural materials are necessary in determining the reactivity effects, the neutron spectra, the neutron balance, radiation damage, the activation of materials, and the heating. For sodium, it is necessary to know the scattering and capture cross sections and have data on the capture and inelastic scattering for Fe, Cr, Ni (in the first place), Ti, V, Mn, Co, Zr, Nb, and Mo. The accuracy requirements amount to 5-10% for capture cross sections and 5% for inelastic scattering cross sections. Data on the resonance structure of cross sections are needed, since resonance self-screening and the Doppler effect are considerable. Data on the (n, p) and (n, α) reactions are required with regard to the problem of radiation damage and, in part, neutron economy.

Absorbers. Natural and enriched boron are used in fast reactors (tantalum is being tested, and the feasibility of europium is under study). The following nuclear data requirements have been elaborated for B, Cd, Eu, Gd, Er, Hf, and Ta absorbers: ±5% for the capture cross section and ±10% for the scattering cross section. Data for individual nuclides are necessary for predicting the variation in reactivity with depletion, the activation, and the heating of absorbers.

radioactive contamination (coolant activation and mass transfer of steel) in the primary circuit, the pump, and the heat exchangers and for calculating the activation of reactor parts to be subsequently extracted, transported, stored, or reprocessed. The basic activation reactions are the following: $^{54}Fe(n, p)^{54}Mn$; $^{58}Ni(n, p)^{58}Co$; $^{59}Co(n, \gamma)^{60}Co$; $^{58}Fe(n, \gamma)^{59}Fe$; $^{50}Cr(n, \gamma)^{51}Cr$; $^{54}Fe(n, \alpha)^{51}Cr$; $^{58}Co(n, \gamma)^{59}Co$; $^{62}Ni(n, \gamma)^{63}Ni$; $^{58}Ni(n, \gamma)^{59}Ni$; $^{54}Fe(n, \gamma)^{55}Fe$; $^{22}Na(n, \gamma)^{23}Na$; $^{40}Ar(n, \gamma)^{41}Ar$. Data averaged with respect to the reactor's neutron spectrum are also necessary. The required accuracy amounts to 10-15%.

In-Reactor Dosimetry. Dosimetric reactions are used for measuring neutron fluxes and spectra in reactors. Knowledge of the irradiation conditions is important for interpreting the results of irradiation experiments, predicting the activation of materials, and correlating the properties of irradiated materials with the irradiation conditions. Two basic factors affect the properties of materials: atomic displacement and helium formation in (n, α) reactions. In order to predict the atomic displacement rate and helium formation, it is necessary to have information on the total flux, the flux spectrum, and the cross sections of the following reactions: $^{27}Al(n, \alpha)^{24}Na$; $^{56}Fe(n, p)^{56}Mn$; $^{63}Cu(n, 2n)^{62}Cu$; $^{238}U(n, f)$ F.P.; $^{237}Np(n, f)$ F.P.; $^{58}Ni(n, 2n)^{57}Ni$; $^{197}Au(n, \gamma)^{198}Au$; $^{239}Pu(n, f)$ F.P. Active work within the framework of IAEA on the selection and evaluation of dosimetric reactions is in progress, and an international data file has been organized.

Transactinides. Nuclear data on transactinides are necessary for determining the storage and depletion of actinides and predicting the neutron activity of the fuel. It is necessary to know the cross sections of the capture and fission reactions and the (n, 2n) reaction.

Some transactinides accumulate in fast power reactors in fairly large quantities. The neutron cross sections of these nuclides must be known with a high degree of accuracy, comparable to the accuracy required for the basic fissionable and fuel nuclides. During reactor operation, there is a buildup of such nuclides, which, due to their relatively short half-life and the characteristics of decay (hard gamma-radiation or neutron emission), cause most of the difficulties in handling the fuel during its transportation and reprocessing. Among such nuclides are ^{232}U, ^{238}Pu, ^{242}Cm, and ^{244}Cm. The reactions essential for ^{232}U formation are $^{233}U(n, 2n)$ and $^{237}Np(n, 2n)$, while the reactions important for the formation of ^{238}Pu, ^{242}Cm, and ^{244}Cm, are $^{237}Np(n, \gamma)$, $^{241}Am(n, \gamma)$, and $^{243}Am(n, \gamma)$.

The required nuclear data accuracy for actinides was investigated in [10, 13, 14] for the purpose of calculating their buildup. The basic results are given below.

The prediction accuracy for certain parameters, calculated by using the achieved nuclear data accuracy is given (for the purpose of calculating the actinide buildup) in Tables 1 and 2. It is evident from Tables 1 and 2 that the achieved nuclear data accuracy for transactinides does not ensure the required accuracy in buildup calculations for fast reactors. More stringent requirements are being formulated for the capture cross sections of ^{240}Pu, ^{241}Pu, ^{242}Pu, and ^{243}Am. The requirements for the (n, 2n) reaction for ^{238}U, ^{237}Np, and ^{238}Pu are essential. The achieved accuracy of fission cross sections is almost sufficient.

The required accuracy of data on transactinide nuclides is determined with a view to ensuring the necessary accuracy in calculating the nuclide production, the neutron yield, and the heat release in the reactor. In addition to the target accuracy for the buildup of a number of nuclides, also the target accuracy for the α-decay energy (5%) and for neutron emission (10)% was considered in [14]. As a result, more stringent accuracy requirements were obtained for the capture cross sections of ^{243}Am, ^{241}Am, and ^{242}Pu and for the ^{242}Cm branching ratio. The most stringent requirements have been imposed on the capture cross sections of ^{237}Np, ^{242}Pu, ^{243}Am, and ^{241}Am and the cross sections of the (n, 2n) reactions for ^{237}Np and ^{238}U.

The most stringent accuracy requirements have been formulated for the following reactions:

$^{237}Np(n, 2n)$ and ^{238}U (n, 2n) for calculating the ^{236}Pu buildup;

$^{238}U\ (n, 2n)$, $^{237}Np\ (n, \gamma)$ for ^{238}Pu;
$^{242}Pu\ (n, \gamma)\ ^{243}Am\ (n, \gamma)$ for ^{244}Cm;
$^{242}Pu\ (n, \gamma)$ for ^{243}Am;

$^{243}Am(n, \gamma)$, $^{242}Pu(n, \gamma)$, and $^{242}Cm_{BRSf}$ for calculating the neutron production.

TABLE 1. Achieved (Numerator) and Required (Denominator) Accuracy of Nuclear Data (%)

Nuclide	Capture cross section	Fission cross section	Cross section of (n, 2n) reaction
^{238}U	8/8	5/4	20/15
^{239}Pu	10/3	4/4	50/50
^{240}Pu	20/4	10/10	50/50
^{241}Pu	20/7	8/5	50/50
^{242}Pu	50/15	30/30	50/50
^{243}Pu	50/50	50/50	50/50
^{242m}Am	30/20	30/30	50/50
^{241}Am	15/15	15/15	—
^{242}Am	30/30	30/30	—
^{243}Am	50/20	50/50	—
^{242}Cm	50/50	50/50	—
^{237}Np	50/15	10/10	50/25

TABLE 2. Achieved and Required Accuracies in Buildup Calculations [10] (%)

Nuclide	Required accuracy	Achieved accuracy	Nuclide	Required accuracy	Achieved accuracy
^{236}Pu	30	55	^{241}Am	5	24
^{238}Pu	20	60	^{242}Am	20	28
^{240}Pu	5	12	^{243}Am	20	59
^{241}Pu	4	24	^{242}Cm	20	28
^{242}Pu	10	31	^{244}Cm	30	71

The requirements for nuclear data connected with calculation of the ^{232}U buildup in nuclear reactors were analyzed in [13]. The most important nuclear constants for calculating the ^{232}U buildup in fast reactors are the characteristics of the reactions (n, 3n) on ^{234}U, (n, γ) on ^{235}U, and (n, 2n) on ^{238}U and ^{237}Np.

Fission Products. In order to determine the total reactivity of fission products (with an accuracy to 5-10%), we must know the capture and scattering cross sections with accuracies of ±10 and ±30%, respectively. It is necessary to know in detail the behavior of the cross sections and their values averaged over the reactor spectrum.

It has been shown in [12, 13] that, if the errors of all the capture cross sections are the same and equal to 30%, and if also the errors of the fission product yields are the same and equal to 3% (in fact, the values of most yields are known with a higher degree of accuracy), we can estimate the acceptable error of the mean cross section (±7%). If a systematic error of 10% is assumed in all capture cross sections of individual fission products, the estimate of the error in the mean capture cross section of fission products amounts to ±12%. This figure also characterizes roughly the scatter of various estimates of this value.

With an allowance for the requirements imposed on the nuclear data obtained in considering the problems of core physics [17], the acceptable error of the mean capture cross section of fission products is equal to 10%. Assuming that there is no correlation between the errors of different cross sections, we can consider that the above accuracy has already been achieved. If we assume that a systematic error is present in these errors, the maximum allowable value is then 7%.

It is important to determine precisely the sense of the error: Depending on the assumption concerning the correlative properties of the error, two opposite conclusions are possible. Assuming the statistical independence of the of the errors of cross sections of various nuclides, we reach the conclusion that there is no need to refine the cross sections of fission products, since it could be considered that a 30% error in the capture cross section for each fission product had already been incurred, as a result of which the 10% requirement for the accuracy of the fission pseudo product would be satisfied. However, if the errors are correlated, this aim could be achieved by striving for an error of 7% in the cross section of each nuclide, for which a very large amount of experimental and evaluation work would be necessary. The second assumption is probably closer to the actual situation. We provide below a list of nuclides whose capture cross sections should be refined, which would be important

for [illegible] tors. (The nuclides are arranged in the order of magnitude of their contribution to the mean cross section, which amounts to 80%.) The contribution of any nuclide in the first group (^{133}Cs, ^{101}Ru, ^{99}Tc, and ^{143}Nd) to the mean cross section amounts to not less than 5%; the contribution of a nuclide in the second group (^{103}Rh, ^{145}Nd, ^{97}Mo, ^{149}Sm, ^{102}Ru, ^{131}Xe, ^{98}Mo, ^{95}Mo, ^{151}Sm, ^{135}Cs, and ^{93}Zr) is equal to 5-2%; a nuclide of the third group ^{105}Pd, ^{141}Pr, ^{100}Mo, ^{153}Eu, ^{103}Ru, and ^{104}Pu) provides 2%; others contribute less than 1%.

CONCLUSIONS

Summarizing, we emphasize again that precise knowledge of estimated microscopic neutron data is necessary in order to ensure the required accuracy in calculating a number of parameters which are important for the reactor operation and decisions on promising reactor concepts, for the technology of the external fuel cycle, including transportation, reprocessing of spent fuel, and the manufacture of new fuel elements, and for investigating the stability of fuel elements in relation to the neutron flux in the reactor. These requirements have not yet been satisfied, in spite of the progress made in the field of experiments and evaluations.

It should also be emphasized that, for effective progress toward the target accuracy of reactor parameters, it is necessary to determine the correlative properties of allowable errors, which, unfortunately, has not yet been done in the WRENDA international list of requirements.

LITERATURE CITED

1. T. Moorhead, "The effects of errors in cross section data on calculation for a large dilute fast reactor," in: Seminar on Physics of Fast and Intermediate Reactors, Vol. 2, Vienna (1962).
2. P. Greebler and B. Hutchins, "User requirements for cross sections in energy range from 100 eV to 100 keV," in: Proc. Conf. on Neutron Cross Section and Technology, Washington (1966).
3. R. Smith, "Nuclear data requirements for fast reactor design and operation," in: Proc. IAEA Symp. on Nuclear Data for Reactors, Vol. 1, Paris (1966), p. 27.
4. P. Greebler et al., "Implication of nuclear data uncertainties to reactor design," in: Proc. IAEA Symp. on Nuclear Data for Reactors, Vol. 1, Helsinki (1970), p. 17.
5. S. M. Zaritskii and M. F. Troyanov, "Requirements for the accuracy of constants in reactor design," in: Nuclear Reactor Physics [in Russian], Vol. 2, Atomizdat, Moscow (1970).
6. S. M. Zaritskii, M. N. Nikolaev, and M. F. Troyanov, "Nuclear data requirements for fast reactor design," in: Neutron Physics [in Russian], Vol. 1, Kiev (1973), p. 5.
7. L. Usachev and G. Bobkov, Planning of an Optimum Set of Microscopic Experiments and Evaluation, INDC(CCP)-19/U, Vienna (1972).
8. L. N. Usachev, V. N. Manokhin, and Yu. G. Bobkov, "Nuclear data accuracy and its effect on fast reactor development. An approach to the development of requirements for nuclear data accuracy" [in Russian], in: Proc. Conf. on Nuclear Data in Science and Technology, Vol. 1, Vienna (1973), p. 129.
9. J. Rowlands, "Nuclear data for reactor design, operation, and safety," in: Proc. Conf. on Neutron Physics and Nuclear Data, Harwell (1978), p. 7.
10. L. Usachev et al., "Determination of transactinide nuclear data required accuracy for burn-up calculation in fast reactors," in: Proc. Conf. on Neutron Physics and Nuclear Data, Harwell (1978), p. 181.
11. Ph. Hammer, "Nuclear data needs for plutonium breeders," in: Proc. Conf. on Nuclear Cross Sections for Technology, Knoxville (1979).
12. Yu. G. Bobkov, A. S. Krivtsov, and L. N. Usachev, "Perturbation theory and product kinetics in reactors," Vopr. At. Nauki Tekh. Ser. Yad. Konstanty, No. 3 (38), 3 (1980).
13. Yu. G. Bobkov, A. S. Krivtsov, and L. N. Usachev, "Nuclear data requirements for fission products and transactinides in fast reactors," in: Neutron Physics [in Russian], Vol. 3, Kiev (1980), p. 234.
14. L. N. Usachev, I. V. Kravchenko, and A. S. Krivtsov, "Required accuracy of transactinide nuclear data for fast reactors with regard to the external fuel cycle," Fourth Conference on Mutual Comparison of Nuclear Data for Transactinides [in Russian], Vienna (1981).

Problem of Nuclear Data for Reactors [in Russian], Atomizdat, Moscow (1980).
16. L. N. Usachev, "Unique determination of errors in nuclear data," in: Nuclear Constants [in Russian], Vol. 20, Atomizdat, Moscow (1975), p. 3.
17. Yu. Bobkov, L. Pyatnitskaya, and L. Usachev, Planning of Neutron Data Experiments and Evaluations for Reactors, INDC(CCP)-46L, Vienna (1974).
18. L. N. Usachev, "Perturbation theory for the breeding ratio and other ratios for various reactor processes," At. Energ., 15, No. 6, 472 (1963).

MEASUREMENT OF THE FISSION CROSS SECTION OF THE ^{235}U ISOMER BY THERMAL NEUTRONS

V. I. Mostovoi and G. I. Ustroev

UDC 621.039.512.23

The isomeric state of ^{235}U ($J^{\pi} = 1/2^{+}$), discovered in 1957 [1, 2], is unique in its extraordinarily low energy, equal to 76.8 eV [3]. In the ground state ($7/2^{-}$), the isomer transforms by means of internal E3-conversion in the outer electron shells, with a half-life of ~26 min. This mechanism of deexcitation specifies the dependence of the half-life and the spectrum of the internal conversion electrons on the nature of the chemical bonds of the uranium atoms.

Information about the fission cross section of the ^{235}U isomer is of interest for the channel concept in the theory of fission. It may prove to be important also for the proposed plasma reactors, with a plasma temperature of a few tens of eV, in which the isomer will be almost stable.

The main difficulties in measuring the fission cross section of the ^{235}U isomer are due to its ultrasmall quantity and its short lifetime. At the present time, the realistic method of obtaining the isomer is the collection of recoil nuclei during the α-decay of ^{239}Pu. For this, because of the relatively large half-life of plutonium, and also the small energy of the recoil nuclei (~90 keV), it is necessary to use thin layers of plutonium of large area (~1 m^2) and to collect the recoil nuclei on very small targets, in order to obtain an acceptable ratio between effect and background. The collection of the recoil nuclei of the isomer is accomplished by means of an electrostatic field in a facility containing 90 mg of plutonium. The facility, with a collection factor of 60%, allowed targets to be obtained containing ~10 ng of the isomer of an area of 0.2 cm^2. Simultaneously, nuclei of the aggregation sputtering of plutonium were accumulated on the target and which were the main source of the background.

The prepared target with the isomer and the control target with ^{239}Pu were placed at the center of the F-1 reactor and, after bringing it to full power (thermal neutron flux $0.7 \cdot 10^{10}$ cm$^{-2} \cdot$sec^{-1}, effective temperature of the neutron spectrum 360°K), the total number of fission fragments versus the time was recorded with semiconductor breakdown detectors [4] in two intervals.

Figure 1 shows the dependence of the number of fission fragments recorded on the time, for one of 15 series of measurements. The upper curve characterizes the first interval, the origin of which is displaced relative to the end of buildup by 13 min (the time necessary for transportation of the sample from the facility to the reactor and for startup of the reactor). The lower curve relates to the second interval, which is started 6 half-lives after completion of the buildup. At this time, the isomer in the target had decayed almost completely and it contained only nuclei of ^{235}U and ^{239}Pu in the ground state. The fission effect of the isomer is clearly seen in the figure. That the observed difference in the total count is due only to fission of the isomer was confirmed in special experiments which showed that during the time of measurements, no desorption of the isomer in the target occurs and that the efficiency of the detectors does not vary appreciably.

In order to determine the ratio of the fission cross section of the ^{235}U isomer (σ_f^m) to its fission cross section in the ground state by thermal neutrons (σ_f^g), the expression

Translated from Atomnaya Énergiya, Vol. 57, No. 4, pp. 241-242, October, 1984. Original article submitted May 8, 1984.

 0038-531X/84/5704-0692$08.50

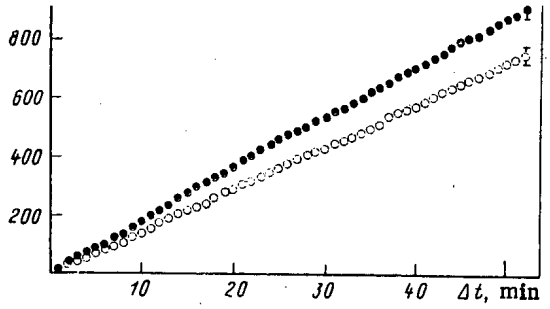

Fig. 1. Total fission fragment count I_f: ●) from the sample containing the ^{235}U isomer; ○) from the sample with the decayed ^{235}U isomer. Time of buildup in the sample of ^{235}U isomer t_0 = 50 min.

$$\frac{\sigma_f^m}{\sigma_f^g} = 1 + \frac{\left(\frac{I_f^m}{I_f} - 1\right)\lambda_m^2 t_0 \Delta t}{(e^{-\lambda m t_1} e^{-\lambda m t_2})(e^{\lambda m t_0} - 1)} \left(\frac{\varepsilon_M N_M^9 I_f}{\varepsilon_M N_M^9 I_f - \varepsilon N^9 I_{fM}}\right)$$

was used, in which only parameters measured in the given experiment occur. Here I_f^m and I_f are the total fission count (after subtraction of the background from the backing and detector) from the target with and without the isomer, respectively; I_{fM} is the total fission count from the control target with ^{239}Pu; N^9 is the number of ^{239}Pu nuclei in the target with the isomer; N_M^9 is the number of ^{239}Pu nuclei in the control target; ε is the fission fragment recording efficiency by the detector for the target with the isomer; ε_M is the fission fragment recording efficiency by the detector for the control target; t_0 is the time during which the isomer built up; $t_1 = t_0 + 13$ is the time of start of recording of the fissions from the target with the isomer (start of first interval); t_2 is the time of completion of recording of the fissions in the target with the isomer (end of first interval); λ_m is the decay constant of the ^{235}U isomer; and $\Delta t = t_2 - t_1$ is the duration of the measurements. The values of I_f^m, I_f, and I_{fM} refer to one and the same measurement duration Δt.

The background from the target backing and the detector was measured periodically between series and was constant (0.98 min^{-1}). Depending on the time of buildup t_0, it amounted to 6-12% of the total count I_f^m and I_f. The same background for the control target was negligibly small.

The recording efficiency of the fission fragments by the detectors (ε and ε_M) was determined before the start and after completion of the measurement of each series, by means of a calibrated fission fragment target of ^{252}Cf. The number of nuclei N^9 and N_M^9 of plutonium in the targets was calculated from the data of α-spectra measurements.

From the data of the measurements made, the required ratio is equal to

$$\frac{\sigma_f^m}{\sigma_f^g} = 2.2 \pm 0.4.$$

The result obtained confirms with a high probability that the fission cross section of the ^{235}U isomer in the thermal neutron energy region is determined by the level of the compound nucleus with spin 0.

LITERATURE CITED

1. F. Asaro and I. Perlman, Phys. Rev., 107, 318 (1957).
2. J. Huizenga et al., Phys. Rev., 107, 319 (1957).
3. V. I. Zhudov et al., Pis'ma Zh. Eksp. Teor. Fiz., 30, No. 8, 549 (1979).
4. A. N. Smirnov, in: Program and Thesis of the Thirtieth Conference on Nuclear Spectroscopy and the Structure of the Atomic Nucleus [in Russian], Nauka, Leningrad (1980), p. 411.

COMPARATIVE ANALYSIS OF ESTIMATES OF NEUTRON RADIATIVE CAPTURE CROSS SECTIONS FOR THE MOST IMPORTANT FISSION PRODUCTS

T. S. Belanova, L. V. Gorbacheva,
O. T. Grudzevich, A. V. Ignatyuk,
G. N. Manturov, and V. I. Plyaskin

UDC 539.172:621.039

At the present time there is a very urgent development of reliable estimated data for the fission products which determine the poisoning of a fast reactor core and the activity of spent fuel. An estimate of the neutron radiative capture cross sections in the energy range from 1 to 10^3 keV is of the greatest practical interest. There are many estimates of the capture cross sections, the most complete of which are the Japanese Evaluated Nuclear Data Library (JENDL-1) [1] and the Evaluated Nuclear Structure Data File (ENDF/B IV) and its revised version ENDF/B V [2]. Kikuchi et al. [1] compare the JENDL-1 values for the main fission products with those of other laboratories. The considerable differences in the various estimates of the capture cross sections for many nuclides show up particularly clearly in the light of new experimental data obtained after the estimates were made. The capture cross sections for the odd nuclides of samarium, neodymium, and europium were revalued [3, 4], and the molybdenum isotopes were analyzed in [5].

In the present article we analyze the estimates and data for the rest of the most important fission products [1, 2]. We divide them into the following three groups: 1) the nuclides ^{99}Tc, ^{101,102,104}Ru, ^{103}Rh, ^{105}Pd, ^{109}Ag, and ^{133}Cs, for which there are direct experimental data on the average neutron capture cross sections; 2) the nuclides ^{107}Pd, ^{129}I, ^{131}Xe, and ^{147}Pm, for which there are no data on the fast neutron capture cross sections, but for which there is experimental information on the average resonance parameters; 3) the nuclides ^{93}Zr, ^{99}Mo, ^{106}Ru, ^{135}Cs, and ^{144}Ce, for which there are no data on the average neutron capture cross sections or on the average resonance parameters.

Nuclides of the First Group

The large amount of new data published during the last five years [6-17] is characterized by an increased level of experimental technique, more accurate methods of taking account of effects accompanying neutron capture, and the reliability of the absolutization of the cross sections. All the measurements were performed by the time-of-flight method at linear or electrostatic accelerators. The detectors used were large-volume nonhydrogenous liquid scintillators. The relative efficiencies of the gamma detector and neutron flux monitor in most measurements were determined by the saturated resonance method, either at low-lying levels of the nuclide under investigation, or at the 4.9-eV gold resonance. Table 1 shows the characteristics of these experiments. The errors in the cross sections (5-10%) obtained in measurements at linear accelerators are due mainly to the errors in determining the fast neutron background. The different methods of taking account of this background are the cause of the systematic divergences (10-30%) [11, 12] in the cross sections. Moreover, the particular methods of taking account of the background above 100 keV contribute to an increase of the cross sections by 20-35% [6, 7, 11, 13]. The estimate included data from [18-33] published up to 1978. The observed discrepancies in these data, as explained, were due most often to the choice of different standards and normalized cross sections, and more rarely to errors in the experiments themselves. The cross sections of ^{103}Rh [19-23], ^{109}Ag [23, 24], and ^{133}Cs [25] were reevaluated to match the standard cross sections taken from ENDF/B V.

Only renormalized data were used in the relative analysis. It should be noted that from an analysis of the experimental data for certain nuclides over the whole neutron energy range from 1 to 1000 keV the use of JENDL or ENDF/B values can be recommended. This information is given below. In these cases the differences between the experimental and estimated values do not exceed 10%. The cross sections of the remaining nuclides were reexamined, taking account

Translated from Atomnaya Énergiya, Vol. 57, No. 4, pp. 243-249, October, 1984. Original article submitted May 14, 1984.

 0038-531X/84/5704-0694$08.50

TABLE 1. Fundamental Characteristics of New Experiments for the First Group of Fission Products*

Nuclide	E, keV	Neutron source	Gamma detector	Flux monitor	Standard	Comments	Ref.
^{99}Tc	2,65--2000	ORELA	C_6F_6, LLSD	^{6}Li (n, α)	SRM ^{197}Au	Absolute measurement	[6]
$^{101, 102}$Ru, ^{104}Ru	2,6—600	ORELA	C_6F_6, LLSD	^{6}Li (n, α) up to 70 keV ^{235}U (n, f) above 70 keV	SRM ^{197}Au	Absolute measurements renormalized to match [11]	[7]
^{103}Rh	2,6—600	ORELA	C_6F_6, LLSD	^{6}Li (n, α) up to 70 keV, ^{235}U (n, f) above 70 keV	SRM ^{197}Au	The same	[7]
	10—70	Van de Graaff accelerator (KFK)	Moxon—Rae detector	—	^{197}Au (n, γ)	Relative measurements	[8]
	500—3000	Van de Graaff accelerator	NaI	Long counter	—	Absolute measurements	[9]
	500—4000	Van de Graaff accelerator (ANL)	LLSD	Gray detector	^{197}Au (n, γ)	Relative measurements	[10]
^{105}Pd	2,6—750	ORELA	C_6F_6, LLSD	^{6}Li (n, α)	—	Absolute measurements	[11]
	1—300	LINAC (Geel)	C_6F_6, LLSD	^{10}B $(n, \alpha\gamma)$	SRM at 55.2-eV resonance	The same	[12]
	3—200	ORELA	C_6F_6, LLSD	^{6}Li (n, α)	SRM ^{197}Au	Absolute measurements renormalized to match [11]	[13]
^{109}Ag	3—2000	ORELA	C_6F_6, LLSD	^{6}Li (n, γ) up to 100 keV, ^{235}U (n, f) above 100 keV	SRM ^{197}Au	Absolute measurements	[14]
	3,2—700	LINAC (JAERI)	C_6F_6, LLSD	^{10}B $(n, \alpha\gamma)$	SRM ^{197}Au	The same	[17]
^{133}Cs	2,7—600	ORELA	C_6F_6, LLSD	^{10}B $(n, \alpha\gamma)$ up to 100 keV, ^{235}U (n, f) above 100 keV	SRM ^{197}Au	Ditto	[15]
	3,2—270	LINAC (Kyoto)	C_6F_6, LLSD	^{10}B $(n, \alpha\gamma)$	$\bar{\sigma}_{n\gamma}$ (24 keV) = = 630mb †	Relative measurements	[16]

*LLSD, large liquid scintillation gamma ray detector; SRM, saturated resonance method.
†1 b = 10^{-28} m^2.

of the new experimental data. The Hauser—Feshbach—Moldauer relations were used in the analysis of the energy changes of the average capture cross sections. The neutron and radiation strength functions appearing in these relations were determined from conditions of optimum description of the set of data assumed [3].

We proceed to a discussion of the data on each nuclide.

^{99}Tc. The experimental data cover the neutron energy range from 0.5 to 2000 keV [6, 18, 26, 27]. In the energy range from 3 to 80 keV the data of Macklin [6], Chou [18], and Little [26] agree with one another to within 5-10%. Above 80 keV the only data are in [6]. The ENDF/B V estimate below 80 keV follows Little's values [27], which are 20-25% higher than those in [26]. Above about 500 keV the ENDF/B V values are appreciably lower than Macklin's results [6]. The JENDL-1 estimate below 100 keV corresponds to the lowest experimental data of Chou [18] in this range, and in the range 400-1000 keV it is higher than all the existing experimental data. The ENDF/B IV estimate is below the JENDL-1 estimate over the whole energy range. Our calculated curve of the capture cross section above 100 keV was based on Macklin's data [6], and up to 100 keV passes between the JENDL-1 and ENDF/B V estimates.

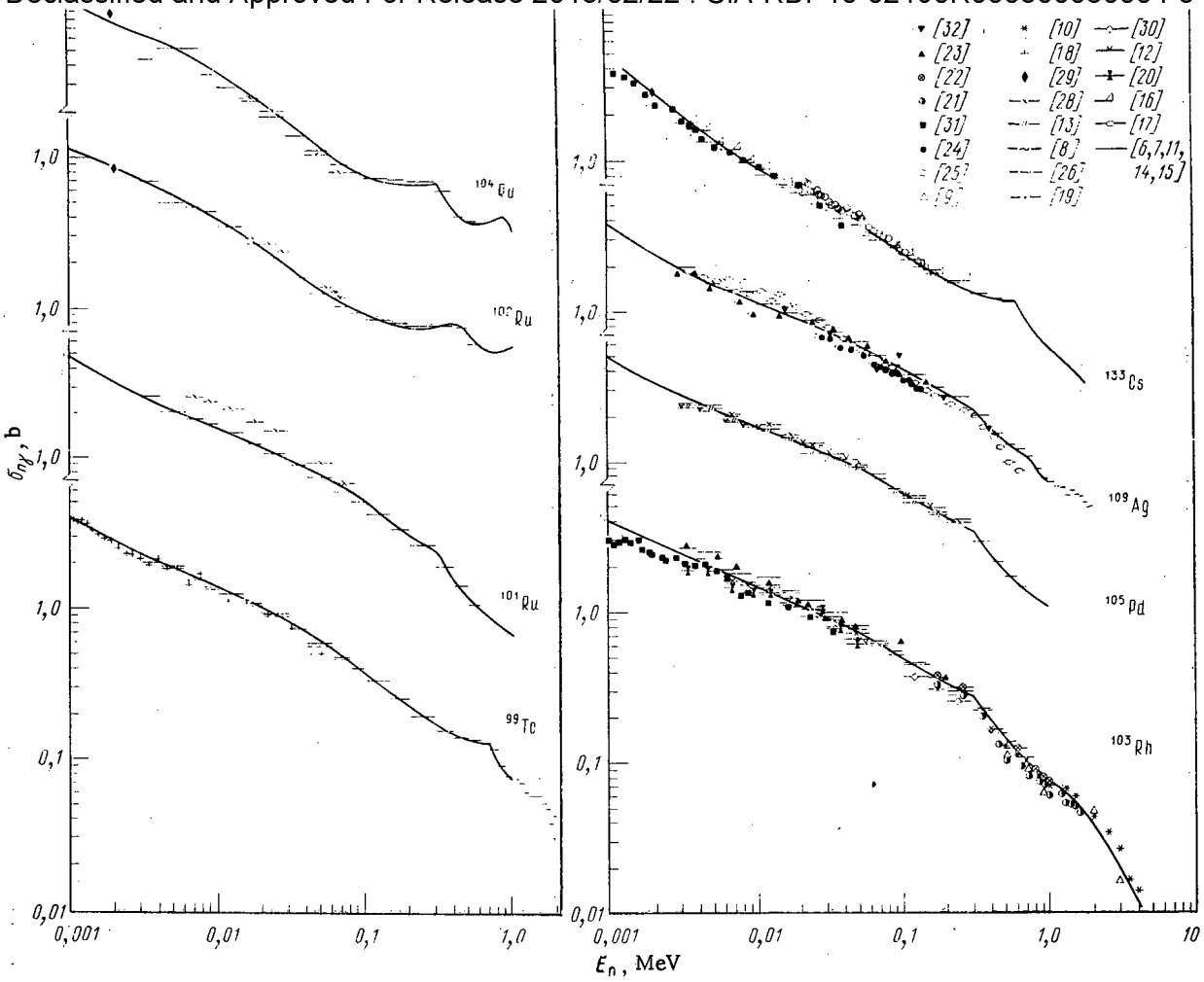

Fig. 1. Recommended curves of estimated neutron capture cross sections for fission products of the first group.

There are just two publications for the nuclides ^{101,102,104}Ru: Hockenbury [28] in the energy ranges 6.5-30 and 49-71.2 keV, and Macklin [7] in the energy range 3-700 keV; their values differ by 10-40%. Since there is no information in [28] on the sources of errors, the corrections, and the absolutization of the cross sections, we used only the data in [7] in estimating the cross sections.

^{101}Ru. The ENDF/B V values agree with Macklin's values [7] within 5-10%, but are systematically above them in the range 4-400 keV. The JENDL-1 and ENDF/B V estimates in the range 20-400 keV agree within 5%. The ENDF/B IV estimate lies below the JENDL-1 and ENDF/B V values by 15% and more. Our recommended curve corresponds to the experimental results in [7].

^{102}Ru. In the energy range 5-700 keV the ENDF/B V cross sections agree with the experimental data in [7] to within 5% on the average. Below 5 keV there is a sharp decrease of the cross section, which at 2 keV is ~30% below Schuman's value [29], and does not join with the resonance region. In view of this, we revised the cross section in the range below 5 keV, and took the ENDF/B V estimate above 5 keV.

^{104}Ru. We recommend the JENDL-1 estimate, which agrees better with Macklin's data [7] (the difference does not exceed 3-5% on the average).

^{103}Rh. As a result of the renormalization of the experimental data in [19-23] we made the following changes: Fricke's values [19] below 80 keV were decreased 10% on the average, Cox's values [21] were decreased 7-18%, the Diven data [22] were decreased 9%, and Weston's [23] by 14-18%. Above 60 keV the published data in [7, 9, 10, 21, 22, 23, 30] agree within 3-10%. Below 60 keV the data in [7, 33] exceed the values in [8, 19, 23, 30, 31] by 10-25% (within each group the agreement is 5-10%). In this energy range the ENDF/B V values agree

well. Above 40 keV the JENDL-1 and ENDF/B V estimates agree with one another and with the published experimental data to within 5-7%. The ENDF/B IV data are systematically lower by 7-10%. In the energy range from 40 to 1000 keV we took the ENDF/B V estimate. Below 40 keV there were not sufficiently strong reasons for preferring either of the two sets of data, and therefore our recommended capture cross section curve was drawn between them.

^{105}Pd. The published experimental data [11, 13, 33] agree within 5-8% on the average. Musgrove's results [13] are systematically lower than Macklin's values [11] by 7-12%. This difference disappears if the data of [13] are corrected by 11.3%, as justified by Macklin [11]. Macklin's values [11] and those of Cornelis [12] agree within 5% on the average. The JENDL-1 estimate is systematically below all the data by 7-20%. The ENDF/B V estimate below 40 keV and above 300 keV agrees with experiment within 5% on the average, but in the range 40-300 keV the values are 10-20% lower than those of Macklin [11] and Cornelis [12]. The ENDF/B IV values are systematically higher than those in ENDF/B V by 10% and more. Our recommended cross section curve is based on the optimum description of all the published experimental data.

^{109}Ag. The cross sections reported by Weston [23] an V. N. Kononov et al. [24] were renormalized: Weston's values were decreased by 30%, and those of Kononov et al., were increased by 10-34% in the range 30-170 keV. The data of [23, 24], renormalized to the new standards, agree with Macklin's results [14] and those of Mizumoto [17] to within 5-15%. The JENDL-1 values are higher than the data analyzed in [14, 17, 23, 24, 31], and the ENDF/B IV values pass through the unrenormalized data of Kononov et al. [24] and lie below Macklin's values [14]. In the 100-keV region the difference between them is more than a factor of two. The ENDF/B V values lie between them, but above Macklin's data [14]. Our recommended capture cross section curve passes through Macklin's data [14].

^{133}Cs. As a result of renormalization, the data of [25] were decreased by 3-10% in the energy range 10-170 keV, but remained on the average 25% above the remaining experimental data [15, 16, 29, 31], which agree with one another within 5-9%. The JENDL-1 values are well confirmed by these data, differing by no more than 5-10%, but the ENDF/B IV and ENDF/B V values are systematically higher. Preference was given to the JENDL-1 estimates.

The experimental data together with our recommended estimated curves for the nuclides discussed above are shown in Fig. 1.

Nuclides of the Second and Third Groups

Since there are no direct experimental data on the average neutron radiative capture cross sections of the nuclei of the second and third groups listed above, cross section estimates can be based only on theoretical calculations. For neutron energies up to ~50 keV the main contribution to the capture cross section comes from s and p neutrons. Since the neutron width corresponding to the elastic scattering channels in this region considerably exceeds the radiative width, and the inelastic scattering channels are still closed, the Hauser–Feshbach–Moldauer relations can be transformed into the simple approximate formula

$$\sigma_{n\gamma}(E_n) \approx \frac{2\pi^2 \lambda_n^2 \Gamma_\gamma}{(2I_0+1)D_0} \overline{F},$$

where λ_n is the neutron wavelength, I_0 is the spin of the target nucleus, Γ_γ is the average value of the radiative width, D_0 is the mean distance between neutron resonances, and F is the correction for the fluctuation of the width. It is clear from this formula that the capture cross sections are determined mainly by the radiation strength function or the ratio $\Gamma_\gamma/(2I_0 + 1)D_0$, whereas in the first approximation the energy dependence of the cross sections is due to the changes in wavelength of the incident neutron. A quantitative description of the capture cross sections is always better made by using relations of the statistical theory of nuclear reactions. It is important to keep in mind. However, that even in this case the calculated values will be determined largely by the assumed values of the radiation strength functions.

Table 2 lists the average values of the resonance parameters used in the ENDF/B IV and JENDL-1 estimates and recommended in later analyses of neutron resonances [34-39]. The main disagreements of the results of the analysis of the radiation strength functions as a rule are connected with the value of D_0. As a result of the development of new methods of determining D_0 which combine probabilistic estimates of missed resonances with direct experimental

TABLE 2. Average Resonance Parameters of Nuclides of the Second Group

Nucleus	Estimate	D_0, eV	Γ_γ, MeV	S_γ, 10^{-4}
^{107}Pd, $I_0=5/2$	ENDF/B IV	10,3	140	136
	JENDL-1	10,0	140	140
	Mughabghab [34]	15±3	125±13	93,3
	Bonifazzi [35]	11,3	125	110
^{129}I, $I_0=7/2$	ENDF/B IV	27,4	117	42,7
	JENDL-1	21,0	100	47,6
	Mughabghab [34]	40±9	(81) *	—
	Fort [36]	30±7	—	—
^{131}Xe, $I_0=3/2$	ENDF/B IV	58,5	117	20
	JENDL-1	33,2	114	34,3
	Mughabghab [34]	70±20	120±20	17,1
	Fröhner [37]	48±4	—	—
	Ribon [38]	58	113	23,1
^{147}Pm, $I_0=7/2$	ENDF/B IV	6,6	68	103
	JENDL-1	4,7	66	140
	Abagyan [39]	3,7	69	186
	Fort [36]	5,0±0,8	—	—
	Fröhner [37]	5,8±0,5	—	—

*Radiative width obtained only for negative resonance [34].

TABLE 3. Cross Sections for the Capture of 30-keV Neutrons by Nuclides of the Third Group

Nucleus	$\sigma_{n\gamma}$, mb	Neighboring nuclei whose cross sections were used
^{93}Zr	120	^{91}Zr·^{92}Zr/^{90}Zr
^{99}Mo	400	^{97}Mo (^{98}Mo/^{96}Mo + ^{100}Mo/^{98}Mo)/2
^{106}Ru	110	^{104}Ru·^{108}Pd/^{106}Pd
^{129}I	320	^{127}I·^{125}Te/^{123}Te
^{135}Cs	118	^{133}Ce (^{136}Ba + ^{135}Ba/^{137}Ba)/2
^{144}Ce	36	^{142}Ce·^{146}Nd/^{144}Nd

information on the number of observed resonances, we consider the results in [35-38] more reliable. Therefore, in calculating the neutron capture cross sections we used the resonance parameters of Bonifazzi et al. [35] for ^{107}Pd, the parameters of Ribon [38] for ^{131}Xe, and the values D_0 = 5.0 eV [36] and Γ_γ = 69 MeV [39] for ^{147}Pm. Our capture cross section curves are shown in Fig. 2a together with the JENDL-1 and ENDF/B V estimates. Since the errors in the determination of D_0 for ^{129}I are appreciable [34, 36], and the data on Γ_γ are not very reliable [34], it is expedient to consider this nuclide together with the fission products of the third group.

Since there are no experimental data on the capture cross sections and the radiation strength functions, the only possible method of estimation is a theoretical or empirical systematization of the existing data on neighboring nuclei. Figure 3 shows the dependences of the observed average 30-keV neutron capture cross sections and the resonance values of $\Gamma_\gamma/(2I_0 + 1)D_0$ on the number of neutrons in the target nucleus. The appreciable similarity of the isotopic dependences of the capture cross sections and the ratio $\Gamma_\gamma/(2I_0 + 1)D_0$ confirm the validity of the simple approximation formula given above. The isotopic dependences for the neighboring elements with the same parity of the number of nucleons are also similar. In the present state of the data this similarity can serve as the soundest criterion for estimating the capture cross sections of the third group of nuclides we are interested in.

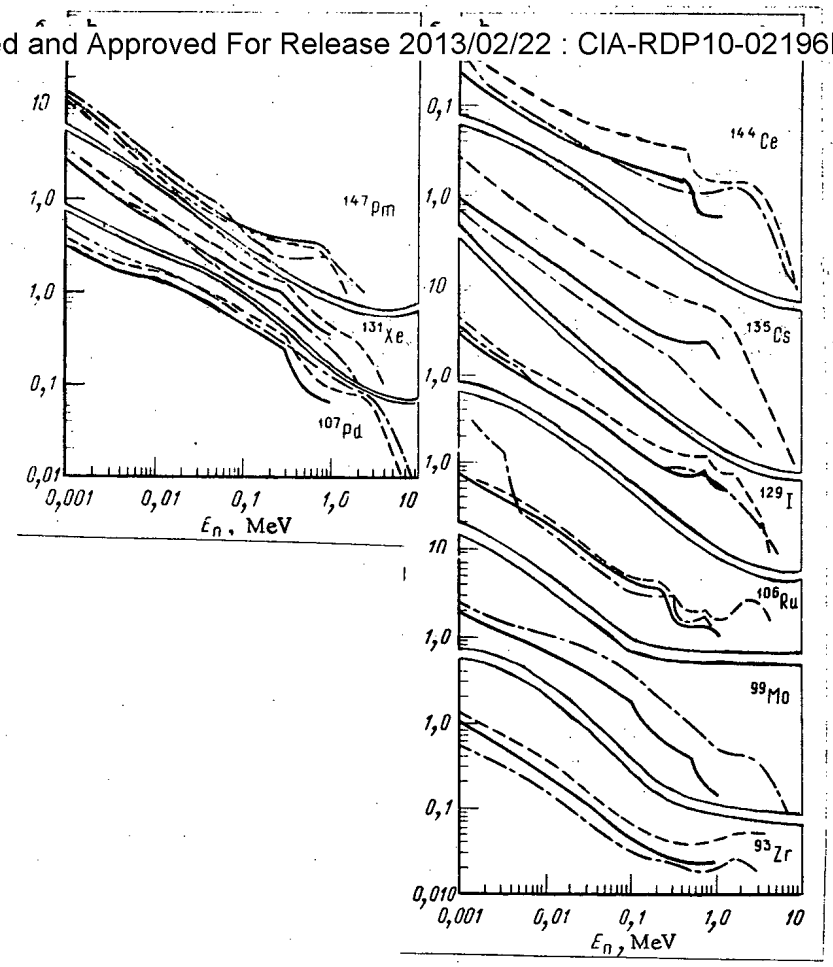

Fig. 2. Neutron capture cross sections for fission products of the a) second and b) third groups: ———) our estimate; -----) JENDL-1; —•—•—•—) ENDF/B V.

TABLE 4. Neutron Capture Cross Sections Averaged over the CFRMF Fast Reactor Spectrum.

Nucleus	Experiment		Estimate ENDF/B IV	Estimate JENDL-1	Estimate ENDF/B V	Our values	C/E*
	$\sigma_{n\gamma}$, b	Δσ, %					
^{99}Tc	0,267	15	0,278	0,333	0,320	0,348	1,31
^{102}Ru	0,0689	6,6	0,125	0,141	0,101	0,102	1,15
^{103}Rh	0,376	24	0,421	0,391	—	0,405	1,08
^{104}Ru	0,0826	6,3	0,0877	0,100	0,083	0,100†	1,21
^{109}Ag	0,507	9,7	0,306	0,544	0,450	0,408	0,80
^{129}I	0,184	6,6	0,233	0,276	0,196	0,208	1,14
^{133}Cs	0,276	6,6	0,302	0,292	0,285	0,292 †	1,06
^{141}Pr	0,073	15	0,102	0,0823	0,080	0,0848	1,16
^{147}Pm	0,641	13	0,777	0,743	—	0,743†	1,16
^{151}Eu	2,39	5,8	2,28	2,12	2,31	2,80	1,17
^{153}Eu	1,45	7,0	1,42	1,41	1,44	1,70‡	1,17

*Ratio of calculated to measured cross section.
†JENDL-1 estimate.
‡Estimate in [4] was used.

The results of such an empirical estimate of the capture cross sections are listed in Table 3. The cross sections obtained are also shown in Fig. 3 together with the ENDF/B V and JENDL-1 estimates. A comparison of the various estimates with the observed isotopic dependences of the capture cross sections shows that for most nuclides of the second and third

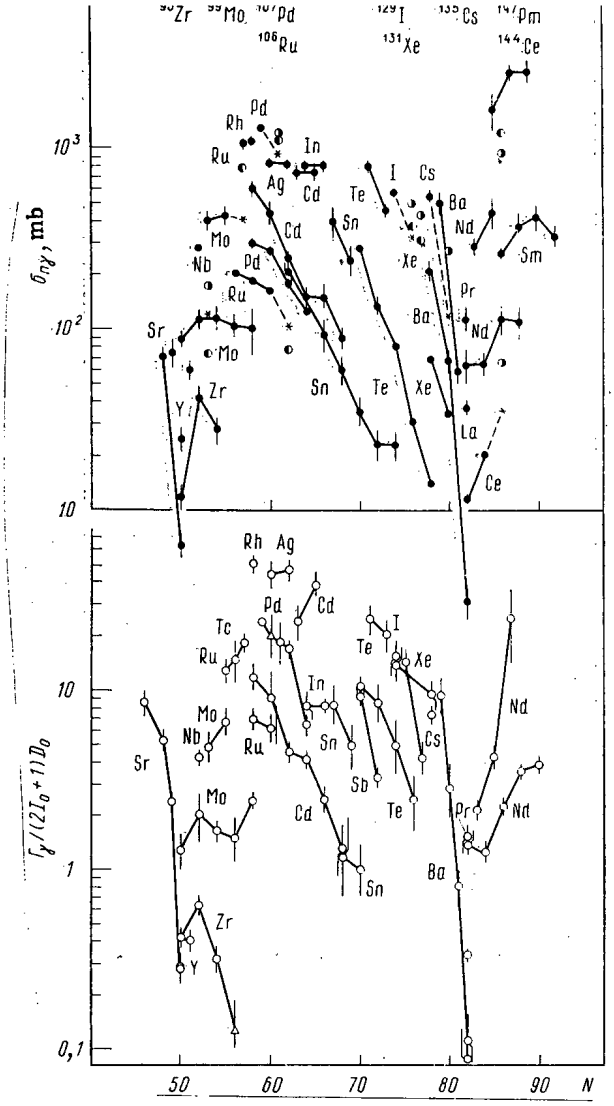

Fig. 3. ●) Systematics of isotopic dependences of 30-keV neutron capture cross sections; ○) resonance values of $\Gamma_\gamma/(2I_0 + 1)D_0$. Estimates for fission products of the second and third groups: ◑) JENDL-1: ◐) ENDF/B V; *) our values.

groups the JENDL-1 estimates represent the upper bound of the possible values of the capture cross sections, whereas the ENDF/B V values do not always underestimate them. The capture cross sections listed in Table 3 were used to normalize the theoretical calculations of the corresponding cross sections. The neutron capture cross sections in the energy range from 1 to 1000 keV obtained in this way are shown in Fig. 2b. It can be seen that the differences between our estimate and those of ENDF/B V and JENDL-1 over the whole energy range are due mainly to the differences in the estimates of the 30-keV neutron capture cross sections.

In the absence of experimental data it is difficult to give a well-substantiated determination of the error of the cross section estimates. On the basis of the spread of the estimated values, the systematic error of the capture cross sections is ~30% for fission products of the second group, and not less than 50% for the third group. These errors are much larger than the admissible errors (10-15%) of the estimates of the capture cross sections of fission product nuclei [40], and therefore it remains very urgent to perform experimental tests of the estimates for nuclides of the second and third groups.

Comparison of Estimates with Integral Values

The average cross sections for certain nuclides have been measured with the CFRMF reactor spectrum [41] (Table 4). Our values and the ENDF/B V estimates on the whole agree better

with experiment than the ENDF/B-IV and JENDL-1 values do. The experimental errors are 7-15%, and the calculated ~10-15%, and therefore the existing divergence lies within the limits of computational and experimental errors. One reason for the observed differences is the failure to take account of resonance self-shielding in either the experiment or calculation.

The rather large difference for ^{99}Tc should be noted. The latest experimental differential values for this isotope indicate an increase in the cross section [6], while the results of integral measurements show the opposite trend. For ^{109}Ag the integral values are inconsistent with the latest differential measurements [14], which caused a decrease of the cross section. Since the calculated value is lower than the experimental by ~20%, the introduction of the correction for resonance self-shielding increases the difference.

CONCLUSIONS

We have reevaluated the neutron capture cross sections of the most important fission products in the neutron energy range from 1 to 1000 keV, taking account of the most recent experimental data. We also used all the available earlier measurements, part of which we renormalized to contemporary standards. The consideration of all the data which agree within 5-10% ensures estimates of high reliability.

The analysis of the experimental data and the theoretical description of the cross sections using the method of maximum probability show that the current accuracy of the estimates of the neutron capture cross sections of fission products of the first group in the energy range from 1 to 1000 keV is 10-15%. Since this accuracy satisfies the requirements for the estimate of fission products [40], we recommend the inclusion of our results in the file of cross section values of the respective nuclei.

A correct comparison with integral data requires taking account of the effects of resonance self-shielding of the cross sections. A preliminary comparison with integral data shows that it is necessary to reconcile the differential and integral measurements of the ^{99}Tc and ^{109}Ag cross sections.

It is difficult to determine the errors of the recommended cross sections of fission products of the second and third groups, for which there is no direct experimental information on the average fast neutron capture cross sections. The possibility of an experimental test of the cross section estimates should be investigated. This question is particularly urgent for ^{107}Pd, ^{131}Xe, and ^{135}Cs, which belong to the first half of the list of the most important fission products.

LITERATURE CITED

1. Y. Kikuchi et al., JAERI-1268, Tokai (1981).
2. R. Schenter and T. England, in: Proc. Meeting on Neutron Cross Sections of Fission Product Nuclei, Bologna (1979), p. 253.
3. T. S. Belanova et al., in: Proc. Twelfth Int. Symp. on Neutron Physics, ZfK-491, Dresden (1982), p. 191.
4. B. D. Yurlov et al., Voprosy Atomnoi Nauki i Tekhniki, Ser. Yadernye Konstanty, No. 1(50), 25 (1983).
5. O. T. Grudzevich et al., [3, p. 194].
6. R. Macklin, Nucl. Sci. Eng., 81, 520 (1982).
7. R. Macklin et al., Nucl. Sci. Eng., 73, 174 (1980).
8. G. Reffo et al., ibid., 80, 630 (1982).
9. S. Joly et al., ibid., 70, 53 (1979).
10. W. Poenitz et al., [2, p. 85].
11. R. Macklin et al., Nucl. Sci. Eng., 78, 110 (1981).
12. E. Cornelis et al., in: Proc. Conf. on Neutron Phys. Antwerp (1982), p. 222.
13. A. Musgrove et al., in: Proc. Conf. on Neutron Phys., Harwell (1978), p. 449.
14. R. Macklin, Nucl. Sci. Eng., 82, 400 (1982).
15. R. Macklin, ibid., 81, 418 (1982).
16. N. Yamamuro et al., [2, p. 19].
17. M. Mizumoto et al., [12, p. 226].
18. C. Chou et al., J. Nucl. Energy, 27, 811 (1973).
19. M. Fricke et al., in: Nuclear Data for Reactors, Vol. 2, Vienna (1970), p. 265.
20. M. Moxon et al., Nucl. Instrum. Methods, 24, 445 (1963).
21. S. Cox, Phys. Rev., B-133, 378 (1964).

22. L. Weston et al., Ann. Phys., 10, 477 (1960).
23. V. N. Kononov et al., At. Energ., 19, No. 5, 457 (1965).
24. D. Kompe, Nucl. Phys., A133, 513 (1969).
25. R. Little et al., Trans. Am. Nucl. Soc., 26, 574 (1977).
26. R. Little et al., EXFOR-10671.002 (1977).
27. R. Hockenbury et al., Prog. Rep. ERDA-NDC, 3, 255 (1976); EXFOR-10552.002-004 (1978).
28. R. Schuman, Prog. Rep. WASH-1127 (1969), p. 72.
29. C. Rigoleur et al., in: Proc. Conf. on Neutron Cross Sections and Technology, Washington (1975), p. 953.
30. Yu. P. Popov et al., Zh. Eksp. Teor. Fiz., 15, 683 (1962).
31. G. Linenberg et al., Rep. LA-467, Los Alamos (1946); EXFOR-11945.004 (1976).
32. R. Hockenbury et al., [30, p. 305].
33. S. Mughabghab, M. Divadeenam, and N. Holden, Neutron Cross Sections, Vol. 1, Academic Press, New York (1981).
34. C. Bonifazzi, E. Menapace, and M. Vaccavi, ENEA-RT/FIMA (82)4, Bologna (1982).
35. E. Fort, H. Derrien, and D. Lafond, [2, p. 121].
36. F. Fröhner, [2, p. 145].
37. P. Ribon, in: IAEA Advisory Group Meeting on Nuclear Level Densities, INDC-092/L New York (1983), p. 245.
38. S. M. Zakharova et al., Library of Multigroup Absorption Cross Sections of Fission Products, Part 2, Promethium Isotopes [in Russian], OB-120, FEI, Obninsk (1981).
39. Status of the Capture Cross Sections for the Most Important Fission Product Nuclei, in: Proc. Meeting on Neutron Cross Sections of Fission Product Nuclei, Bologna (1979), p. 403.
40. Y. Harker and R. Anderl, ibid., p. 5.

ABSOLUTE MEASUREMENTS OF THE ^{239}Pu FISSION CROSS SECTION FOR 8.5-MeV NEUTRONS

R. Arlt, H. Bohn, W. Wagner, M. Josch, G. Musiol, H.-G. Ortlepp, G. Pausch, K. Herbach (GDR), I. D. Alkhazov, E. A. Ganza, L. V. Drapchinskii, V. N. Dushin, S. S. Kovalenko, O. I. Kostochkin, V. N. Kuz'min, K. A. Petrzhak, B. V. Rumyantsev, S. M. Solov'ev, P. S. Soloshenkov, A. V. Fomichev, and V. I. Shpakov (USSR)

UDC 539.173.4

Since ^{239}Pu is the basic fissionable isotope in fast breeder reactors, its fission cross section should be known within ±2% over a wide range of neutron energy. Although the published error of the latest estimate of this cross section [1] is ±3% in the neutron energy range up to 5 MeV, and 4-4.5% for higher energies, the current experimental data differ by 10% and more. The overwhelming majority of the experimental data on the ^{239}Pu fission cross section were obtained in measurements relative to the standard value of σ_f of ^{235}U, and absolute measurements have been performed in only a few cases [2-4].

As a result of the meeting at Smolenits from March 28 to April 1, 1983, the IAEA Conference on the Standard Value of σ_f for ^{235}U recommended the time-correlated associated-particle method (TCAPM) as the most promising way of increasing the accuracy of the fission cross section data. Such measurements have already been performed for ^{239}Pu using 14-15-MeV neutrons [5, 6]. We have measured the ^{239}Pu fission cross section for 8.5-MeV neutrons by this method. The measurements were the joint effort of the V. G. Khlopin Radium Institute (USSR) and the Dresden Technical Univeristy (GDR). The work was performed at the Tandem generator at the Central Institute of Nuclear Research in Rossendorf (GDR).

Translated from Atomnaya Énergiya, Vol. 57, No. 4, pp. 249-251, October, 1984. Original article submitted May 23, 1984.

 0038-531X/84/5704-0702$08.50

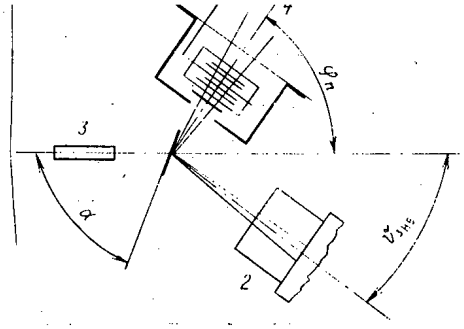

Fig. 1. Schematic diagram of experiment: 1) fission ionization chamber; 2) associated-particle channel telescope; 3) deuteron beam collimator; 4) neutron cone.

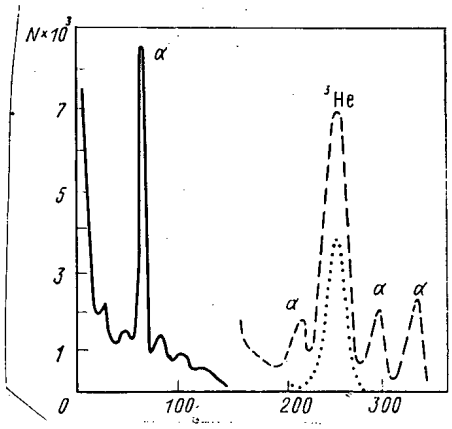

Fig. 2. Amplitude spectrum in the associated-particle channel.

Since the TCAPM was described in detail in [5], we dwell here only briefly on its principle. A schematic diagram of the experiment is shown in Fig. 1. The neutrons were produced in the reaction D(d, n)^{3}He by using 9-MeV deuterons. The associated helions were recorded by a detector at an angle of 42° with the deuteron beam. The neutrons emitted at an angle of 55° with the beam bombarded the ^{239}Pu target. Fission–associated-particle coincidences were recorded. The cross section was determined from the relation

$$\sigma_f = N_c/N_{He}n,$$

where N_{He} is the number of helions recorded, N_c is the number of coincidences, and n is the number of ^{239}Pu nuclei per cm^2 of the target.

The experimental data were corrected for: the background in the associated-particle channel, the background of random coincidences, the distortion of the neutron flux as a result of absorption and scattering by structural materials and target backings, and the efficiency of recording fissions.

The most difficult problem was the recording of the associated particles. The target of the tandem generator — the neutron source — was a deuterated polyethylene film 1-2 mg/cm^2 in thickness. The helions were recorded against the background of scattered deuterons and alpha particles from the (d, α) reaction on the carbon of the target. The spectrum in the associated-particle channel is shown in Fig. 2. The helions were recorded with a ΔE–E_r telescope of two completely depleted semiconductor detectors 10 and 40 μg/cm^2 in thickness. The two-dimensional spectrum in ΔE–E_r coordinates is shown in Fig. 3. The helions were separated by using a fast-acting analyzer with an analysis time of ~200 nsec [7]. The background in the associated-particle channel was determined by replacing the deuterated polyethylene by ordinary polyethylene. The background of random coincidences was found from an analysis of the fission–associated-particle time spectrum.

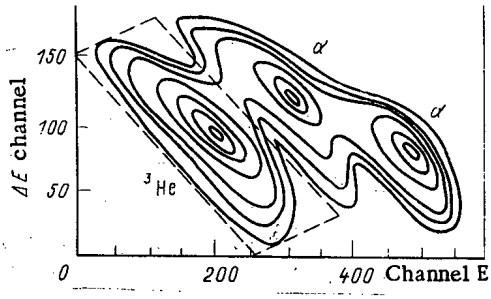

Fig. 3. Two-dimensional spectrum in ΔE–E_r coordinates in the associated-particle channel: -----) recorded part of spectrum.

TABLE 1. Corrections and Component Errors of the Result of Measuring σ_f of ^{239}Pu, %

Effect	Correction	Error
Statistics of coincidences	—	2,5
Random coincidences	3,01	0,5
Background in associated-particle channel	1,35	0,4
Extrapolation of fission fragment energy to zero	1,52	0,5
Absorption of fission fragments in layer	1,22	0,3
Neutron flux distortion	0,23	0,12
Uniformity of layer in targets	—	0,5
Total error of result	—	2,7

The distortion of the neutron flux was calculated by a method which is the inverse of the problem of the transport of neutron radiation. The transport equation was solved by the Monte Carlo method with modeling of the actual geometry of the experimental arrangement.

Fissions were recorded by an ionization chamber in 2π geometry. Four fissionable targets with a total density of 754.9 $\mu g/cm^2$ positioned in tandem were used in the experiments. The efficiency of counting fissions was computed by determining the absorption of fragments in the active layer of the targets, and the counting loss resulting from alpha particle discrimination. The absorption of fragments was calculated on the basis of the thickness of the target layers, taking account of the translational velocity due to the pulse of neutrons and the anisotropy of fission [8]. The counting losses resulting from discrimination were determined by analyzing the amplitude spectrum of the fission fragments. The values of the corrections introduced and the partial errors of the result are listed in Table 1.

The targets of isotopically pure fissionable material were prepared in the Radium Institute by sputtering onto a rotating backing. The number of nuclei in the target was determined by alpha counting in an arrangement with a small solid angle. The number of nuclei was calculated by using the value of the half-life $T_{1/2}$ = 24,110 ± 30 yr from [9]. The uniformity of the layers was determined by scanning the target surface of the alpha detector with a 1-mm-diameter diaphragm. The deviation from uniformity did not exceed 0.5-0.7%.

Statistical data for the 1670 events obtained in the measurements enabled us to achieve measurement errors less than 3%. Therefore, the result is preliminary. We propose to repeat the measurements in the future. Our value of 2.40 ± 0.07 b (1 b = 10^{-28} m^2) for the cross section is substantially different from the most recent estimate 2.28 ± 0.087 [1].

LITERATURE CITED

1. G. Antsipov et al., INDC (CCP)-166, IAEA, June (1981).
2. K. Kari and S. Cierjaks, in: Proc. Int. Conf. Neutron Physics and Nuclear Data, Harwell (1978), p. 905.
3. I. Szabo and J. Marquette, in: Proc. Spec. Meeting on Fast Fission Cross Sections, Argonne, ANL-76-90 (1976), p. 203.

4. [illegible], J. Nucl. Energy, 24, 671 (1970).
5. R. Arlt et al., in: Proc. Int. Conf. Nuclear Cross Sections for Technology, NBS Spec. Publ. 594, Washington (1980), p. 990.
6. M. Cance and G. Grenier, Nucl. Sci. Eng., 80, 282 (1982).
7. R. Arlt et al., Report ZfK-350, Dresden (1978), p. 209.
8. R. Arlt et al., Preprint 05-23-79, Dresden Technical University, Dresden (1979).
9. A. Lorenz, INDC (NDS)-121/NE, IAEA, December (1980).

MEASUREMENT OF THE α VALUE AT ^{235}U RESONANCES

Yu. V. Adamchuk, M. A. Voskanyan,
G. V. Muradyan, P. Yu. Simonov,
and Yu. G. Shchepkin

UDC 539.172.4.162.2

Formulation of the Problem. The ratio α of the capture cross section of neutrons to the fission cross section of ^{235}U is one of the basic constants used in the design of nuclear reactors. The ratio must be determined with an error of less than 5% in a wide range of neutron energies. But the available information on the α value does not satisfy the accuracy requirements.

The errors in the measurement of α have two main reasons: 1) methodological difficulties of uniquely separating neutron capture events from the background of fission events and capture events of scattered neutrons and fission neutrons in the structural materials; and 2) errors in the determination of the parameters of the setup, which relate the experimentally measured spectra with the α value, i.e., errors in the calibration.

A number of known α values (calibration values) are used for calibration in some neutron-energy range which overlaps with the range of the measurements. The precision in the determination of α depends greatly upon both the position and the variability range of the α values of the calibration. One usually employs α values of the thermal energy range of the neutrons for calibration; in this range, the absolute value of the parameter is known with great precision. But the calibration values of α do not provide the high accuracy required at the present time because the variability range of α is not broad enough in the case of thermal neutrons and difficulties are encountered in the determination of the background level at these neutron energies.

The goal of our work was to obtain absolute calibration values of α at resonances of ^{235}U. The resonance range is advantageously distinguished from the thermal range by the fact that the α values at the resonances change in a greater variability range from 0.08 to approximately 8, and the resonances proper can be separated from the background, i.e., in the case of the resonances, the background influences the precision of the measurements to a lesser degree.

The measurements were based on the spectrometry of the multiplicity of the radiation from excited nuclei [1-3]. The method made it possible to distinguish with high accuracy between capture events and fission events, to substantially reduce the background of the scattered neutrons and the fission neutrons, and, owing to the almost 100% recording efficiency, to obtain in the resonance region absolute α values without employing additional calibration values. The error made in the determination of α amounted to at most 2% in the majority of resonances. In addition to the improved calibration data, our work made it possible to verify the various methods of measuring α, which were used in the energy range including the resonances. More specifically, it is interesting to compare the results of our work with the results of the Oak Ridge Laboratory [4] because the data of the preceding α measurements which were made in the I. V. Kurchatov Institute of Atomic Energy on ^{235}U by spectrometry of the multiplicity [3] at 0.1-10 keV were systematically below the results given in [4].

Details of the Measurements and of the Resonance Range. In the present work, as in [3], the spectrometry of the multiplicity was employed. But a transition into resolved resonances

Translated from Atomnaya Énergiya, Vol. 57, No. 4, pp. 251-257, October, 1984. Original article submitted January 18, 1984.

0038-531X/84/5704-0705$08.50

(E_n ch sufficed for shielding from scattered neutrons. As a consequence, the absorption in the converter of the γ quanta leaving the sample could be substantially reduced. This helped to improve the separation of capture events from fission events. The efficiency of recording interactions of neutrons with nuclei increased and reached almost 100%. The high efficiency made it possible to obtain absolute α values without using calibration values and to exclude the background resulting from fission products, i.e., the fission neutrons and the emission from fission fragments. The background could be eliminated by shutting off the electronic equipment of the detector after each recording of an interaction. The level of the remaining background was determined from the region near a resonance and eliminated by subtracting the "uranium substrate." Part of the useful events can be assumed as background because in regions neighboring a resonance, the neutron cross sections are small but nonvanishing. When the background is taken into account in this way, the α value obtained differs to some extent from the true α value. Therefore, when the values indicated were used for calibration (or for comparison with the results of other authors), an operation which is the analog of the subtraction of the "noise base" must be made in the calibrated (or compared) data within the same energy limits.

Let us note that our measurements were made with a new spectrometer of the multiplicity, which guaranteed high reliability of the results. The spectrometer volume (~200 liters), was about two times greater than the volume of the spectrometer used in [3]. The volume of the detector sections was also increased and the mutual shielding of the sections was reduced. In this way, the efficiency of recording γ quanta was increased and the number of efficiently working sections was raised.

Method and Measurements. The measurements were made on the 26-m flight base of the Linear Electron Accelerator of the I. V. Kurchatov Institute of Atomic Energy; a 48-section scintillation detector (48SSD) with the NaI(Tl) crystal and a ^{10}B converter with a thickness of ~0.3 g/cm^2 was used (Fig.1). The detector sections consisted of individual blocks in the form of rectangular parallelepipeds. The central part of the detector consisted of crystals with a size of 300 × 132 × 132 mm; the detector faces were composed of crystals with a size of 150 × 132 × 132 mm. The smallest thickness of the scintillator in the direction of the gamma quanta leaving the sample was ~13 cm; the geometrical efficiency of the detector was ~98%. The total scintillator volume was ~200 liters. The inner detector cavity had a size of 40 × 40 × 45 cm. The detector was shielded on its outside with ~150-mm-thick boron carbide and with 100-200-mm-thick lead layers.

An electron pulse of the accelerator had a duration of 100 nsec; the pulse frequency was 270 Hz. Filters of cadmium (1 mm thick), aluminum (16 mm thick), and lead (5 mm thick) were placed on the path of the beam. The ^{235}U sample under inspection was placed in the center of the converter. In order to reduce the absorption of γ quanta in the sample, the sample was given the form of six identical disks with a diameter of 29 mm and a thickness of 0.06 g/cm^2; the spacing of the disks was 1 cm. The amount of material in the converter and the sample cassette was minimized.

Each of the detector sections was viewed with an FEU-110 photomultiplier. The photomultiplier signal was split into two channels. In the first channel, the signal passed through an integral discriminator, was shaped to a standard pulse with a length of 0.3 μsec, and was applied to an encoder of the multiplicity of coincidences. In the second channel, the photomultiplier signal was applied to a summing stage wherein the amplitudes of the pulses of all detector sections were linearly superimposed. The output pulse of the summing stage was applied to four integral discriminators ID_j (j = 1, 2, 3, 4) at which discrimination levels corresponding to the energy liberation E_j^{Σ} within the entire detector volume were adjusted to 0.6, 0.8, 1.1, and 1.5 MeV. A 0.6-μsec-long strobing pulse from the first discriminator was applied to the input of the encoder of the frequency of coincidences. During this pulse, pulses from the integral discriminator of the detector sections could be received. The coding pulse generated by the encoder of the frequency of coincidences and the pulse of the discriminators ID_j of the summing stage were applied to a time encoder and a computer. A time channel had a width of 160 nsec; 32,767 channels were available.

As a result of the measurements in each time channel (interval) i corresponding to a certain neutron energy, four groups (j = 1-4) of spectra of the frequency of coincidences of 1-15 events were stored in the computer under the condition that the energy dissipation in the entire detector volume had exceeded 0.6, 0.8, 1.1, or 1.5 MeV. A coincidence frequency above

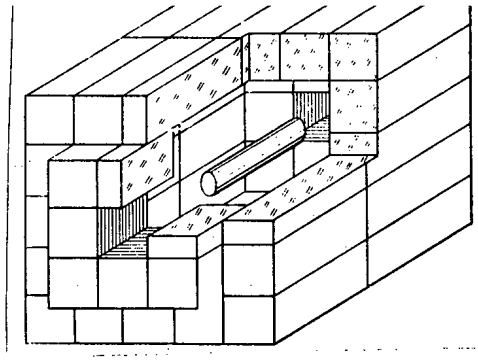

Fig. 1. 4π scintillation detector consisting of 48 sections.

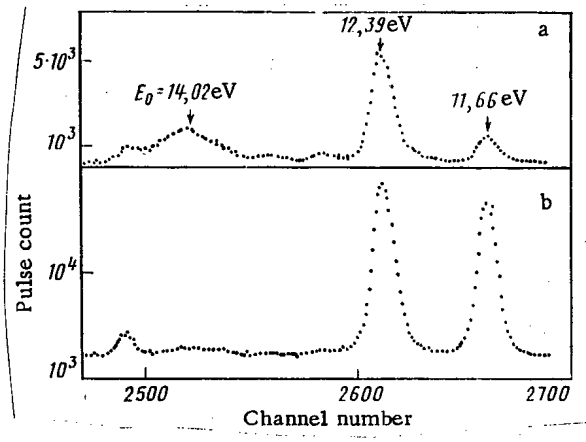

Fig. 2. Time-of-flight spectra in measurements involving ^{235}U for the coincidence multiplicities k = 10 (a) and k = 4 (b).

15 was accumulated in a 16th spectrum. The energy discrimination threshold in each section was kept as low as possible and amounted to ~25 keV. The four groups of spectra were simultaneously measured. After each event recorded, the detector equipment was shut off for 50 μsec (to preclude the recording of the background produced by fragments). Counting losses were taken into account with the aid of a random pulse generator. The generator pulses were passed through the entire electronic system of the detector along with the pulses from the detector sections.

The following measurements were made in the investigations: 1) a multidimensional spectrum $N_j(i, k)$ of the flight time and the frequency of coincidences of gamma quantum recordings in the detector sections were simultaneously measured at four discrimination thresholds E_j^{Σ} (j = 1, 2, 3, 4) via the total energy dissipation in the entire 48SSD volume in interactions of neutrons with ^{235}U nuclei; 2) the spectra of the multiplicity of gamma quanta in the spontaneous fission of ^{252}Cf were measured with the same discrimination thresholds E_j^{Σ}; 3) the absolute number of decays of ^{137}Cs and ^{60}Co sources were measured with a detector having a 100% efficiency; this detector was assembled from the same units as the 48SSD but had a minimum thickness of 26 cm in the direction of the gamma quantum flight path; and 4) the dependence of the number of counts of the 48SSD upon the discrimination threshold E_j^{Σ} was determined with ^{137}Cs, ^{60}Co, and ^{252}Cf sources.

Evaluation of the Measurement Data. In the spectrometry of the multiplicity, each of the interactions of a neutron with a nucleus is recorded as a function of the number of particles emitted in a particular channel of the spectrum of the frequency of coincidences (i.e., in a certain multiplicity). Fission results, on the average, in the emission of ~9 gamma quanta and neutrons, whereas radiative capture causes the emission of ~4 gamma quanta. Therefore, the distributions f(k) of fission event recordings and γ(k) of capture recordings over the multiplicity of the events must differ strongly (for the sake of simplicity, we term the functions f(k) and γ(k) the forms of fission and capture, respectively). For example, at

multiplicities $k \geq 5$ capture events must be predominantly recorded, whereas fission events must occur mainly at multiplicities $k \geq 7$.

The functions $f(k)$ and $\gamma(k)$ do not coincide with the spectrum of the multiplicity of the particles emitted because several gamma quanta can be incident on a single detector section or, conversely, one gamma quantum can be recorded in several detector sections. The greater the differences between the forms $f(k)$ and $\gamma(k)$, the easier the separation of fission events from capture events and, hence, the greater the accuracy with which α can be determined. The precision with which fission events can be separated from capture events depends in many ways upon the number of sections, the detector volume, the efficiency of recording γ quanta, and several other parameters of the spectrometer of the multiplicity.

In order to illustrate the possibilities of the spectrometer of the multiplicity, the time-of-flight spectra for the multiplicities $k = 4$ and $k = 10$ are shown in Fig. 2. Excellent separation of capture events from fission events is clearly visible. For example, the areas of the resonances at $E_0 = 11.66$ eV ($\alpha \approx 8.7$) and $E_0 = 12.39$ eV ($\alpha \approx 1.6$) are about the same in the spectrum for $k = 4$, whereas the area of the resonance with $\alpha = 8.7$ is about 5 times smaller than in the spectrum with $k = 10$. Resonances with small α values appear more clearly in the spectrum with $k = 10$ than in the spectrum with $k = 4$. The resonance at $E_0 = 14.02$ eV ($\alpha \approx 0.1$) can serve as an example.

We selected for evaluation 15 resonances which were well separated on the energy scale. In the determination of the absolute α value (which we will denote by α_0), the numbers Γ^l and F^l of the capture events and fission events recorded, respectively, must be known for the l-th resonance; in addition, the recording efficiency of capture events (ε_γ) and fission (ε_f) must be known. As indicated above, the measurements were made at four threshold values of the discrimination with respect to the total energy liberated in the detector. When the threshold was increased, the efficiency decreased, and therefore in general

$$\alpha_0^l = \frac{\varepsilon_{fj}}{\varepsilon_{\gamma j}} \frac{\Gamma_j^l}{F_j^l}, \tag{1}$$

where $j = 1, 2, 3, 4$ denotes the number of the discrimination threshold.

Since $\gamma(k)$ and $f(k)$ overlap, an additional processing of the spectra is required for the determination of Γ_j^l and F_j^l. Assume that $N_j^l(k)$ events of neutron interactions with nuclei are recorded with multiplicity k of the l-th resonance at the j-th discrimination threshold. The number $N_j^l(k)$ can be easily obtained from the experimental spectra by determining the area under a resonance and subtracting the background. In the general case, both $F_j^l(k)$ fission events and $\Gamma_j^l(k)$ capture events are recorded with multiplicity k.

We use the concept of forms and set

$$\begin{aligned} \Gamma_j^l(k) &= \Gamma_j^l \gamma_j(k); \\ \Gamma_j^l(k) &= F_j^l f_j(k), \end{aligned} \tag{2}$$

where

$$N_j^l(k) = \Gamma_j^l \gamma_j(k) + F_j^l f_j(k). \tag{3}$$

The problem is therefore reduced to the determination of Γ_j^l and F_j^l from an experimental $N_j^l(k)$ value. It is also known that the forms $\gamma_j(k)$ and $f_j(k)$ are the same for all resonances (some dependence of the form of the capture upon the spin of a level will be considered below). As will be shown below, at multiplicities $k \geq 10$ capture events are not recorded, i.e., $\gamma(k) = 0$ for all $k \geq 10$. This means that

$$\sum_{k \geqslant 10} N_j^l(k) = F_j^l \sum_{k \geqslant 10} f_j(k) \tag{4}$$

and, hence,

$$F_j^{(l)} = \frac{\sum_{k \geqslant 10} N_j^l(k)}{\sum_{k \geqslant 10} f_j(k)}. \tag{5}$$

$\sum_{k\geq m} N^{(2)}$ upon the Limits of Summation

m	$\sum_{k\geq m} N^{(1)} / \sum_{k\geq m} N^{(2)}$	m	$\sum_{k\geq m} N^{(1)} / \sum_{k\geq m} N^{(2)}$
1	0,37	8	0,08
2	0,37	9	0,07
3	0,34	10	0,06
4	0,29	11	0,06
5	0,22	12	0,06
6	0,15	13	0,06
7	0,10	16	0,06

The Γ_j^l value can be calculated with Eq. (3) in any given interval between k_1 and k_2:

$$\Gamma_j^l = \frac{1}{\sum_{k=k_1}^{k_2} \gamma(k)} \left[\sum_{k=k_1}^{k_2} N_j^l(k) - F_j^l \sum_{k=k_1}^{k_2} f(k) \right]. \tag{6}$$

When the Γ_j^l are calculated, the first multiplicity is conveniently omitted (i.e., $k_1 = 2$ is assumed) because the main part of the background events and only 3% of the total effect are concentrated in the first multiplicity. The k_1 value was assumed equal to 6 because only 8% of all capture events and the major part of the fission events (>80%) are recorded at $k > 6$.

Let us show that Eq. (5) holds, i.e., that really only fission events are recorded at multiplicities $k \geq 10$. Let us consider the two resonances $l = 1$ and $l = 2$. We form the ratio $\sum_{k\geq m} N^1(k) / \sum_{k\geq m} N^2(k)$ and analyze how it changes with a variation of the limits of summation ($m = 1, 2, \ldots$). We omit the subscript j and indicate the values obtained for $j = 1$; the spectra for all thresholds E_j^{Σ} are treated in the same way. The results are listed in Table 1 for the resonances with $E_0^{(1)} = 11.66$ eV and $E_0^{(2)} = 8.78$ eV.

We use Eq. (3) and write

$$\frac{\sum_{k\geq m} N^{(1)}(k)}{\sum_{k\geq m} N^{(2)}(k)} = \frac{\Gamma^{(1)} \sum_{k\geq m} \gamma(k) + F^{(1)} \sum_{k\geq m} f(k)}{\Gamma^{(2)} \sum_{k\geq m} \gamma(k) + F^{(2)} \sum_{k\geq m} f(k)}.$$

It follows from Table 1 that the ratio no longer changes for $k > 9$. Since the forms $\gamma(k)$ and $f(k)$ differ and since fission is recorded with greater probability at high multiplicities, the behavior of the ratio can be explained only by a lack of fission-event reeordings at $k \geq 10$, i.e., we have $\gamma(k) = 0$ for $k \geq 10$. This had to be shown.

We term the range with $k \geq 10$ the range of "pure fission." It is then easy to determine the ratio of the fission events recorded at the two resonances:

$$\frac{F^{(1)}}{F^{(2)}} = \frac{\sum_{k\geq 10} N^{(1)}(k)}{\sum_{k\geq 10} N^{(2)}(k)}. \tag{7}$$

One must know $\gamma(k)$ and $f(k)$ for determining F^l and Γ^l from Eqs. (5) and (6). For determining these quantities, two resonances with different α values are employed. We write down Eq. (3) for these resonances:

$$N^{(1)}(k) = \Gamma^{(1)}\gamma(k) + F^{(1)}f(k);$$
$$N^{(2)}(k) = \Gamma^{(2)}\gamma(k) + F^{(2)}f(k).$$

By multiplying the second of these equations with the coefficient $\nu = \Gamma^{(1)}/\Gamma^{(2)}$ and subtracting the result from the first equation, we obtain

$$N^{(1)}(k) - \nu N^{(2)}(k) = (F^{(1)} - \nu F^{(2)})\, f(k)$$

After summation over all multiplicities and taking into account that $\sum_{k=1}^{\infty} f(k) = 1$, we obtain

$$F^{(1)} - \nu F^{(2)} = \sum_{k=1}^{\infty} [N^{(1)}(k) - \nu N^{(2)}(k)].$$

It follows from the last two equations that

$$f(k) = \frac{N(k) - \nu N^{(2)}(k)}{\sum_{k=1}^{\infty} [N^{(1)}(k) - \nu N^{(2)}(k)]}. \tag{8}$$

Similarly, by multiplying the formula for $N^{(2)}(k)$ with the coefficient $\beta = F^{(1)}/F^{(2)}$ and taking into account that $\sum_{k=1}^{9} \gamma(k) = 1$, we obtain

$$\gamma(k) = \frac{N^{(1)}(k) - \beta N^{(2)}(k)}{\sum_{k=1}^{9} [N^{(1)}(k) - \beta N^{(2)}(k)]}. \tag{9}$$

The coefficient β can be easily determined from the region of "pure fission" (see Eq.(7)).

The coefficient β cannot be determined in analogy because a region of pure capture does not exist. However, the spectrum of the multiplicity comprises a region in which mainly capture events are recorded. For example, for multiplicities $k \leq 3$, only 3% of all fission events are recorded. The existence of such a region makes it possible to determine with adequate precision f(k) for the entire range $k \geq 1$ on the basis of an approximation of the contribution to fission. For this purpose, additional measurements of the spectrum of the multiplicity in the spontaneous fission of ^{252}Cf were made. The goal of the measurements was to determine those values characterizing the form f(k) which depend only slightly upon the uncertainty of our knowledge of f(k) and which at the same time make it possible to determine ν with rather high accuracy. As will be shown below, the ratio $f(5)/[f(4) + f(3)] \equiv \mu$ can be used for this purpose.

In order to exclude the background of radioactive fragments in measurements involving ^{252}Cf, the "time gates" for the coincidence counting were "opened" through the pulse of a semiconductor detector which recorded fission fragments and was mounted, along with a thin ^{252}Cf layer, in the center of the 48SSD unit.

Various forms f(k) of the spontaneous fission of ^{252}Cf were obtained for analyzing the change of μ. The forms were changed by changing the experimental conditions: the number of sections used, the width of the time gates, and the trigger threshold of the semiconductor detector. It was observed that at a given position of the maximum of f(k), only a small change of at most 4% occurs in μ. The explanation is that the form of the curve f(k) at $k \leq 4$ is given by events with high multiplicity of the gamma quanta and by the incidence of particles on a single section. Therefore, the relative form of the curve at low multiplicities is in many ways predetermined by the position of the maximum. Thus, we may assume that for a certain position of the maxima of the forms of uranium and californium fission, the ratios f(5)/[f(4) + f(3)] are almost identical for the nuclei of these elements.

The corresponding μ value can be easily determined once the position of the maximum of the form of the ^{235}U fission has been determined on the base of the total multiplicity pattern. The ratio $\mu = f(f)/[f(4) + f(3)]$ allows us to take into account the contribution of fission at small multiplicities and to determine the coefficient $\nu = \Gamma^{(1)}/\Gamma^{(2)}$. We obtain with Eq. (3) for ν

$$\nu = \frac{\mu [N^{(1)}(3) + N^{(1)}(4)] - N^{(1)}(5)}{\mu [N^{(2)}(3) + N^{(2)}(4)] - N^{2}(5)}.$$

Exc[illegible] $\nu_1(k)$ of the fission can be determined with Eq.(8) when ν is known.

The forms of fission, which were obtained in the evaluation of various pairs of levels, coincided with high accuracy. The forms $\gamma(k)$ of capture coincide only for levels with identical spin. The forms of fission and capture are listed in Table 2 and were calculated for the pair of levels $E_0^{(1)} = 11.66$ eV and $E_0^{(2)} = 8.78$ eV with the spin $J = 4$; Table 2 includes the form $\gamma(k)$ determined for the pair $E_0^{(1)} = 12.39$ eV and $E_0^{(2)} = 18.05$ eV with the spin $J = 3$. These forms correspond to the threshold of discrimination for a total energy liberation of 0.6 MeV in the detector.

The forms $\gamma_j(k)$ and $f_j(k)$ were obtained with this method at all discrimination thresholds E_j^{Σ} ($j = 1, 2, 3, 4$). Equations (5) and (6) were used to determine the numbers F_j^{ζ} of fission events recorded and Γ_j^{ζ} of capture events recorded in each of the resonances under consideration. Thus, the recording efficiencies ε_{fj} and $\varepsilon_{\gamma j}$ for fission events and capture events, respectively, had still to be determined for calculating the absolute α values with Eq. (1) at the resonances. We constructed for this purpose for each of the resonances the dependence of the numbers Γ_j and F_j upon the discrimination threshold E_j^{Σ}. By extrapolating the curves to the discrimination threshold zero ($E_0^{\Sigma} = 0$ MeV), we calculated the absolute numbers Γ_0 and F_0 of capture events and fission events. When Γ_0 and F_0 are known, the efficiency of recording $\varepsilon_{\gamma j} = \Gamma_j/\Gamma_0$ or $\varepsilon_{fj} = F_j/F_0$ can be easily determined at each discrimination threshold. In order to show the validity of the determination of the absolute Γ_0 and F_0 values by extrapolation of the Γ and F dependencies upon E^{Σ}, we measured the dependence of the 48SSD count upon the discrimination threshold via the total energy liberation in the detector in the case of radioactive ^{137}Cs and ^{60}Co sources with known source intensities. The intensities of the ^{137}Cs and ^{60}Co sources were determined with the same 4π detector in which a small channel with a cross section of 1×0.5 cm was provided for introducing a source. The smallest thickness of the crystals for γ quanta was ~26 cm. In the case of ^{60}Co, the extrapolation to count zero of the 48SSD from the discrimination level rendered a value which coincided with the intensity of the source. This confirms the validity of the determination of Γ_0 and F_0 in the case of ^{235}U because in the case of neutron capture in ^{235}U (and even more in the case of fission), the multiplicity of the gamma radiation and its total energy are greater than in the ^{60}Co decay. The values which we found for the efficiencies $\varepsilon_{\gamma j}$ and ε_{fj} are shown in Fig. 3 in the form of curves. We have for the first discrimination thresholds $E_1^{\Sigma} = 0.6$ MeV the values $\varepsilon_{\gamma j} = (96.8 \pm 0.6)\%$ and $\varepsilon_{fj} = (99.76 \pm 0.1)\%$.

TABLE 2. Forms of Fission and Capture in Dependence upon the Multiplicity

Parameter	k															
	1	2	3	4	5	6	7	8	9	10	11	12	13	14	15	16
$f_1(k)$, %	0,02	0,53	1,47	3,30	5,63	8,02	9,92	11,03	11,20	10,53	9,26	7,75	6,16	4,69	3,47	7,00
$\gamma_1(k)$, % ($J=4$)	2,68	10,95	21,28	25,00	20,24	11,89	5,37	1,95	0,64	—	—	—	—	—	—	—
$\gamma_1(k)$, % ($J=3$)	1,52	11,80	22,15	25,34	19,66	11,34	5,08	2,24	0,87	—	—	—	—	—	—	—

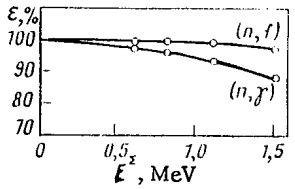

Fig. 3. Dependence of the recording efficiency ε_γ of capture events and the recording efficiency ε_f of fission events upon the discrimination threshold E_j^{Σ}.

ing Δt = 10 μsec in Dependence upon the Delay Time t_{del}

t_{del} (μsec)	$N(t_{del})\,10^3$	t_{del}, (μsec)	$N(t_{del})\,10^3$
0,6	203	70	6,8
10	13,6	90	7,5
20	9,3	120	6,8
30	8,4	140	7,3
40	8,1	160	6,7
50	7,7	180	7,5
60	7,7	190	7,4

Thus, the above-described method of evaluating the experimental spectra $N_j(k)$ of the multiplicity allows the separation of recorded fission events and capture events, i.e., it is possible to determine F_j and Γ_j and also the recording efficiencies ε_{fj} and $\varepsilon_{\gamma j}$ of these processes.

The absolute α values were determined with Eq. (1). Since the recording efficiency of fission events and capture events in the 48SSD spectrometer is high, $\varepsilon_{\gamma j}$ and ε_{fj} depend only slightly upon E^{Σ} (see Fig. 3) and therefore an extrapolation for the determination of Γ_0 and F_0 is possible. A high recording efficiency is also important for excluding the activity of the fission products from being recorded. As indicated, this type of background can be excluded by shutting off the equipment for a time t_{block} = 50 μsec with the aid of a pulse produced by each event recorded. Obviously, the higher the efficiency ε_f, the smaller the probability of recording the radioactive radiation of fragments. The "aftereffect" time of a fission was determined for the proper selection of t_{block}. We measured for this purpose the count of delayed coincidences of 48SSD pulses and semiconductor-detector pulses produced by fission fragments in the "time window" Δt = 10 μsec in the spontaneous fission of ^{252}Cf. The delay time t_{del} of the pulse generated in the detector of the fission fragments was varied. The count $N(t_{del})$ of the delayed coincidences in the 10-μsec window is listed in Table 3 reduced to one fission event.

It follows from Table 3 that the count of the coincidences hardly changes at delays exceeding 50 μsec. This means that the aftereffect of a fission has disappeared 50 μsec after a fission event. The constant count at t_{del} > 50 μsec resulted from the background of random coincidences. Owing to the high efficiency in the fission, the error resulting in the α value from the background of the fission products amounted to at most 0.015% according to our estimates. When no shutoff was introduced in the case t_{del} > 50 μsec after a fission event, the aftereffect of the fission, if such an effect exists at all, is extremely small and, owing to its slow development, it was subtracted along with the "background base."

Results. The absolute α values obtained for 15 resonances are listed in Table 4. Table 4 includes the energy intervals in which the average values of the effect and the background were determined. The background was determined from two regions in the case of certain resonances (3rd and 4th columns of Table 4). The systematic error, which is included in the total error, accounts for the error in the determination of μ_j and also for the errors of the efficiencies ε_γ and ε_f. As indicated above, the errors amount to $\Delta\mu/\mu \approx 4\%$, $\Delta\varepsilon_\gamma/\varepsilon_\gamma \approx 0.6\%$, and $\Delta\varepsilon_f/\varepsilon_f \approx 0.1\%$.

The relation between $\Delta\mu$ and $\Delta\alpha$ was expressed as follows:

$$\frac{\Delta\alpha}{\alpha}=\frac{\alpha+1}{\alpha}\,\frac{f(3)+f(4)}{\gamma(5)-\mu[\gamma(3)+\gamma(4)]}\,\Delta\mu=0.0069\,\frac{\alpha+1}{\alpha}\,\Delta\mu.$$

It follows from Table 4 that the accuracy of the α values obtained is high. The error amounts to at most 2% for many levels. The smallest absolute error is $\Delta\alpha$ = 0.01. The small error and the large variability range of α at these resonances make it possible to calibrate with about the same accuracy the α values obtained from the measurements of the relative form of this parameter. Moreover, the wide variability range of α makes it possible to perform this calibration with any unique (not only linear) relation between the characteristics measured in the experiment and the α value.

TABLE 4. α Values at Several Resonances of ^{235}U

E_0, eV	Limits (eV) of the effect	Limits (eV) of background-1	Limits (eV) of background-2	Our work	Ref. [4]
3,61	3,509–3,720	4,144–4,274	2,299–2,352	0,732	–
4,85	4,754–4,945	4,242–4,403	–	8,262	–
6,39	6,287–6,507	7,857–7,928	6,689–6,802	3,033	3,64
7,08	6,957–7,213	7,857–7,928	–	1,188	1,44
8,78	8,609–8,982	7,618–7,928	–	0,397	0,437
9,28	9,178–9,381	9,432–9,643	–	0,595	0,658
11,66	11,520–11,820	10,671–10,941	–	7,692	8,68
12,39	12,192–12,599	10,612–10,941	–	1,451	1,66
14,02	13,617–14,270	14,765–15,116	–	0,077	0,088
15,40	15,243–15,568	14,765–15,074	17,307–17,489	0,843	0,938
16,08	15,904–16,250	17,307–17,489	–	1,882	2,14
18,05	17,835–18,274	18,387–18,586	17,282–17,489	0,351	0,331
19,30	19,084–19,539	18,387–18,586	17,230–17,621	0,681	0,759
21,07	20,87–21,25	21,83–22,23	–	1,345	1,65
32,07	31,80–32,35	32,68–32,95	31,23–31,48	0,658	0,679

Table 4 includes the results of [4]. In order to be able to make comparisons of the α values, that portion of the cross section σ_γ and σ_f which was subtracted in our work along with the "background base" was subtracted. Obviously, the results of [4] are systematically too large. The comparison could not be made for levels with E_0 below 6 eV because the step width of the averaging of the results of [4] was too large. The explanation of the differences will stimulate further measurements of α and the investigation of the relation between the experimentally determined parameters and the capture cross section values, fission cross section values, and the α value.

LITERATURE CITED

1. G. V. Muradyan, Yu. V. Adamchuk, and Yu. G. Shchepkin, in: Problems of Atomic Science and Technology [in Russian], Some Problems in Solid-State Physics, Press of the Inst. of Atomic Energy, Moscow (1974), p. 52.
2. G. V. Muradyan, At. Energ., 50, No. 6, 394 (1981).
3. G. Muradyan et al., in: Proc. Int. Conf. Nuclear Cross Sections from Technology, Knoxville (1980), p. 488.
4. R. Gwin et al., Nucl. Sci. Eng., 59, 79 (1976).

EXPERIMENTAL INVESTIGATION OF THE FORM OF THE ENERGY DISTRIBUTION OF NEUTRONS IN THE SPONTANEOUS FISSION OF ^{252}Cf

M. V. Blinov, G. S. Boikov,
and B. A. Vitenko

UDC 539.173.84.164

In the last few years certain progress has been made in the investigation of the spectrum of instantaneous neutrons from the ^{252}Cf fission, with the ^{252}Cf being an international standard [1-5]. However, the accuracy with which the spectrum is known to date does not satisfy the requirements which must be met by such a standard. Therefore, new precision measurements must be made in the entire energy range (particularly above 5 MeV) in which the experimental data differ substantially.

We measured in our work the neutron spectrum in the energy range 0.01-10 MeV with the time-of-flight technique. We used an ionization chamber with current measurements and ^{235}U layers as a neutron detector. The cross section of the reaction $^{235}U(n, f)$ has been studied in detail in a wide energy range and is one of the standards of nuclear physics. The chamber was an assembly of five aluminum foil disks (diameter 100 mm, thickness 0.05 mm) with uranium (99.9% ^{235}U) applied to both sides of the disks. The layer homogeneity was ±5% at an average thickness of 1 mg/cm^2. The total mass of the uranium in the chamber was 0.8 g. The chamber housing was made from 0.2-mm-thick cadmium foil. The amplitude distribution which was obtained for the fission fragments with the chamber under operational conditions is illustrated in Fig. 1. The efficiency of recording fission fragments amounted to ~85% at the threshold so that practically full discrimination from the α particles was guaranteed. The intrinsic background of the chamber was $2 \cdot 10^{-3}$ pulses per sec.

A miniature ionization chamber with the design resembling that described in [6] served as the detector of the fission fragments of californium. Californium layers with a diameter of 4 mm, a mass of 0.75 μg ($5.1 \cdot 10^5$ fissions per sec) or 0.3 μg ($2.1 \cdot 10^5$ fissions per sec) were used. The admixed spontaneous fissions resulting from other nuclides of californium and curium were less than 0.2%. The efficiency of recording the fission fragments exceeded 99%.

The total time resolution of the experimental setup amounted to 1.5 nsec. The main uncertainty in the resolution resulted from the uranium chamber. The time scale was calibrated with an accuracy of 0.1% with the aid of a quartz generator of time intervals. The "zero" of the time was determined with three methods: from the coincidence of the spectra on the three flight bases, from the simultaneous application of generator pulses to the current-pickup electrodes of the californium and uranium chambers, and from the replacement of the uranium layers in the working chamber by a single uranium layer with a diameter of 10 mm under conservation of the capacity. The data obtained with the three methods agreed satisfactorily, and the accuracy with which the zero of the time scale was determined was ±0.08 nsec. The error which was made in the determination of the base did not exceed ±2.5 mm. The background of true random coincidences was reduced by a superposition-revision circuit [7] and amounted to less than 2% at a neutron energy of 50 keV on the 50-cm base.

The neutron spectrum was measured on three flight bases of 25, 50, and 100 cm outside the premises at a distance of 8 m from the earth's surface. The measurements were made in three series of 5 days each on each of the flight bases.

When the experimental results were processed, corrections for the scattering of neutrons by the detectors and the ambient medium were introduced. Since the mass of the fission chambers was small (the mass of the uranium chamber was 65 g, that of the californium chamber 1.5 g), the corrections varied between 3% at 10 keV and 0.7% at 1 MeV. Correction functions for the scattering of neutrons by the air were determined by calculations using the method described in [8]. The correction for the scattering of neutrons by air varied between 30% for the 25-m base at E = 10 keV and 0.5% at E = 1 MeV. Corrections for the time resolution

Translated from Atomnaya Énergiya, Vol. 57, No. 4, pp. 257-259, October, 1984. Original article submitted May 23, 1984.

 0038-531X/84/5704-0714$08.50

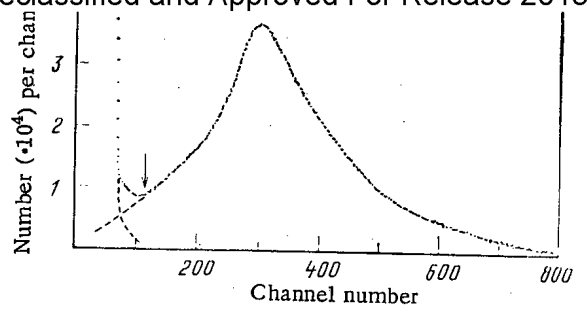

Fig. 1

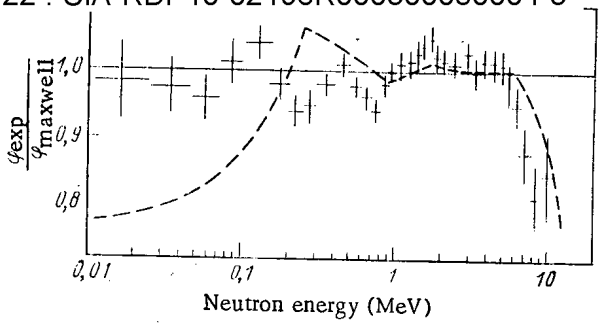

Fig. 2

Fig. 1. Amplitude distribution of the fission fragments of α particles of ^{235}U. The arrow denotes the threshold of recording fragments in the actual measurements.

Fig. 2. Ratio of the experimental results obtained in our work to a Maxwell distribution. The errors indicated do not include the uncertainty of the fission cross-section; -----) data of [9].

were also introduced. The correction on the 100-cm base amounted to 5% at the neutron energy 10 MeV. A correction was also introduced for the anisotropy of the emission of the fission fragments from the uranium layer; the kinematic effect for the various neutron energies was taken into account. This correction had a maximum value of 2.5% at a neutron energy of 10 MeV.

When the errors made in the determination of the intensity of the neutron spectrum were analyzed, the following factors were taken into account: uncertainties in the corrections of the flight distance, the time resolution, the zero of the time scale, and the cross section of the $^{235}U(n, f)$ reaction. The accuracy of the determination of the neutron energy depends mainly upon the error in the zero of the time scale, the "weight" of the channel, and the flight distance.

The results of the measurements are illustrated in Fig. 2 in the form of the ratio of our results to a Maxwell distribution (temperature T = 1.42 MeV of the spectrum). The data were normalized to the integral of the energy interval 10 keV-10 MeV. It follows from the figure that the experimental results of our work coincide with an accuracy of ±5% with the distribution indicated in the neutron energy interval 0.01-5 MeV. The slight deviations observed in this energy interval may be associated with the imprecision with which the cross section of the reaction $^{235}U(n, f)$ is known. At energies >5 MeV a systematic deviation of the data from the Maxwell distribution is observed. The values obtained agree within the error limits with the estimates of [9] in the neutron energy interval 0.2-10 MeV.

LITERATURE CITED

1. M. V. Blinov, V. A. Vitenko, and Yu. I. Yurevich, in: Neutron Physics [in Russian], Central Scientific-Research Institute of Atomic Information (TsNIIatominform), Part 3, Moscow (1980), p. 109.
2. R. Bottger, H. Klein, A. Chalupka, and B. Strohmaier, in: Proc. Conf. Nucl. Data for Science and Technology, Brussels (1983), p. 484.
3. M. Blinov, G. Boykov, and V. Vitenko, in: Proc. Conf. Nucl. Data for Science and Technology, Brussels (1983), p. 479.
4. W. Pönitz and T. Tamura, in: Proc. Conf. Nucl. Data for Science and Technology, Brussels (1983), p. 470.
5. H. Märten, D. Seeliger, and B. Stobinski, INDC (DDR)-17/L, Vienna (1982).
6. A. Chalupka, Nucl. Instrum. Methods., 164, 105 (1979).
7. M. V. Blinov, V. A. Vitenko, and V. I. Yurevich, in: Neutron Physics [in Russian], Central Scientific-Research Institute of Atomic Information (TsNIIatominform), Part 4, Moscow (1980), p. 96.
8. M. Blinov, V. Vitenko, V. Dushin, and V. Yurevich, Nucl. Instrum. Methods, 198, 455 (1982).
9. J. Grundle and C. Eisenhauer, NBS-425, Washington (1975), p. 250.

EFFECTS OF THE FLUCTUATION OF THE RESONANCE PARAMETERS IN THE AVERAGE NEUTRON CROSS SECTIONS

N. Koyumdzhieva, S. Toshkov, and N. Yaneva

UDC 539.172.4

Theoretical modeling of the energy dependence of neutron cross sections in the range of unresolved resonances, where direct information on the dependence is not available, is important for both interpretation and analysis of data on the transmission of neutrons through relatively thick samples, with the transmission averaged over the energy $\langle\exp(-n\sigma)\rangle$, the self-indication $\langle\sigma_\alpha\exp(-n\sigma)\rangle$ averaged over the energy (where σ denotes the total cross section; σ_α denotes the cross section of the reaction α; and n denotes the thickness of the absorbing sample in nuclei per barn), and some other averaged functional cross sections $\langle f(\sigma)\rangle$. The resonance structure of the cross sections is obtained indirectly as the difference between the measured $\langle f(\sigma)\rangle$ values and $f(\langle\sigma\rangle)$.

The multilevel modeling of the energy dependence of the cross sections of our work was based on the general results of the R-matrix theory of nuclear reactions (in the Reich–Moor approximation) and has been expounded in [1, 2]. When we restrict the considerations to a single system of resonance states, in the simplified form the cross sections can be expressed in the usual manner through the elements S_{nn} and $S_{n\alpha}$ of the collision matrix S. It is generally accepted that the S matrix can be represented in the form

$$S=e^{-i\varphi}(1-iK)^{-1}(1+iK)e^{-i\varphi}, \tag{1}$$

where φ denotes the phase of potential scattering.

When we assume that radiative capture involves a large number of channels α, we can restrict our considerations in the S matrix to channels differing from the radiative channels for which

$$K_{n\alpha}=\frac{1}{2}\sum_{\lambda}\frac{\Gamma_{n\lambda}^{1/2}\Gamma_{\alpha\lambda}^{1/2}}{E_\lambda-E-i\Gamma_\gamma/2}, \tag{2}$$

where $\Gamma_{n\lambda}^{1/2}$ and $\Gamma_{\alpha\lambda}^{1/2}$ denote the widths of the levels λ in the corresponding channels, and Γ_γ denotes the radiative width which is the same for all levels [1].

When the energy dependence of the cross sections was modeled, we used the scheme of the Monte Carlo method in which the width of the levels and the level spacings $E_{\lambda+1}-E_\lambda$ are generated by Porter–Thomas and Wigner distributions, respectively [2]. It has been shown earlier that the statistical spread of the resonance parameters relative to their average values does not significantly influence the total cross sections averaged over the energy [2]. However, in the case of the reaction cross sections, the statistical fluctuations can rather significantly modify the calculated cross sections (up to about 30%). Therefore, in the range of partially overlapping resonances ($\Gamma_n \leq D$), specific numerical calculations must be made in the model and the results must be compared with known results for isolated levels.

In the simplest case, namely single-channel scattering and radiative capture, the cross section of radiative capture in our model can be represented as in [1]:

$$\sigma_{n,\gamma}=\pi\lambda^2(1-|S_{nn}|^2), \tag{3}$$

where

$$S_{nn}=e^{-2i\varphi}(1-iK_{nn})^{-1}(1+iK_{nn}); \tag{4}$$

Institute of Nuclear Research and Nuclear Power Engineering of the Bulgarian Academy of Sciences, Sofia. Translated from Atomnaya Énergiya, Vol. 57, No. 4, pp. 259–260, October, 1984. Original article submitted May 18, 1984.

 0038-531X/84/5704-0716$08.50

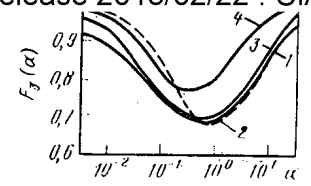

Fig. 1. The function $F(\alpha)$ for the single-level approximation (1) as calculated with the method of [3] (2), and obtained with the multilevel model for $\overline{\Gamma}_n/\overline{D} = 0.2$ (3), and $\overline{\Gamma}_n/\overline{D} = 1$ (4). $\alpha = \Gamma_\gamma/\Gamma_n$.

$$K_{nn} = \frac{1}{2}\sum_\lambda \frac{(E_\lambda - E)\,\Gamma_{\lambda n}}{(E_\lambda - E)^2 + \Gamma_\gamma^2/4} + i\,\frac{\Gamma_\gamma}{4}\sum_\lambda \frac{\Gamma_{\lambda n}}{(E_\lambda - E)^2 + \Gamma_\gamma^2/4} = K_1 + iK_2. \tag{5}$$

We obtain a simple formula for σ_γ from Eqs. (3)-(5):

$$\sigma_{n,\gamma}(E) = 4\pi\lambda\,\frac{K_2(E)}{[1+K_2(E)]^2 + [K_1(E)]^2}. \tag{6}$$

In our scheme the average cross section was obtained as a result of averaging the $\sigma_{n,\gamma}$ generated by a large number of events in Monte Carlo calculations:

$$\langle\sigma_{n,\gamma}\rangle = 4\pi\lambda^2\left\langle\frac{K_2(E)}{[1+K_2(E)]^2 + [K_1(E)]^2}\right\rangle. \tag{7}$$

The average cross sections were calculated with the program described in [2]. The cross section of radiative capture was calculated according to Eq.(7) taking into account that

$$\Gamma_{\lambda n} = \beta_{\lambda n}\overline{\Gamma}_n;\quad \frac{E_\lambda - E}{\overline{D}} = Z_\lambda, \tag{8}$$

where $\overline{\Gamma}_n$ and $\overline{D}$ denote the average values of the neutron line width and interresonance spacing, respectively.

The $\beta_{\lambda n}$ and Z_λ values were obtained as random numbers with a normal distribution and a Wigner distribution, respectively. The λ values in Eq. (5) were varied between 1 and 30 so that 15 levels were on both sides of each of the points in the calculation of the cross section. The step width in the change of E in the interval of averaging over the energy was so small that the resonance structure in the interval under consideration was described in detail. The step width on the energy scale and the number of levels and events considered in the Monte Carlo calculations were optimized by making comparative calculations.

We calculated the dependence of the cross section for each set of resonance parameters and determined its average over the energy. The final result was obtained by averaging over the number of events in the Monte Carlo method (this number was not less than 100). The error in the determination of the cross section was estimated with the standard formula of the Monte Carlo method and did not exceed 3-5%.

Figure 1 illustrates the function F_γ, in which the effect of the fluctuations of the resonance parameters in the cross section of radiative capture was taken into account. We obtained curves 2 and 3 as the ratios of the average values $\sigma_{n,\gamma}$, calculated with the method described above for the values $\overline{\Gamma}_n/\overline{D} = 0.2$ and 1, respectively, to the same quantities obtained without fluctuations of the resonance parameters. In the first case, a significant interference in the resonance levels must exist, whereas the resonance levels fully overlap in the second case.

The calculations show that in the region of overlapping levels ($\overline{\Gamma}_n \approx \overline{D}$), the fluctuations of the resonance parameters are substantial as in the case of isolated resonances. The values of the corresponding functions F_γ (see Fig. 1) differ from the corrections calculated with the method of [3].

discussions.

LITERATURE CITED

1. A. A. Luk'yanov, Moderation and Absorption of Resonance Neutrons [in Russian], Atomizdat, Moscow (1974).
2. N. Koyumdzhieva and N. Yaneva, Problems of Atomic Science and Technology, Nuclear Constants Series [in Russian], No. 42(3) (1981), p. 88.
3. J. Teppel, H. Hofmann, and H. Weidenmuller, Phys. Lett., 49B (1974).

TOTAL NEUTRON CROSS SECTIONS OF RADIOACTIVE ^{153}Gd AND STABLE ^{152}Gd

V. P. Vertebnyi, P. N. Vorona, A. I. Kal'chenko, V. G. Krivenko, and V. Yu. Chervyakov

UDC 539.125.5.162.2

Measurements were made on the VVR-M nuclear reactor of the Institute of Nuclear Research, Academy of Sciences of the Ukrainian SSR, of the cross sections for thermal and epithermal neutrons of ^{152}Gd and radioactive ^{153}Gd ($T_{1/2}$ = 241.6 days), as these data are essential for estimating the feasibility of accumulating the latter in large amounts. The isotopes ^{152}Gd and ^{153}Gd appear in the transformation chain of ^{151}Eu during its irradiation in a reactor [1]. Earlier, we determined the neutron cross sections for the following isotopes of this chain: ^{151,152,153,154,155}Eu, ^{152,153,154}Sm, and partially ^{152,154}Gd. The study of ^{152,153}Gd almost concludes the determination of the neutron cross sections of the isotopes occurring in the transformation chain of ^{151}Eu during irradiation in a nuclear reactor. ^{153}Gd, with a half-life of 241.6 days, is interesting in that it is found in a number of odd isotopes of ^{155,157}Gd, having very large neutron cross sections in the region of thermal neutron energies. Calculations of the density of neutron resonances indicate an even greater density of the levels for ^{153}Gd (D = 1.2 eV) by comparison with ^{155,157}Gd [2], and therefore it can be expected that ^{153}Gd also has a large cross section in the thermal neutron region. Already, after the start of our experiment, an estimate has appeared [3] of the effective capture cross section of ^{153}Gd, averaged over the reactor spectrum, and which was obtained by a study of the spectrum of (n, γ) reactions on ^{152}Gd and ^{153}Gd, and amounts to 26,000 ± 10,000 b (1 b = 10^{-28} m^2).

Radioactive ^{153}Gd is obtained by irradiation in the reactor of stable ^{152}Gd. One of the difficulties of conducting the experiment was caused by the presence in the sample of ^{152}Gd of impurities of strongly absorbing ^{155,157}Gd, which should be burned during irradiation in the reactor. These impurities led to a marked self-screening of the sample. In order to avoid a strong reduction of the neutron flux in the sample, it had to be made quite thin. Unfortunately, planning of the experiments was complicated because of the absence of reliable data about the neutron cross section of ^{152}Gd, serving as the starting product for the production of ^{153}Gd. We had available the results of our earlier investigations [4]: with v = 2200 m/sec, $\sigma_t(^{152}\text{Gd}) = 600^{+600}_{-480}$ b; the activation cross section $\sigma_\gamma(^{152}\text{Gd})$ = 1100 ± 100 b was taken from the publication [5]. The experiment was conducted by the procedure described in [6]. Samples with a size of 15.0 × 2.25 × 25.9 mm were prepared for irradiation, the mass of gadolinium oxide amounted to 71.64 mg, and aluminum powder with a mass of 1990 mg was used for dilution.

The isotopic composition of the starting sample of ^{152}Gd is shown in Table 1. According to the data of the Isotope Foundation of the SSSR, there were also impurities of samarium (2.6 ± 0.4%) and europium (1.0 ± 0.25%) in the sample. In order to obtain radioactive ^{153}Gd, the samples of ^{152}Gd were irradiated three times in the reflector of the VVR-M nuclear reactor in the Institute of Nuclear Research, Academy of Sciences of the Ukrainian SSR (15.2, 8.7, and 23.9 days, respectively) at nominal power. The thermal neutron fluence at the end of each irradiation amounted to $0.236 \cdot 10^{20}$, $0.444 \cdot 10^{20}$, and $0.910 \cdot 10^{20}$ cm^{-2}. The radioactive ^{153}Gd was produced in the reaction

Translated from Atomnaya Énergiya, Vol. 57, No. 4, pp. 260-262, October, 1984. Original article submitted May 18, 1984.

 0038-531X/84/5704-0718$08.50

tial Sample of ^{152}Gd

Isotope	Content, %	Concentration of nuclei, 10^{20} cm^{-2}
152	30±0,1	2,05
154	9,5±0,1	0,65
155	22,1±0,1	1,51
156	14,9±0,1	1,02
157	8,5±0,1	0,58
158	9,1±0,1	0,62
160	5,9±0,1	0,40

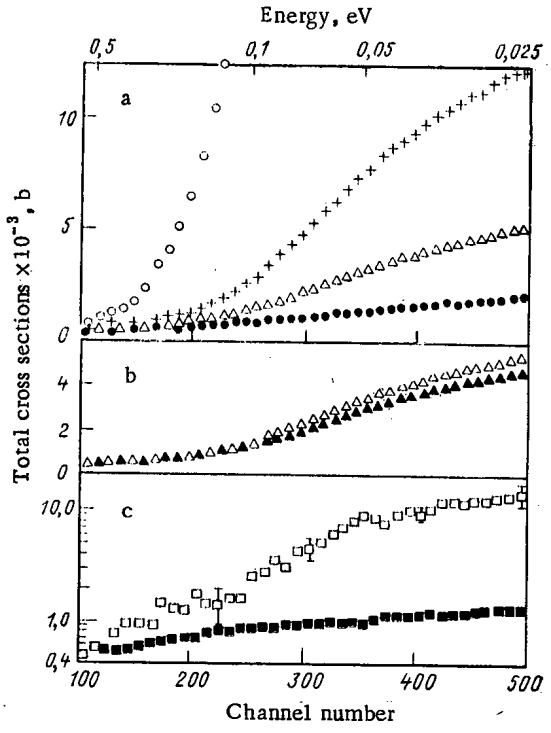

Fig. 1

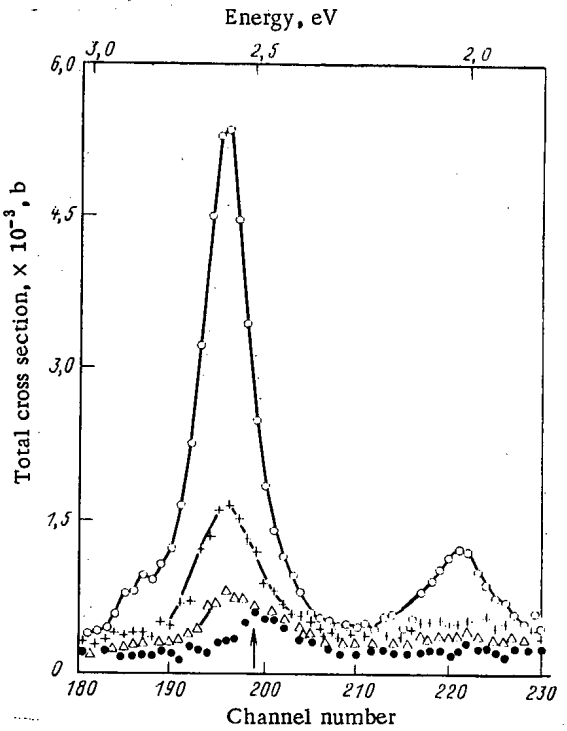

Fig. 2

Fig. 1. Total neutron cross sections of gadolinium isotopes: a) cross section of sample of ^{152}Gd before irradiation (○) and after irradiation in the reactor during 15.2 days at a neutron fluence of $0.236 \cdot 10^{20}$ cm^{-2} (×), during 23.9 days at a fluence of $0.444 \cdot 10^{20}$ cm^{-2} (Δ), and during 47.8 days at a fluence of $0.910 \cdot 10^{20}$ cm^{-2} (●); b) cross section of irradiated sample of ^{152}Gd at a neutron fluence of $0.444 \cdot 10^{20}$ cm^{-2} before (Δ) and after decay (▲) of the radioactive ^{153}Gd built up in it (holding time of sample t = 287 days; c) total neutron cross section of ^{153}Gd (□) and ^{152}Gd (■).

Fig. 2. Observed neutron cross section of a sample of ^{152}Gd before irradiation (○) and after irradiation in the reactor during 15.2 days with a neutron fluence of $0.236 \cdot 10^{20}$ cm^{-2} (×), during 23.9 days with a fluence of $0.444 \cdot 10^{20}$ cm^{-2} (Δ), and during 47.8 days with a fluence of $0.910 \cdot 10^{20}$ cm^{-2} (●). The resonance at E_o = 2.658 and 2.008 eV belong to the impurity isotope ^{155}Gd. The resonance of ^{153}Eu, appearing as a result of the decay of radioactive ^{153}Gd, is denoted by the arrow.

$$^{152}Gd + n \rightarrow {}^{153}Gd\ (241.6\ \text{days}) \xrightarrow{E.C} {}^{153}Eu,$$

where E.C is electron-capture.

Measurements were made of the transmission of the sample before irradiation and after each irradiation with a resolution of 1, 0.22, and 0.55 μsec/m. After the irradiations, a weakening of the resonances $^{155,157}Gd$ and an intensification of the $^{156,158}Gd$ resonances was

TABLE 2. Change of Concentration of Gadolinium Isotopes, Relative Units

Time of irradiation	^{152}Gd	^{153}Gd	^{155}Gd	Neutron fluence, 10^{20} cm^{-2}
Before irradiation	1,0	0	1,0	0
First irradiation, 15.2 days	0,960	0,0365	0,28	0,236
Second irradiation, 23.9 days	0,926	0,0483	0,091	0,444
Third irradiation, 47.8 days	0,855	0,0623	0,007	0,910

observed in the transmission, as a result of burnup of the strongly absorbing ^{155,157}Gd and their transition to ^{156,158}Gd. Resonances caused by the buildup in the sample of ^{153}Gd were not detected. In order to observe the resonances, according to estimates a sample thicker by a factor of 10 is necessary. The results of the measurements in the region of 0.025-4 eV (resolution 1 μsec/m) of the observed cross section of the sample, referred in all cases to the initial concentration of ^{152}Gd, are shown in Fig. 1a. The main contribution to the cross section after the first two irradiations is made by ^{155,157}Gd (22.1%, and 8.5% of the initial composition of the sample). Observation after the change of strength of the resonance with energy 2.56 eV, belonging to ^{155}Gd, allowed the change of concentration of this isotope in the sample to be followed, after the first and second irradiations, and the neutron fluence to be estimated (Fig. 2). This made it possible to calculate the burnup of ^{152}Gd and the concentration of the ^{153}Gd formed (Table 2). From a comparison of the values of the parameters $g\Gamma_n^0$ obtained after irradiation with the original, it follows that after the first irradiation the concentration of ^{155}Gd in the sample amounted to 28% of the original, and after the second irradiation – 9.1 ± 0.2%. After the third irradiation, the resonance with energy 2.56 eV was not observed, and the neutron fluence was estimated from the burnup of a sample-verifier containing ^{10}B: it amounted to $0.47 \cdot 10^{20}$ cm^{-2}, which corresponds to a ^{155}Gd concentration of 0.7% of the original.

In all cases, the contribution of ^{155}Gd was subtracted from the observed cross section of the sample (the contribution of ^{157}Gd is negligibly small, as the isotope burns up almost completely after the first irradiation). The results obtained, equal to (after the i-th irradiation)

$$\sigma_{i\,\mathrm{obs}} = [n_i\sigma(^{152}\mathrm{Gd}) + n_i\sigma(^{153}\mathrm{Gd})]/n_0\sigma(^{152}\mathrm{Gd}),$$

were used for finding the energy dependence of the ^{152}Gd and ^{153}Gd cross sections. Moreover, an additional experiment was run: After the lapse of 287 days after the second irradiation, the measurements of the transmission of the irradiated sample were repeated (see Fig. 1b). This was done in order to determine the contribution of ^{153}Gd to the observed cross section. With E_n = 0.0253 eV, the difference in the observed cross sections amounted to 410 ± 90 b. Figure 1c shows the final results of the determination of the cross sections of ^{152}Gd and ^{153}Gd in the energy range 0.0253-0.6 eV. With a neutron energy of 0.0253 eV, the total cross sections amount to 1100 ± 230 b for ^{152}Gd, and 14,000 ± 3000 b for ^{153}Gd. The energy dependence $\sigma_t(E_n)$ for ^{152}Gd is close to linear; the energy dependence $\sigma_t(E_n)$ for ^{153}Gd is similar in form to the dependence $\sigma_t(E)$ for ^{155}Gd, for which there is a resonance for E_n = 0.0268 eV. It may be supposed, therefore, that there exists a resonance also for ^{153}Gd, for a neutron energy close to zero.

LITERATURE CITED

1. V. P. Vertebnyi et al., Preprint Kharkov Institute of Nuclear Research-75-14 [in Russian], Kiev (1975).
2. Zh. I. Pisanko and L. A. Golovach, Preprint IF-69-16 [in Russian], Kiev (1969).
3. A. Spits et al., in: Proceedings of the Fourth International Symposium on Neutron Capture Gamma-Ray Spectroscopy, Grenoble, p. 85 (1981).
4. V. P. Vertebnyi et al., Ukr. Fiz. Zh., 14, 520 (1969).

5. [illegible], J. Inorg. Nucl. Chem., 34, 2099 (1972).
6. V. P. Vertebnyi et al., Preprint Kharkov Institute of Nuclear Research-76-17 [in Russian], Kiev (1976).

CROSS SECTIONS OF THE INTERACTION OF FAST NEUTRONS WITH CHROMIUM AND ITS ISOTOPES

I. A. Korzh, V. A. Mishchenko,
M. V. Pasechnik, and N. M. Pravdivyi

UDC 539.172.4

Apart from the interest in terms of pure physics, research on the scattering of fast neutrons by chromium and its isotopes, the determination of the scattering cross sections, and research on the scattering dynamics are of great practical importance because chromium is one of the most important components in the building materials of nuclear installations, and its use in relatively large amounts (~30% of the composition) in the fuel elements of fast reactors with a dissociating gaseous coolant appears promising. Therefore, many measurements of neutron cross sections have been made on chromium: Measurements were made of the total cross section [1-3], the cross section of elastic scattering [3-17], and the cross section of inelastic scattering in the excitation of discrete levels of isotopes by recording the gamma quanta released [18-20] or by recording the inelastically scattered neutrons [3, 16, 17, 21]. In all cases, except for [17], the scattering cross sections were measured on chromium samples with the natural isotope composition. But the energy range of interest from a practical viewpoint was not always adequately investigated. Apart from this, there exist substantial differences between the results of the various authors, particularly at energies below 3 MeV. It is therefore necessary to make systematic cross section measurements of adequate precision.

When measurements are made on the separated isotopes, the cross sections of inelastic neutron scattering in the excitation of discrete levels can be obtained with high precision and reliability. We used the time-of-flight technique with high resolution of [22, 23] to measure the cross sections of elastic and inelastic scattering of neutrons at the energies 1.5, 2.0, 2.5, and 3.0 MeV at ^{50}Cr, ^{52}Cr, and ^{54}Cr samples [24-26] and at the energies 5.0, 6.0, and 7.0 MeV at a ^{53}Cr sample [27, 28].

Figure 1 shows as an example the differential cross sections which we obtained for the elastic and inelastic scattering of neutrons under excitation of the two lowest levels of the ^{52}Cr nucleus and at a neutron energy of 1.5-7.0 MeV. The data were compared with the results of calculations based on the optical model (OM) and averaged parameters of the potential [29] or with the method of strong coupling of channels (ChC) [30] or with the statistical Hauser–Feshbach–Moldauer (HFM) model [31]. The authors of [34, 35] have described the calculation of the cross sections according to a statistical model in which both discrete ^{52}Cr levels up to an energy of 4.8 MeV and higher excited levels in the form of a continuum with a level density defined by the Fermi gas model of [32] were taken into account with the parameters from [33]. It follows from Fig. 1 that the reduced scattering cross sections indicated can be rather well described with the optical-statistical approach.

Figure 2 illustrates energy dependences of the integral cross sections of elastic scattering. The dependencies were obtained by us and by other authors. Figure 2 includes data on the total cross sections and the average cosine of the angle of inelastic neutron scattering. For the purpose of comparing with the results of model calculations, all cross sections obtained with a resolution <50 keV were averaged over an energy interval of 200 keV. It follows from the figure that the differences between the results of measurements which were made of the cross sections in three different laboratories do not exceed 7-10%. The situation in the case of cross sections of elastic scattering is similar. A rather large number of data for the cross section of elastic scattering, particularly for the lower part of the energy range considered, is available, but the spread of the data is increased at energies <3 MeV.

Translated from Atomnaya Énergiya, Vol. 57, No. 4, pp. 262-266, October, 1984. Original article submitted May 21, 1984.

0038-531X/84/5704-0721$08.50

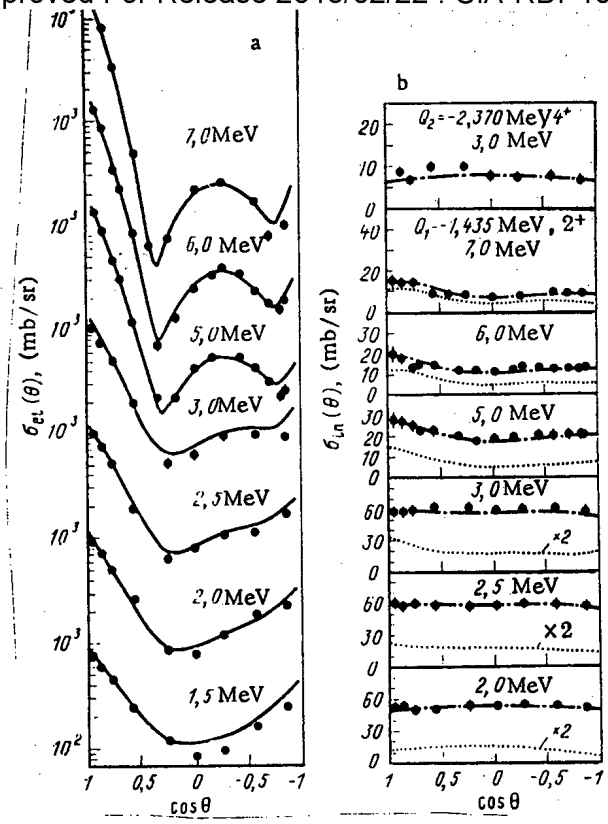

Fig. 1. Differential cross sections of elastic (a) and inelastic (b) scattering of neutrons by ^{52}Cr nuclei: ●) experimental cross sections; ———) cross sections calculated with the optical model and the statistical Hauser—Feshbach—Moldauer model; —•—•—•—•—) cross sections calculated with the model of strong channel coupling and with the statistical Hauser—Feshbach—Moldauer model; •••••) cross sections calculated with the model of strong channel coupling.

A rather strong resonance structure is observed in the data on the average cosines of the angle of elastic scattering at neutron energies <2 MeV; though the form of the energy dependence is the same in the three groups of data [7-9], considerable systematic differences can be observed. The agreement between the data of the various researchers is better at higher energies.

Figure 3 illustrates the energy dependences of the integral cross sections of inelastic scattering of neutrons at 0.5-9.0 MeV and with an excitation of the three lowest levels of the ^{52}Cr nucleus. It follows from the figure that at neutron energies <3 MeV, a considerable spread of the data exists, with the spread often exceeding the experimental errors. But this refers to data obtained in measurements of the yield of gamma quanta accompanying the inelastically scattered neutrons. The results of the present work are in good agreement with the general form of the energy dependence and help to eliminate the existing inconsistencies between the data of many authors. In addition, our data at energies >5 MeV fill the gaps in the cross section data.

The experimental data represented by Figs. 2 and 3 were compared with the results of model calculations made with the optical-statistical approach in the optical model, the strong channel-coupling model, the Hauser—Feshbach—Moldauer model, and the statistical Hauser—Feshbach model of [36]. Even when a set of averaged parameters of the optical potential was employed, a rather good description of the experimental results in the energy range under consideration was obtained, except for the total cross section and the cross section of elastic scattering at energies <3 MeV. For the purpose of comparing with experimental data, with the results of model calculations, and of the data among themselves, Figs. 2 and 3 include the results of the well-known calculations made with BNAB-78 (TsYaD-1) [37], TsYaD-2 [38], ENDF/B IV [39], ENDF/B V [40], KEDAK-3 [41], and JENDL-1 [42] with the corresponding averaging over the energy interval.

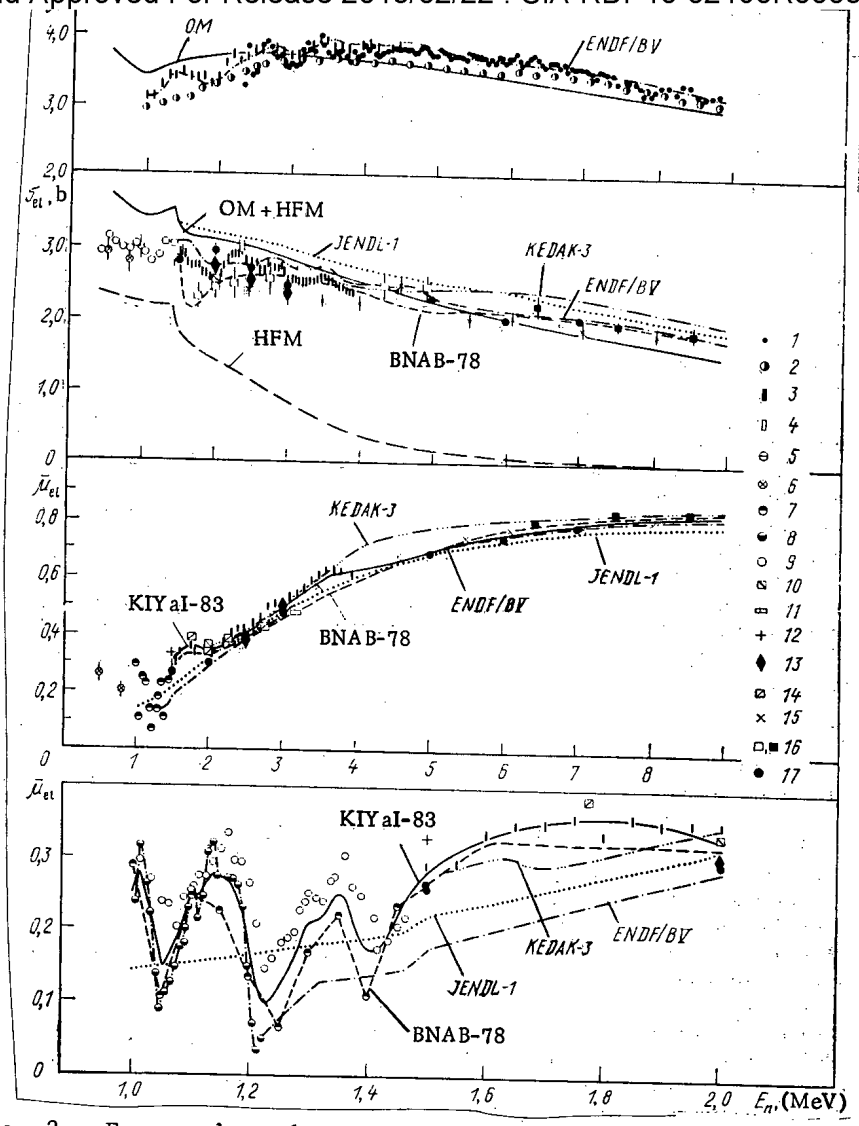

Fig. 2. Energy dependences of the total cross sections, the integral cross sections of elastic scattering, and the average cosine of the angle of elastic scattering of neutrons in the energy range 0.5-9.0 MeV: 1) data of [1]; 2) data of [2]; 3) data of [3]; 4) data of [4]; 5) data of [5]; 6) data of [6]; 7) data of [7]; 8) data of [8]; 9) data of [9]; 10) data of [10]; 11) data of [11]; 12) data of [12]; 13) data of [13]; 14) data of [14]; 15) data of [15]; 16) (isotope) data of [17]; 17) data of [24-28]. The curves represent the results of calculations made with the optical model and the Hauser—Feshbach—Moldauer model and also the data of new calculations with BNAB-78 (TsYaD-1) [37], ENDF/ BV [40], KEDAK-3 [41], JENDL-1 [42], and KIYaI-83.

As put into evidence by the example of the ENDF/B V calculation, the results of the calculation of the total cross sections are, in general, in good agreement with the experimental data. The results of calculations of the cross sections of elastic scattering differ significantly. The total set of experimental cross section values is in best agreement with the ENDF/B V calculation data. Substantial differences, particularly at energies <2 MeV, are observed between the calculated results of the average cosines of the angle of elastic scattering. The discrepancies may be explained by the fact that some of the calculations were based on one or the other experimental work. Naturally, calculated values of greater reliability can be obtained when all experimental data are included in the considerations. We used this principle when we calculated the average cosine of the angle of elastic scattering (KIYaI-83), as indicated in Fig. 2.

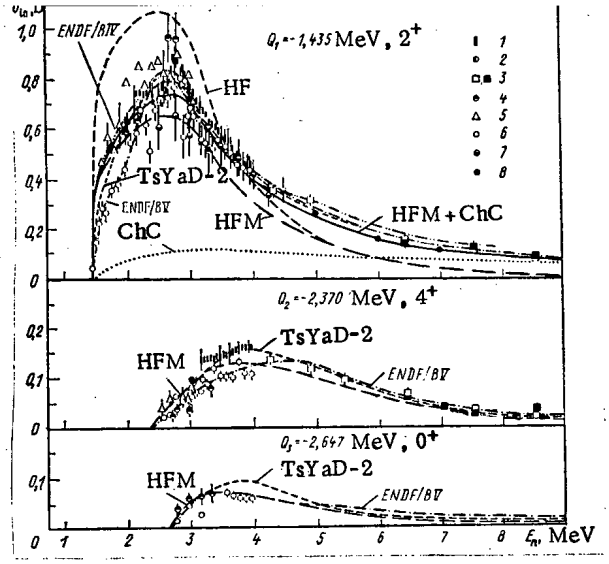

Fig. 3. Energy dependences of the cross sections of inelastic scattering of neutrons in the case of excitation of the three lowest levels of the ^{52}Cr nucleus: 1) data of [2]; 2) data of [16]; 3) (isotope) data of [17]; 4) data of [18]; 5) data of [19]; 6) data of [20]; 7) data of [21]; 8) data of [24-28]. The curves represent the results of calculations which were made with the statistical theory, disregarding the fluctuations of level widths (HF, Hauser—Feshbach model) or with the fluctuations included (HFM, Hauser—Feshbach—Moldauer model), with the model of channel coupling (ChC); the curves also relate to the data of the modern calculations with TsYaD-2, ENDF/B IV, and ENDF/B V.

The significant differences between the results of the calculations of the cross sections of inelastic scattering (see Fig. 3) reflect the differences in both the approach and the calculation procedure itself. The results of calculations based on the totality of available data on cross sections can be accepted with greater confidence. In view of the information represented in Fig. 3, we may say that at the present time the TsYaD-2 calculations reflect the contemporary state of the data in a better way than any other calculation.

It follows from Figs. 2 and 3 that new experimental cross section data for chromium and its isotopes would be useful for both removing the remaining inconsistencies in the data characterizing the lower part of the energy range considered and filling the gaps in the data of the upper part of the range. However, reliable estimates of the scattering cross section can be obtained for chromium on the basis of the available experimental data; the development state of the optical-statistical model allows a rather precise interpolation and extrapolation of the data to energy ranges for which no data are available or where the data are not adequately reliable.

The authors thank A. V. Ignatyuk and V. P. Lunev for useful discussions of their results.

LITERATURE CITED

1. D. Foster and D. Glasgow, Phys. Rev., C3, 576 (1971).
2. C. Neustead and S. Cierjacks, KFK-2060, Karlsruhe (1974).
3. A. Smith, P. Guenther, and J. Whalen, in: Proc. Int. Conf. Nucl. Cross Sections for Technology, NBS Spac. Publ. N 594, Washington (1980), p. 168; P. Guenther, A. Smith, and J. Whalen, Nucl. Sci. Eng., 82, 408 (1982).
4. O. A. Sal'nikov, At. Energ., 3, No. 1, 106 (1957).
5. W. Gilboy and J. Towle, Nucl. Phys., 42, 86 (1963).
6. I. A. Korzh, N. T. Sklyar, and I. A. Totskii, Ukr. Fiz. Zh., 9, 577 (1964).
7. A. Smith, and P. Guenther, Some Elastic Angular Distributions, A Status Report, INDSWG-48, ANL, Argonne (1964).

8. -0-12 (1970).
9. A. Smith, in: Angular Distributions in Neutron-Induced Reactions, BNL-400, II, 24-0-27 (1970).
10. L. Kazakova, V. Kolesov, V. Popov, et al., in: Proc. Int. Conf. Nucl. Struct. Study with Neutrons, Antwerpen (1966), p. 576.
11. A. Becker, W. Guindon, and C. Smith, Nucl. Phys., 89, 154 (1966).
12. I. A. Korzh, V. A. Mishchenko, M. V. Pasechnik, et al., Ukr. Fiz. Zh., 12, 1571 (1967).
13. M. V. Pasechnik, I. A. Korzh, I. E. Kashuba, et al., Yad. Fiz., 11, 958 (1970).
14. B. Holmqvist, S. Johansson, G. Lodin, et al., AE-Repts. AE-385, Studsvik (1970).
15. B. Holmqvist and T. Wiedling, AE-Repts. AE-430, Studsvik (1971).
16. M. B. Fedorov and T. I. Yakovenko, in: Neutron Physics [in Russian], Part 3, Obninsk (1974), p. 56.
17. W. Kinney and F. Perey, Rept. ORNL-4806, Oak Ridge (1974).
18. D. van Patter, N. Nath, S. Shafroth, et al., Phys. Rev., 128, 1246 (1962).
19. D. L. Broder, V. E. Kolesov, I. P. Lashuk, et al., At. Energ., 16, No. 2, 103 (1964).
20. P. Karatzas, G. Couchel, B. Barnes, et al., Nucl. Sci. Eng., 67, 37 (1968).
21. E. Almen-Ramström, AE-Repts. AE-503, Studsvik (1975).
22. V. V. Zhuk, A. A. Kozar', I. A. Korzh, et al., in: Neutron Physics [in Russian], Part, 4, Obninsk (1974), p. 203.
23. I. A. Korzh, V. A. Mishchenko, and I. E. Sanzhur, Ukr. Fiz. Zh., 25, 109 (1980).
24. I. A. Korzh, V. A. Mishchenko, É. N. Mozhzhukhin, et al., in: Neutron Physics [in Russian], Part 4, Moscow (1976), p. 220.
25. I. A. Korzh, V. A. Mishchenko, É. N. Mozhzhukhin, et al., Yad. Fiz., 26, 1151 (1977).
26. M. Pasechnik, I. Korzh, and E. Mozhzhukhin, in: Proc. Int. Conf. Nucl. Cross Sections for Technology, NBS Spec. Publ. N 594, Washington (1980), p. 893.
27. I. A. Korzh, V. A. Mishchenko, and N. M. Pravdivyi, Yad. Fiz., 35, 1097 (1982).
28. I. Korzh, V. Mishchenko, M. Pasechnik, and N. Pravdivy, in: Proc. Int. Conf. Nucl. Data for Science and Technology, Dordrecht—Boston—London (1983), p. 159.
29. M. V. Pasechnik, I. A. Korzh, and I. E. Kashuba, in: Neutron Physics [in Russian], Part 1, Kiev (1972), p. 253.
30. A. V. Ignatyuk, V. P. Lunev, and V. S. Shorin, Problems of Atomic Science and Technology [in Russian], Nuclear Constants Series, No. 13, 59 (1974).
31. P. Moldauer, Phys. Rev., 129, 754 (1963); B135, 642 (1964); B136, 947 (1964).
32. A. Gilbert and A. Cameron, Can. J. Phys., 43, 1446 (1965).
33. W. Dilg, W. Schantl, H. Vonach, and M. Uhl, Nucl. Phys., A127, 269 (1973).
34. I. A. Korzh, I. E. Kashuba, and A. A. Golubova, in: Neutron Physics [in Russian], Part 4, Moscow (1976), p. 203.
35. G. V. Antsipov, V. A. Kon'shin, V. P. Korennoi, and E. Sh. Sukhovitskii, Problems of Atomic Science and Technology [in Russian], Nuclear Constants Series, No. 20, 164 (1975).
36. W. Hauser and H. Feshbach, Phys. Rev., 87, 366 (1952).
37. V. M. Bychkov, V. V. Vozyakov, V. N. Manokhin, et al., Neutron Physics [in Russian], Part 4, Moscow (1977), p. 91; L. P. Abagyan, N. O. Bazazyants, M. N. Nikolaev, and A. M. Tsybulya, Group Constants for the Calculation of Reactors and Shields [in Russian], Energoizdat, Moscow (1981).
38. V. V. Vozyakov, V. M. Bychkov, V. P. Lunev, and V. I. Popov, Problems of Atomic Science and Technology [in Russian], Nuclear Constants Series, No. 48, 44 (1982).
39. A. Prince, Evaluation of Chromium Neutron and Gamma Production Cross Sections for ENDF/B IV, Upton, New York (1976).
40. A. Prince and T. Burrows, Evaluation of Natural Chromium Neutron Cross Sections for ENDF/B V, Upton, New York (1979).
41. B. Goel, Graphical Representation of the German Nuclear Data Library KEDAK, Part I, Non-fissile Materials, KFK-2233, Karlsruhe (1975).
42. S. Igarasi, T. Nakagawa, Y. Kikuchi, et al., Rept. JAERI-1261 (1979).

SPECTRUM OF SECONDARY NEUTRONS AND CROSS SECTION OF THE (n, 2n) REACTION AT NIOBIUM

A. A. Lychagin, V. A. Vinogradov,
O. T. Grudzevich, B. V. Devkin,
G. V. Kotel'nikova, V. I. Plyaskin,
and O. A. Sal'nikov

UDC 539.171.017

The present article reports on the results of measurements and on an evaluation of the emission spectra of neutrons from niobium nuclei; the results were obtained with the time-of-flight technique. The initial neutron energy was 14 MeV. In order to obtain high resolution at high energies, a lower energy threshold, and high statistical precision in the low-energy part of the spectrum, the measurements were made with two flight bases. On a flight base of 7 m, the time resolution was 0.65 nsec/m at a threshold of 0.5 MeV; on a flight base of 2.4 m, the corresponding values were 1.3 nsec/m and 0.1 MeV, respectively. A detailed description of the spectrometer, the measurement procedure, and the calculation of the errors has been published in [1, 2].

The spectra of scattered neutrons were measured under angles of 30, 45, 60, 75, 90, 105, 120, and 135°. The evaluation of the spectra rendered for each of the flight bases the integral spectra which are in good agreement except for the spectral region above 9 MeV. Owing to the better time resolution, the elastic peak could be established with greater precision in the spectra measured on the 7-m flight base. Therefore, in the high-energy part of the spectrum a peak which seems to result from collective excitation of lower levels could be observed. The peak is smeared because the initial energy of the neutrons changed in the measurements with the variation of the angle of scattering; the angle of scattering was varied by moving the sample.

The analysis made use of the integral spectrum which had been obtained as follows: The energy range between 0.2 and 1.5 MeV was determined on the basis of the measurements with the 2.4-m flight base; the range above 9 MeV was considered with the 7-m flight base; the range between 1.5 and 9 MeV was determined by averaging the results of both measurements and by taking into account the errors of each. In Fig. 1 the spectrum is compared with the data of other authors [3-5].

We calculated the spectrum of the primary neutrons to obtain the spectrum of the secondary neutrons. The spectrum of the primary neutrons was subtracted from the experimental total spectrum of the inelastically scattered neutrons. Two versions of the approach to the determination of the spectrum of the primary neutrons were used: 1) description of the spectrum in the form of a sum of an equilibrium part calculated with the statistical theory in the Hauser—Feshbach—Moldauer formalism and a contribution of direct processes in accordance with [6]; and 2) description in the form of a sum of an equilibrium part defined as above and a preequilibrium part described with the exciton model.

In the first version, the equilibrium part of the spectrum was described with the SMT-80 program of [7]. The permeability coefficients were calculated with the optical model having the potentials of [8]. The density of the nuclear levels was calculated with the Fermi gas model with a "backward shift." The value of the "backward shift" was $\Delta = 0.25$ MeV and the parameter of the nuclear level density was $a = 11.07$ MeV^{-1} in accordance with [9] for an initial neutron energy of 5-8 MeV. The nonequilibrium part of the spectrum was calculated as in [6].

A combined calculation was made in the second version with the STAPRE program of [10], wherein the equilibrium part was described in the same fashion as in the first version, but with $\Delta = -0.25$ MeV and $a = 10.94$ MeV^{-1}. By contrast to [11] where the parametrization of the pre-equilibrium part was made with the set of experimental data of other researchers, we used in the present work the experimental spectrum we had obtained.

Translated from Atomnaya Énergiya, Vol. 57, No. 4, pp. 266-267, October, 1984. Original article submitted May 7, 1984.

 0038-531X/84/5704-0726$08.50

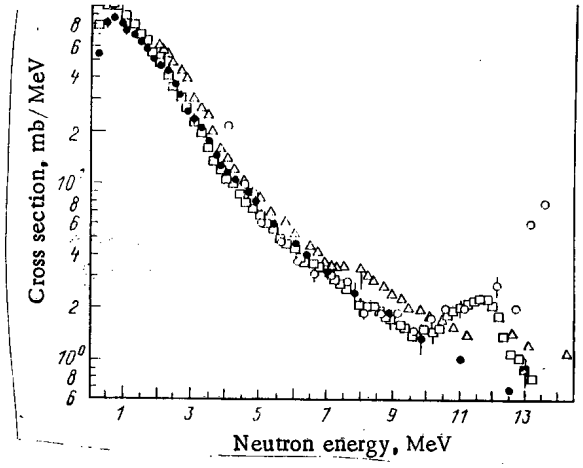

Fig. 1. Integral spectra of neutrons inelastically scattered at niobium nuclei: □) our work; ●) [3]; ○) [4]; Δ) [5]. The cross section divided by 4π is plotted to the ordinate.

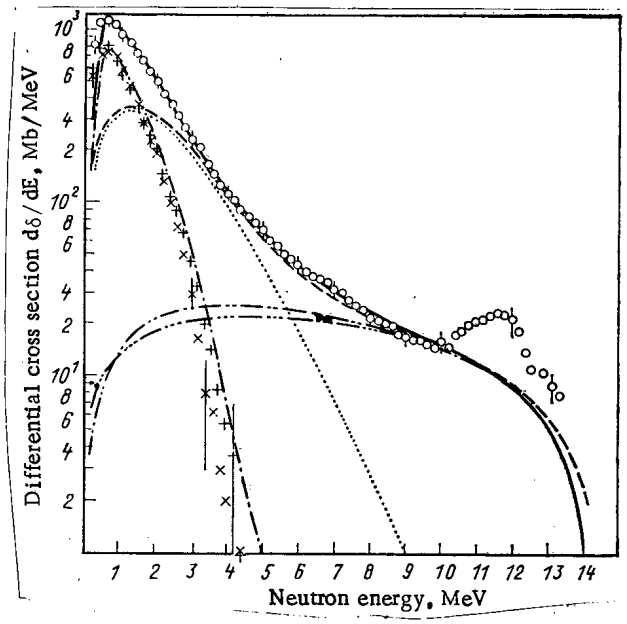

Fig. 2. Comparison of the results of the calculation with the experimental data:) experiment; ———) total spectrum calculated with the STAPRE program; – – – –) spectrum of the primary neutrons (version 1); •••••) equilibrium part of the spectrum (version 1); —••—) contribution of the direct processes (version 1); —•••—) pre-equilibrium emission (version 2); ×) spectrum of the secondary neutrons (version 1); +) spectrum of the secondary neutrons (version 2); —•—) spectrum of the secondary neutrons according to the STAPRE program.

The primary-neutron spectra calculated in the two versions are in good agreement and therefore only one of them is shown in Fig. 2. Apart from the primary-neutron spectrum, the STAPRE program also allows the calculation of the secondary-neutron spectrum, wherein the possible cascades of the emitted particles and competing channels, among them the γ transitions, can be taken into account. It is therefore possible to compare the results of the calculations with the experimental data in the entire energy range. Good agreement of the calculated spectrum with the experimental spectrum is observed at scattered-neutron energies of up to 9 MeV. The discrepancies between the data at energies in excess of 9 MeV can obviously be explained by the contribution of collective excitations which are not described with the model used in the calculations.

Figure 2 also illustrates the secondary-neutron spectra corresponding to the two versions of the calculation of the primary-neutron spectrum and the secondary-neutron spectrum calculated with the STAPRE program. All spectra agree within the experimental error limits. A certain difference in the low-energy part of the secondary-neutron spectrum calculated with the STAPRE program can be explained by the fact that the program takes into account two competing (n, n'γ) channels and the emission of secondary neutrons due to the exclusion principle imposed by the condition of conservation of the angular momentum, whereas this influence is compensated for in the experimental spectrum by the possible competition between (n, γn') channel of the decay of highly excited states, as indicated in [12].

The data processing rendered the following values for the cross section of the (n, 2n) reaction: in the first version of the calculation, 1360 ± 96 mb, in the second version, 1375 ± 96 mb, and in the version calculated with the STAPRE program 1347 mb. These values are obviously in good agreement among themselves and with the results of [13] where the cross section $\sigma_{n,2n}$ = 1350 ± 98 mb was obtained.

LITERATURE CITED

1. A. A. Lychagin et al., Preprint FEI-1406, Obninsk (1983).
2. A. A. Lychagin et al., Preprint FEI-923, Obninsk (1979).
3. O. A. Sal'nikov et al., Nuclear Constants [in Russian], No. 7, Atomizdat, Moscow (1971), p. 134.
4. J. Kammerdiener, UCRL-51232, Lawrence Livermore Laboratory (1972), p. 133.
5. D. Hermsdorf et al., ZFK-277, Dresden (1974), p. 2265.
6. O. A. Sal'nikov, "Inelastic scattering of neutrons in the range of overlapping levels," Doctoral Dissertation, Physics and Mathematics, RIAN, Leningrad (1975).
7. N. N. Titarenko, Preprint FEI-1260 [in Russian], Obninsk (1982).
8. C. Lagrange, in: Neutron Physics [in Russian], Part 3, Moscow (1976), p. 65.
9. S. P. Simakov et al., Yad. Fiz., 38, No. 1(7), 3 (1983).
10. M. Uhl and B. Strohmaier, Report IRK 76/01, Institute für Radiumforschung und Kernphysik, Vienna (1976), p. 27.
11. A. A. Lychagin et al., Preprint FEI-1385 [in Russian], Obninsk (1983).
12. Yu. E. Kozyr' and G. A. Prokopets, Yad. Fiz., 26, No. 5, 927 (1977).
13. J. Frehaut and G. Mosinsky, in: Neutron Physics [Russian translation], Press of the Central Scientific-Research Inst. of Atomic Information (TsNIIatominform), Moscow, Vol. 4, (1976), p. 303.

NEUTRON GENERATOR WITH YIELD OF 10^{12} sec^{-1}

G. G. Voronin, A. N. Dyumin, A. V. Morozov,
V. A. Smolin, G. V. Tarvid, and B. B. Tokarev

UDC 621.039.556

Neutron generators with energies of 14 MeV based on deuterium-beam accelerators employing the reaction T(d, n)^{4}He are one of the most practical sources of neutrons. They are widely used in investigations in physics and radiobiology and also when solving a number of applied problems (including the engineering problems of thermonuclear synthesis, activation analysis, problems of radiotherapy, etc.). Neutron generators NG-150 with a yield of $2 \cdot 10^{11}$ sec^{-1} [1] are presently manufactured in the Soviet Union, and while these are widely used, they do not meet the requirements of several fields of science and technology.

Investigations have been carried out with the aim of creating a neutron generator with a yield of up to 10^{12} sec^{-1}. These investigations have led to the solution of many of the problems concerned with the creation and formation of a beam of deuterium ions at currents of up to 20 mA and energies of 160 keV in the continuous mode. Target assemblies have been developed capable of receiving up to 4 kW [2]. A neutron generator of this type has been started up and tests carried out on the first trial batch of tritium targets made by the Institute of Nuclear Research of the Academy of Sciences of the Ukrainian SSR.

A diagram of the neutron generator is given in Fig. 1. An accelerator with a vertical accelerating tube enables deuterium-ion beams at currents up to 20 mA and energies of 160 keV to be focused on the target with spot diameters of ~20 mm. Vacuum pumping is carried out by NMDO-025-1 pumps.

A duoplasmotron ion gun enables deuteron beams of up to 30 mA to be achieved at discharge currents of $\sim$5 A. The nascent component of the beam comprises 70%. The use of cermet joints and metal seals for the gun electrodes reduces the content of heavy ions in the beam and improves the operating conditions of the KP-25V directly heated distributor cathode. Cathodes of this type are already in production and have extremely high emission properties and resistance to ion bombardment and a high margin in active material [3]. Several cathodes have been run up to 1000 h during tests on ion guns, at a discharge current of ~5 A, without any marked deterioration in emission properties. The continuous operating life of the gun is determined by the enlargement of the emission aperture in the tungsten anode during operation. For a beam current of up to 20 mA, the best size of emission hole is an initial diameter of 0.3 mm, at which the leakage of gas into the gun does not exceed 25 cm^3/h, while the service life of the anode reaches 300 h. The ions are taken from the surface of the plasma penetrating into the conical expander. The beam passes through the aperture of the extraction electrode virtually without losses at an extraction voltage of ~16 kV, which avoids the need to cool the electrode system of the initial beam former.

The acceleration tube is glued together out of porcelain insulators and flat disks made of stainless steel in which the conical electrodes are set. The physical dimensions of the ion beam are controlled and the distribution of current density throughout its cross-sectional area set by varying the voltage on the focusing electrode. Figure 2 shows the way in which the section of the phase volume and the distribution of current density change with increase in beam current. The shape of the observed phase diagram is determined by aberrations in the region of the focusing electrode. The multivelocity structure that arises from the action of nonlinear focusing forces at beam currents up to 15 mA enables the beam to form on the target with a distribution close to being uniform, which is important as a means of reducing the thermal loads on the target and fully utilizing the tritium in the active layer of the target. Higher values of beam current distort the increase in size, and a proportion of the deuterons strike the aperture stop ahead of the target, due to the increase in beam diameter.

Translated from Atomnaya Énergiya, Vol. 57, No. 4, pp. 268-270, October, 1984. Original article submitted May 28, 1984.

0038-531X/84/5704-0729$08.50

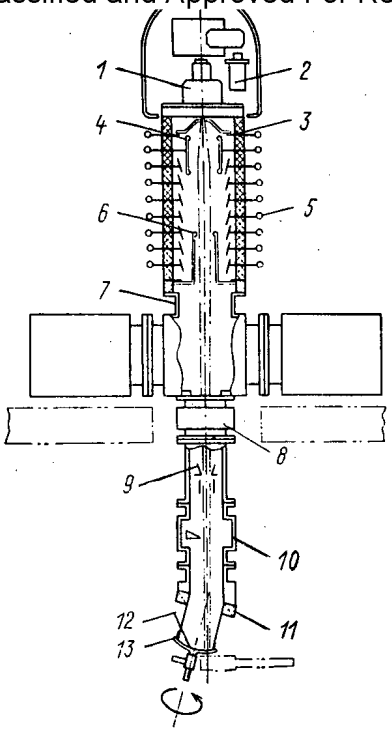

Fig. 1

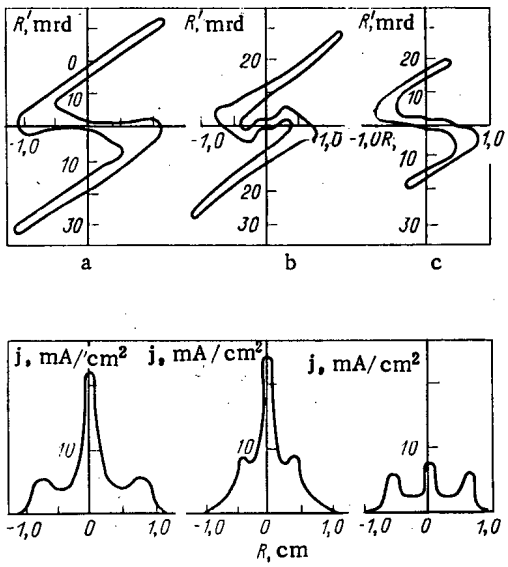

Fig. 2

Fig. 1. Diagrammatic representation of neutron generator: 1) ion gun; 2) palladium filter for introducing deuterium; 3, 4) extraction and focusing electrodes; 5) accelerating tube; 6) accelerating electrode; 7) vacuum chamber with magnetic-discharge pumps; 8) vacuum trap; 9) aperture stop; 10) beam chopper; 11) rotating vacuum connection; 12) target; 13) system for cooling target.

Fig. 2. Section of phase volume of beam and distribution of current density for different values on target: a) I = 18 mA; b) I = 12 mA; c) I = 8 mA.

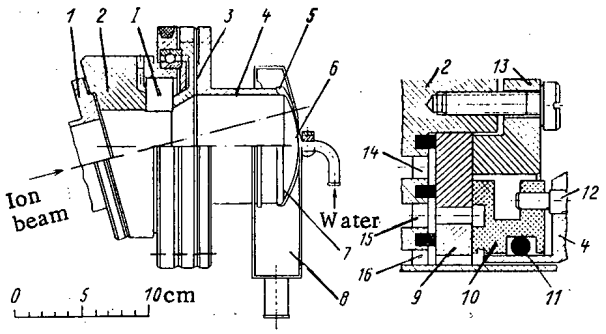

Fig. 3. Target assembly: 1) ion guide from accelerator; 2) base of target; 3) flange; 4) target holder; 5) vacuum seal; 6) target; 7) screen; 8) water intake; 9) bush; 10) sealing ring; 11) rubber seal; 12) pin; 13) pressure flange; 14) channel for cooling water; 15) channel for prevacuum pump; 16) channel for high-vacuum pump; I) rotating vacuum seal unit.

A target assembly has been created for a neutron generator for use with a 90-mm-diameter target having a spherical substrate and an active layer in the form of a ring. The output surface of the target is cooled by water which is fed into the gap between the substrate of the target and the screen that rotates with it. The vacuum seal for the connection to the rotating assembly takes the form of a ring with two sealing surfaces made of expanded fluoro-

is additionally pumped out by the prevacuum pump (Fig. 3). The average wear rate of the seal material does not exceed 10^{-4} g/h at 1000 rpm, while the service life of the seal rings reaches several thousand hours. No variations were observed in a total of ~1500 h of operation. A study of the temperature conditions of the target using a radiation temperature transducer installed in the vacuum ahead of the target showed that the element temperature did not exceed 50°C when the beam was deflected from it. The flow rate of the water cooling the target was 6 liters/min.

The neutrons were obtained via the reaction T(d, n)^{4}He. A tritium–titanium target was used. The layer of titanium was applied to the substrate from annealed oxygen-free copper in the form of a ring with external and internal diameters of 70 and 30 mm, respectively. The thickness of the layer was 1.5-4 mg/cm^2. The total activity due to the tritium was 20-90 Ci (1 Ci = $3700 \cdot 10^{10}$ Bq), which corresponds to a ratio between the number of atoms of tritium and titanium of 0.7:1.

The irradiated target was mounted immediately following the accelerating tube. The deuterium beam comprises both atomic and molecular components. The yield of neutrons was proportional to the target current over quite a wide range. The absolute value of the yield was determined from the activity of the copper foil in the reaction ^{63}Cu(n, 2N)^{62}Cu with an accuracy of ~5%. Its initial value was 10^{12} sec^{-1} at a deuteron current of 15 mA and an accelerator voltage of 160 kV.

The variation in the neutron yield as the target was irradiated by deuterons was monitored by a scintillation detector and proportional counter filled with ^{3}He. The fall in the neutron yield with irradiation time was found by finding the summated number of deuterons hitting the target. This relationship was practically exponential for all targets studied. The yield was halved after about 2 h at a target current of 15 mA. This corresponds to a total charge of 100 C or 3.5 C/cm^2.

The proposed equipment is relatively simple and reliable in operation. The generator was switched on and controlled from a control desk. The warm-up time comprised several minutes. This prevented the deuteron beam from striking the electrodes of the accelerator tube and heating them up. The passage of the beam through the ion-optical system was monitored by instruments on the control desk. The ion generator is relatively small in size, its length from the ion gun to the target (see Fig. 1) being 1840 mm.

A voltage doubler scheme based on an IOM-100 transformer serves as the source of high voltage. This can supply a direct current of up to 50 mA on a continuous basis. The heater supply to the ion gun, which is at high potential relative to ground, is obtained from an ac generator which is insulated from ground. The voltage on the electrodes of the accelerator tube comes from a voltage divider with a total resistance of 30 MΩ.

The neutron yield of 10^{12} sec^{-1} is about an order of magnitude greater than that obtainable from the best Soviet-produced equipment of this type. Finally, the minimum distance between the active layer of the rotating target and the sample being irradiated, situated outside the equipment, is 5 mm. Under these circumstances, the neutron flux is several units times 10^{11} sec$^{-1} \cdot$cm^{-2}, for a deuteron beam of ~20 mm.

In conclusion, we would like to express our gratitude to Yu. B. Evdokimov and L. M. Nikitin for their considerable assistance in carrying out this work.

LITERATURE CITED

1. G. G. Voronin, E. I. Gerasimov, G. M. Latmanizova, et al., Preprint D-0412, NIIEFA, Leningrad (1978).
2. G. G. Voronin, A. V. Morozov, A. I. Solnyshkov, and G. V. Tarvid, in: Proceedings of the All-Union Conference on the Use of Accelerators in the National Economy, Vol. 1, NIIEFA, Leningrad (1979), p. 228.
3. A. M. Ievlev, Elektron. Tekh., Ser. 4, Elektrovakuumnye i Gazorazryadnye Prib., No. 6, p. 53 (1974).
4. R. Booth, IEEE Trans. Nucl. Sci., NS-14, No. 3, 943 (1967).
5. L. I. Katsaurov and A. I. Kuznetsov, At. Energ., 21, No. 5, 390 (1966).

USING A LINEAR POLARIMETER FOR INVESTIGATING THE γ RADIATION OF AN (n, n'γ) REACTION

L. I. Govor, A. M. Demidov, O. K. Zhuravlev, V. A. Kurkin, and Yu. K. Cherepantsev

UDC 539.17:539.14

When fast neutrons are inelastically scattered, in the majority of cases an oriented nucleus is formed in an excited state which is dexcited through linearly polarized gamma quanta having an angular anisotropy with respect to the beam of the incoming neutrons. In the last few years, measurements of the angular distributions of the gamma quanta of the (n, n'γ) reaction with fast reactor neutrons have often been made. The high intensity of the neutron beam at the target and the excellent noise conditions of such experiments have made it possible to measure angular distributions of 15-20 γ transitions between the lower levels of a nucleus. In spherical even–odd nuclei, the transitions are of the type $2^+ \to 0^+$, $2^+ \to 2^+$, $3^+ \to 2^+$, $3^+ \to 4^+$, $4^+ \to 2^+$, etc. States with J = 2 or 3 have the maximum population in this reaction, and, therefore, favorable conditions for investigations of transitions of the type $2^+ \to 2^+$ and $3^+ \to 2^+$ exist. By contrast to the investigations of the gamma–gamma angular correlations, in the case of $2^+ \to 2^+$ transitions, the variability range of the coefficient a_4 (in the expansion in Legendre polynomials with $a_0 = 1$) as a function of δ is small ($-0.03 \leqslant a_4 \leqslant 0$). It is not always possible to reach the experimental precision which in the determination of a_4 would suffice for a unique determination of the multipole mixture parameter δ.

Measurements of the linear polarization P of γ quanta are an independent source of information on the angular moments of the levels and the multipole mixture parameters in γ transitions. The inspection of the δ and P ellipses in a_2 and a_4 coordinates for $2^+ \to 2^+$ transitions (Fig. 1) has shown that in the majority of cases, a unique determination of the parameter δ is possible even when the measurements of P are not very accurate and the a_2 value is known from angular distributions. A similar situation is encountered in other transitions with small a_4 values.

By contrast to the angular distributions of the γ quanta, the linear polarization depends strongly upon the difference in the parity of the states between which the transition takes place. This results from the relation $P(E2M1) = P(M2E1)^{-1}$. Thus, when measurements of the angular distribution of the γ quanta are combined with measurements of the linear polarization, in the majority of cases a unique determination of the parameters of multiple mixing of γ transitions is possible and both spins and parities can be determined for nuclear states which are well populated in an (n, n'γ) reaction. Earlier results of measurements of the linear polarization of the γ quanta in (n, n'γ) reactions have not been published.

We made measurements on the horizontal channel of the IR-8 reactor of the I. V. Kurchatov Institute of Atomic Energy. The neutron beam was passed through a filter consisting of a 1-mm-thick cadmium layer, a 10-mm-thick B_4C layer, and a 50-mm-thick uranium layer. The beryllium cassettes of the reflector of the reactor core had an air gap opposite the bottom plate of the channel. This implied a neutron flux increase by a factor of 2.7. The smallest size of the neutron beam collimator at a distance of 1 m from the target was 25 mm; the beam diameter at the target was ~40 mm. The target was mounted under an angle of 45° with respect to the neutron beam. We used in our work a ^{148}Nd sample with a mass of 20 g of the element and a size of 4 × 5 cm; the ^{148}Nd enrichment was 91.6%.

We measured the linear polarization with a Compton polarimeter consisting of two germanium detectors with a volume of ⌀ 40 × 40 mm each. One of the detectors acted as a scatterer of γ quanta and a collimator with a size of 20 × 40 mm was placed before the detector to transmit the γ quanta from the target. The other detector was operated only as an absorber of the scattered γ quanta. The distance between the surfaces of the germanium crystals was selected so that the polarimeter properties were optimized (product of the efficiency of the Compton spectrometer times the square of the polarization sensitivity). In two different

Translated from Atomnaya Énergiya, Vol. 57, No. 4, pp. 270-272, October, 1984. Original article submitted May 10, 1984.

 0038-531X/84/5704-0732$08.50

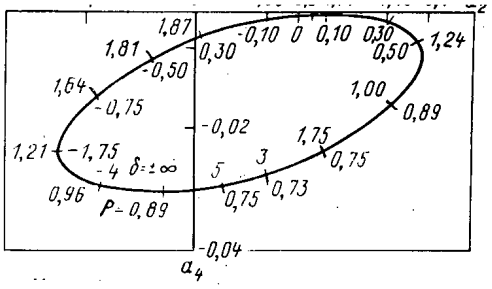

Fig. 1. P and δ ellipse for the $2^+ \to 2^+$ transition in ^{148}Nd.

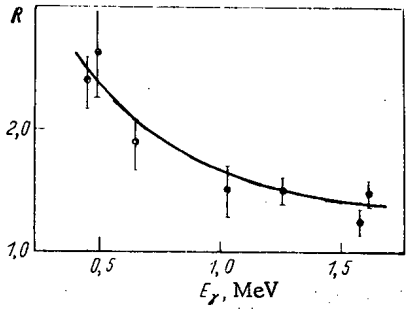

Fig. 2. Polarization sensitivity of the polarimeter.

measurement series, the distance was 3 and 5 cm with an average angle of 67° between the primary and scattered γ quanta. The γ radiation from the target was recorded under an angle of 90° with respect to the direction of the neutron beam (upwards). The pulses of the two detectors were applied to a summing circuit and to fast and slow coincidence circuits and thereafter fed into an analog–digital converter with 8192 channels. The resolution of the Compton spectrometer was 2.3 keV at E_γ = 1.6 MeV. The total load of the polarimeter was 40 pulses per second in the case of the ^{148}Nd sample and a load of $5 \cdot 10^3$ pulses per second in the scattering detector. The detectors were shielded from the neutron beam by a 250-mm-thick layer of polyethylene containing boron carbide, a 100-mm-thick lead layer, and a 3-mm-thick ^{6}Li layer. The γ-quanta beam from the target was filtered with a 100-mm-thick pure polyethylene block.

The linear polarization was defined by the ratio $P = (1 - NR)/(N - R)$, where $N = N_{90°}/N_{0°}$ denotes the ratio of the counting rates for a particular γ line when the plane of the Compton scattering of the γ quanta was perpendicular ($N_{90°}$) and parallel ($N_{0°}$) to the plane of the reaction (n – γ plane). The polarization sensitivity $R(E_\gamma)$ was determined with the aid of the a_2, a_4, and δ values which we had measured in the case of pure E2 and E1 transitions in ^{148}Nd and ^{140,142}Ce. The sensitivity is illustrated in Fig. 2 for a detector spacing of 5 cm. The time of the $N_{90°}$ and $N_{0°}$ measurements was ~50 h. The geometrical anisotropy of the setup was taken into account by normalizing to the intensity of the γ lines which have an isotropic angular distribution.

The main results of the experiment are listed in Table 1, which indicates the energy of the transition, the characteristics of the initial state (J^π_i) and of the final state (J^π_f) (the square brackets include the characteristics which we earlier assumed [1]), the a_2, a_4, and δ values obtained from the measurements of the angular distributions [2], the type of the transition, the polarization P_{ant} to be anticipated theoretically on the basis of the a_2, a_4, and δ values, the experimental polarization P_{exp}, and the results concerning J^π and δ. In addition, linear polarization values, which allow certain conclusions on the multipole character of the γ transitions and J^π_i values, were obtained for the following γ lines: 527.1 keV (P = 3.4 (9), E2 transition); 759.32 keV (P = 0.7 (3), E2M1 transition); 825.23 keV (P = 1.7 (6), $J^\pi = 4^+, 3^-, 2^-$); and 935.83 keV (P = 0.58 (14), E2M1 transition, $J^\pi_i = 3^+, 4^+$).

The authors thank S. A. Nikolaev and Yu. V. Shcherbakov, who participated in the initial stage of the development of our method.

^{148}Nd(n, n'γ) Reaction

E_γ, keV	$J_i^\pi \to J_f^\pi$	a_2	a_4	δ	P_{ant} E2M1	P_{ant} E1M2	P_{exp}	Result
489,96	[3] → 4⁺	−0,20 (4)	0,04 (5)	$1/\delta = 0{,}01^{+0{,}05}_{-0{,}03}$	0,61 (6)	1,64 (16)	2,35 (19)	$J_i^\pi = 5^-$
				$0{,}12^{+0{,}05}_{-0{,}04}$	0,88 (5)	1,14 (7)		$\delta = 0{,}03$
	[5] → 4⁺			0,03 (2)	0,49 (4)	2,08 (18)		
869,23	2⁺ → 2⁺	0,01 (4)	0,02 (5)	$8{,}3^{+11}_{-2{,}4}$	0,77 (8)	1,29 (13)	0,75 (7)	π = +
				−0,32 (8)	1,87 (6)	0,53 (2)		δ = 8,3
947,09	2⁺ → 2⁺	−0,06 (4)	0,01 (4)	$1/\delta = -0{,}03^{+0{,}04}_{-0{,}08}$	0,81 (7)	1,23 (11)	0,95 (14)	π = +
				−0,47 (10)	1,84 (5)	0,54 (2)		$1/\delta = -0{,}03$
1209,92	[3] → 2⁺	0,05 (5)	0,06 (6)	$1/\delta = -0{,}015^{+0{,}025}_{-0{,}021}$	1,55 (21)	0,65 (8)	1,71 (38)	$J_i^\pi = 3^+$
				0,20 (4)	0,40 (4)	2,50 (25)		$1/\delta = -0{,}015$
1427,4	[3] → 2⁺	0,20 (5)	0,02 (6)	0,37 (5)	0,34 (3)	2,9 (3)	0,57 (33)	$J_i^\pi = 3^+$
	4 → 2⁺				2,0 (4)			

Remark. The errors corresponding to the 68% confidence interval are indicated in parentheses.

LITERATURE CITED

1. A. Demidov et al., in: Neutron-Capture γ-Ray Spectroscopy and Related Topics, Conference Series No. 62, The Institute of Bristol and London (1982), p. 728.
2. P. Taras, Can. J. Phys., 49, 328 (1971).

MATHEMATICAL MODELING OF AN NONEQUILIBRIUM FLOW CONSISTING OF WATER, STEAM, AND AIR

N. I. Kolev

UDC 621.039.534.2.44

It is necessary in the mathematical modeling of transitional processes in nuclear power plants with water-cooled nuclear reactors to use the model of a flow consisting of water, steam, and air. This model has been developed by means of integration of the conservation equation [1]. The eigenvalues of the characteristic matrix as well as the form of the system have not been investigated. However, these important elements of the model determine the physical essence of the phenomenon being described, since the propagation velocity of perturbations of the dependent variables, which corresponds to the eigenvalues, is finite. Also an expression has not been presented for the critical mass flow density which corresponds to the adopted assumptions about the nonequilibrium nature and inhomogeneity of the flow. It is necessary in the development of this kind of model to bear in mind that one should use a single mathematical formulation to describe the nonsteady, steady, and critical states of the flow. Such an approach has been applied in [2] in the description of a nonsteady homogeneous equilibrium flow consisting of water, steam, and air in distributed parameters. A further development of this approach for homogeneous nonequilibrium and homogeneous equilibrium flows has been presented in [3-5]. The aim of this paper is to attempt to create a model of a nonsteady nonequilibrium inhomogeneous flow consisting of water, steam, and air.

Institute of Nuclear Investigations and Nuclear Power, Bulgarian Academy of Sciences, Sofia. Translated from Atomnaya Energiya, Vol. 57, No. 4, pp. 272-277, October, 1984. Original article submitted March 9, 1983.

 0038-531X/84/5704-0734$08.50

the pressure of both phases is identical; Dalton's law is valid for both components of the gaseous phase; the temperature and velocity of both phases are different; and the air is the only ideal gas.

The thermodynamic state of the flow is completely described by the vector

$$\mathbf{U}^{*T} = (p,\ T_g,\ T_f,\ \rho_L). \tag{1}$$

The necessary equations of state are as follows:

$$p_L = \rho_L R_L T_g,\ dp_L = R_L \rho_L dT_g + R_L T_g d\rho_L; \tag{2, 3}$$

$$p_D = p - p_L;\ dp_D = dp - dp_L; \tag{4, 5}$$

$$dh_L = c_{pL} dT_g; \tag{6}$$

$$\rho_D = \rho_D (p,\ T_g,\ \rho_L);$$

$$d\rho_D = \left(\frac{\partial \rho_D}{\partial p_D}\right)_{T_g} dp_D + \left(\frac{\partial \rho_D}{\partial T_g}\right)_{p_D} dT_g = \left(\frac{\partial \rho_D}{\partial p_D}\right)_{T_g} dp + \left[\left(\frac{\partial \rho_D}{\partial T_g}\right)_{p_D} - \left(\frac{\partial \rho_D}{\partial p_D}\right)_{T_g} R_L \rho_L\right] \times \tag{7, 8}$$

$$\times dT_g - R_L T_g \left(\frac{\partial \rho_D}{\partial p_D}\right)_{T_g} d\rho_L = \left(\frac{\partial \rho_D}{\partial p}\right)_{T_g, \rho_L} dp + \left(\frac{\partial \rho_D}{\partial T_g}\right)_{p, \rho_L} dT_g + \left(\frac{\partial \rho_D}{\partial \rho_L}\right)_{p, T_g} d\rho_L,$$

where

$$\left(\frac{\partial \rho_D}{\partial p}\right)_{T_g, \rho_L} = \left(\frac{\partial \rho_D}{\partial p_D}\right)_{T_g},\ \left[\hat{=} \frac{\partial \rho_D}{\partial p}\right]; \tag{9}$$

$$\left(\frac{\partial \rho_D}{\partial T_g}\right)_{p, \rho_L} = \left(\frac{\partial \rho_D}{\partial T_g}\right)_{p_D} - R_L \rho_L \left(\frac{\partial \rho_D}{\partial p_D}\right)_{T_g},\ \left[\hat{=} \frac{\partial \rho_D}{\partial T_g}\right]; \tag{10}$$

$$\left(\frac{\partial \rho_D}{\partial \rho_L}\right)_{p, T_g} = -R_L T_g \left(\frac{\partial \rho_D}{\partial p_D}\right)_{T_g},\ \left[\hat{=} \frac{\partial \rho_D}{\partial \rho_L}\right]; \tag{11}$$

$$h_D = h_D (p,\ T_g,\ \rho_L);\ dh_D = \left(\frac{\partial h_D}{\partial p}\right)_{T_g, \rho_L} dp + \left(\frac{\partial h_D}{\partial T_g}\right)_{p, \rho_L} dT_g + \left(\frac{\partial h_D}{\partial \rho_L}\right)_{p, T_g} d\rho_L. \tag{12, 13}$$

Here

$$\left(\frac{\partial h_D}{\partial p}\right)_{T_g, \rho_L} = \left(\frac{\partial h_D}{\partial p_D}\right)_{T_g},\ \left[\hat{=} \frac{\partial h_D}{\partial p}\right]; \tag{14}$$

$$\left(\frac{\partial h_D}{\partial T_g}\right)_{p, \rho_L} = \left(\frac{\partial h_D}{\partial T_g}\right)_{p_D} - R_L \rho_L \left(\frac{\partial h_D}{\partial p_D}\right)_{T_g} \left[\hat{=} \frac{\partial h_D}{\partial T_g}\right]; \tag{15}$$

$$\left(\frac{\partial h_D}{\partial \rho_L}\right)_{p, T_g} = -R_L T_g \left(\frac{\partial h_D}{\partial p_D}\right)_{T_g},\ \left[\hat{=} \frac{\partial h_D}{\partial \rho_L}\right]; \tag{16}$$

$$h_f = h_f (p,\ T_f);$$

$$dh_f = \left(\frac{\partial h_f}{\partial p}\right)_{T_f} dp + \left(\frac{\partial h_f}{\partial T_f}\right)_p dT_f. \tag{17, 18}$$

We shall further restrict ourselves to consideration of only a one-dimensional flow. The very same equations of state can be used in the analysis of a multidimensional flow. We shall adopt the equations of mass conservation of the water, steam, and air and the entropy conservation equation of the gaseous and liquid phases multiplied by the temperature of the corresponding phase as the initial point of our discussions:

$$\rho_L \left(\frac{\partial \alpha}{\partial \tau} + w_g \frac{\partial \alpha}{\partial z}\right) + \alpha \left(\frac{\partial \rho_L}{\partial \tau} + w_g \frac{\partial \rho_L}{\partial z}\right) + \alpha \rho_L \frac{\partial w_g}{\partial z} = 0; \tag{19}$$

$$\rho_D \left(\frac{\partial \alpha}{\partial \tau} + w_g \frac{\partial \alpha}{\partial z}\right) + \alpha \left(\frac{\partial \rho_D}{\partial \tau} + w_g \frac{\partial \rho_D}{\partial z}\right) + \alpha \rho_D \frac{\partial w_g}{\partial z} = \mu; \tag{20}$$

$$-\rho_f \left(\frac{\partial \alpha}{\partial \tau} + w_f \frac{\partial \alpha}{\partial z}\right) + (1-\alpha) \left(\frac{\partial \rho_f}{\partial \tau} + w_f \frac{\partial \rho_f}{\partial z}\right) + (1-\alpha) \rho_f \frac{\partial w_f}{\partial z} = -\mu; \tag{21}$$

$$\alpha \left[\rho_L \left(\frac{\partial h_L}{\partial \tau} + w_g \frac{\partial h_L}{\partial z}\right) + \rho_D \left(\frac{\partial h_D}{\partial \tau} + w_g \frac{\partial h_D}{\partial z}\right)\right] - \alpha \left(\frac{\partial p}{\partial \tau} + w_g \frac{\partial p}{\partial z}\right) = \tag{22}$$

$$= \dot{q}_g''' + \mu \left[h_{ex} - h_D + \Delta w_g (\bar{w}_g - w_g)\right];$$

$$(1-\alpha) \rho_f \left(\frac{\partial h_f}{\partial \tau} + w_f \frac{\partial h_f}{\partial z}\right) - (1-\alpha) \left(\frac{\partial p}{\partial \tau} + w_f \frac{\partial p}{\partial z}\right) = \dot{q}_f''' - \mu \left[h_{ex} - h_f + \Delta w_f (\bar{w}_f - w_f)\right]. \tag{23}$$

sibility of the liquid is completely justified:

$$\rho_f \approx \text{const.} \tag{24}$$

Equation (21) simplifies to

$$\frac{\partial \alpha}{\partial \tau} + w_f \frac{\partial \alpha}{\partial z} - (1-\alpha)\frac{\partial w_f}{\partial z} = \mu/\rho_f. \tag{25}$$

Eliminating $\partial\alpha/\partial\tau$ from Eqs. (19) and (21) and making use of the equation of state for elimination of the derivatives of the density and enthalpy, we shall solve the equations obtained with respect to the time derivatives. Then we obtain

$$\left\{\begin{aligned}
&\frac{\partial \rho_L}{\partial \tau} + w_g \frac{\partial \rho_L}{\partial z} + \Delta w \frac{\rho_L}{\alpha}\frac{\partial \alpha}{\partial z} + \rho_L \frac{\partial w_g}{\partial z} + \frac{1-\alpha}{\alpha}\rho_L \frac{\partial w_f}{\partial z} = -\mu \frac{\rho_L}{\alpha \rho_f}; && (26)\\
&\frac{\partial T_g}{\partial \tau} + w_g \frac{\partial T_g}{\partial z} - \Delta w A_g \frac{\partial \alpha}{\partial z} - \alpha A_g \frac{\partial w_g}{\partial z} - (1-\alpha) A_g \frac{\partial w_f}{\partial z} = B_g; && (27)\\
&\frac{\partial T_f}{\partial \tau} + w_f \frac{\partial T_f}{\partial z} - \Delta w A_f \frac{\partial \alpha}{\partial z} - \alpha A_f \frac{\partial w_g}{\partial z} - (1-\alpha) A_f \frac{\partial w_f}{\partial z} - \Delta w \frac{A_f}{\rho_g a^2}\frac{\partial p}{\partial z} = B_f; && (28)\\
&\frac{\partial p}{\partial \tau} + w_g \frac{\partial p}{\partial z} + \Delta w \rho_g a^2 \frac{\partial \alpha}{\partial z} + \alpha \rho_g a^2 \frac{\partial w_g}{\partial z} + (1-\alpha)\rho_g a^2 \frac{\partial w_f}{\partial z} = C; && (29)\\
&\frac{\partial \alpha}{\partial \tau} + w_f \frac{\partial \alpha}{\partial z} - (1-\alpha)\frac{\partial w_f}{\partial z} = -\mu/\rho_f, && (30)
\end{aligned}\right.$$

where

$$a = a_g/\alpha^{1/2}; \tag{31}$$

$$c_{pf} = \partial h_f/\partial T_f; \quad c_{pD} = \partial h_D/\partial T_g; \tag{32, 33}$$

$$\rho_g c_{pg} = \rho_L c_{pL} + \rho_D c_{pD}; \tag{34}$$

$$h_{pf} = \rho_f \frac{\partial h_f}{\partial p} - 1; \quad h_{pg} = \rho_D \frac{\partial h_D}{\partial p} - 1; \tag{35, 36}$$

$$\bar{\rho}_L = -\rho_L \frac{\partial h_D}{\partial \rho_L} = p_L \frac{\partial h_D}{\partial p_D}; \tag{37}$$

$$\rho_L^* = -\rho_L \frac{\partial \rho_D}{\partial \rho_L} = p_L \frac{\partial \rho_D}{\partial p_D}; \tag{38}$$

$$c_{pg}^* = \rho_g c_{pg}/(\partial \rho_D/\partial T_g); \tag{39}$$

$$\rho_g a_g^2 = [c_{pg}^*(\rho_D + \rho_L^*) - \rho_D \bar{\rho}_L] \Big/ \left(c_{pg}^* \frac{\partial \rho_D}{\partial p} - h_{pg}\right); \tag{40}$$

$$C = \frac{-\dot{q}_g''' - \mu[h_{ex} - h_D + \Delta w_g(\bar{w}_g - w_g) - \rho_D \bar{\rho}_L/\rho_f - c_{pg}^*(1-\rho_L^*/\rho_f)]}{\alpha\left(c_{pg}^* \frac{\partial \rho_D}{\partial p} - h_{pg}\right)}; \tag{41}$$

$$A_g = (-\rho_D \bar{\rho}_L + \alpha h_{pg} \rho_g a^2)/(\alpha \rho_g c_{pg}); \tag{42}$$

$$A_f = h_{pf} \rho_g a^2/(\rho_f c_{pf}); \tag{43}$$

$$B_g = \{\dot{q}_g''' + \mu[h_{ex} - h_D + \Delta w_g(\bar{w}_g - w_g) - \rho_D \bar{\rho}_L/\rho_f] - \alpha h_{pg} C\}/(\alpha \rho_g c_{pg}); \tag{44}$$

$$B_f = \{\dot{q}_f''' - \mu[h_{ex} - h_f + \Delta w_f(\bar{w}_f - w_f) - (1-\alpha) h_{pf} C\}/[(1-\alpha)\rho_f c_{pf}]. \tag{45}$$

No assumptions of any kind have been made up to now about exchange of momentum between the two phases. Equations (26)-(30) are valid independently of further assumptions about the interphase force interaction.

The authors of [6] have assumed in their description of pneumatic transporting of a solid monodisperse phase that the pressure acts only in the gaseous phase and the solid phase is carried away by the gas by means of mechanical interaction. Thus, the pressure gradient appears only in the equation of momentum conservation of the gaseous phase. This idea has been used in [7] to describe a two-phase one-component flow in which the gaseous phase carries away the dispersed liquid. The author of [8] used this idea to describe a one-component flow consisting of both a continuous gaseous phase and a dispersed liquid and of a continuous liquid and a dispersed gaseous phase. We shall consider these cases for a two-component flow.

liquid:

$$\frac{\partial w_g}{\partial \tau} + w_g \frac{\partial w_g}{\partial z} + \frac{1}{\alpha \rho_g} \frac{\partial p}{\partial z} = -Z_g/(\alpha \rho_g);$$

$$Z_g = \alpha \rho_g g \cos \varphi + f_{Rg}; \tag{46, 47}$$

$$\frac{\partial w_f}{\partial \tau} + w_f \frac{\partial w_f}{\partial z} = -Z_f/[(1-\alpha)\rho_f];$$

$$Z_f = (1-\alpha)\rho_f g \cos \varphi + f_{Rf}. \tag{48, 49}$$

These equations together with Eqs. (26)-(30) completely describe the flow when the vector of dependent variables

$$\mathbf{U}^T = (\rho_L,\ T_g,\ T_f,\ p,\ w_g,\ w_f,\ \alpha)$$

is used.

We obtain

$$\lambda_{1,2} = w_g; \quad \lambda_3 = w_f; \quad \lambda_{4,5} = w_g \pm a; \quad \lambda_{6,7} = w_f, \tag{50-56}$$

for the eigenvalues of the characteristic matrix of the system, where

$$a = a_g/\alpha^{1/2} - \tag{57}$$

is the speed of sound and $\lambda_{4,5}$ characterize the propagation velocity of a pressure perturbation and the velocity of the gas.

2. For a bubble flow the system takes on the following form:

$$\left\{\begin{array}{l} \cdot\ \cdot\ \cdot\ \cdot \qquad (26) \\ \cdot\ \cdot\ \cdot\ \cdot \qquad (27) \\ \cdot\ \cdot\ \cdot\ \cdot \qquad (28) \\ \cdot\ \cdot\ \cdot\ \cdot \qquad (29) \\ \dfrac{\partial w_g}{\partial \tau} + w_g \dfrac{\partial w_g}{\partial z} = -Z_g/(\alpha \rho_g); \qquad (58) \\ \dfrac{\partial w_f}{\partial \tau} + w_f \dfrac{\partial w_f}{\partial z} + \dfrac{1}{(1-\alpha)\rho_f} \dfrac{\partial p}{\partial z} = -Z_f/[(1-\alpha)\rho_f]; \qquad (59) \\ \cdot\ \cdot\ \cdot \qquad (30) \end{array}\right.$$

$$\lambda_{1,2} = w_g; \quad \lambda_3 = w_f; \quad \lambda_4 = w_f + a; \quad \lambda_5 = w_g;$$
$$\lambda_6 = w_f - a; \quad \lambda_7 = w_f, \tag{60-65}$$

where

$$a = a_g \Big/ \left(\frac{\rho_f}{\rho_g}\alpha\right)^{1/2} \tag{66}$$

is the speed of sound and $\lambda_{4,6}$ characterize the propagation velocity of a pressure perturbation and the velocity of the liquid.

Let us consider the limiting case of a homogeneous flow when $\Delta w = 0$, $w_g = w_f = w$. It is convenient to adopt

$$\mathbf{U}^T = (\rho_L,\ T_g,\ T_f,\ \rho,\ p,\ w). \tag{67}$$

as the vector of dependent variables. We write instead of Eq. (30) the equation of mass conservation of a two-phase flow. It is noteworthy that the assumption of incompressibility of the liquid is absent from this equation:

$$\frac{\partial \rho_L}{\partial \tau} + w \frac{\partial \rho_L}{\partial z} + \frac{\rho_L \partial w}{\alpha \partial z} = -\mu \frac{\rho_L}{\alpha \rho_f}; \tag{68}$$

$$\frac{\partial T_g}{\partial \tau} + w \frac{\partial T_g}{\partial z} - A_g \frac{\partial w}{\partial z} = B_g; \tag{69}$$

$$\left\{\begin{array}{l} \dfrac{\partial T_f}{\partial \tau} + w \dfrac{\partial T_f}{\partial z} - A_f \dfrac{\partial w}{\partial z} = B_f; \qquad (70) \\ \dfrac{\partial p}{\partial \tau} + w \dfrac{\partial p}{\partial z} + \rho a^2 \dfrac{\partial w}{\partial z} = C; \qquad (71) \end{array}\right.$$

$$\frac{\partial w}{\partial \tau} + w\frac{\partial w}{\partial z} + \frac{1}{\rho}\frac{\partial p}{\partial z} = -Z/\rho; \tag{72}$$

$$\frac{\partial \rho}{\partial \tau} + w\frac{\partial \rho}{\partial z} + \rho\frac{\partial w}{\partial z} = 0. \tag{73}$$

This system of equations has already been derived and investigated by the author in [5]. The eigenvalues of the characteristic matrix of this system are [5]

$$\lambda_{1,2,3,6} = w;\ \lambda_{4,5} = w \pm a, \text{ where}$$
$$a = a_g \Big/ \left(\frac{\rho}{\rho_g}\alpha\right)^{1/2}. \tag{74-80}$$

Thus, we have obtained for the case under discussion hyperbolic systems of quasilinear inhomogeneous partial differential equations. It is not difficult with the help of the eigenvalues to obtain linearly independent eigenvectors and to impart a canonical form to the system. One can use it immediately to construct a numerical solution by applying the method of characteristics or any of its modifications with specified initial and boundary conditions.

Applicability of the Models. It is necessary to answer an important question about the region of application of each of these three systems of equations. If the assumption of incompressibility of the liquid was not made, we would obtain Eqs. (81)-(83) for the speed of sound. A rigorous derivation of these equations is given in [9], in which they are a particular case of a three-phase three-component flow with the solid phase missing. The conclusions are very extensive; therefore, we shall restrict ourselves here to just recording them. Assuming $a_f \to \infty$, we obtain Eqs. (57), (66), and (80):

$$a^{-2} = \rho_g\left(\frac{\alpha}{\rho_g a_g^2} + \frac{1-\alpha}{\rho_f a_f^2}\right) \quad (81);\ a^{-2} = \rho_g\frac{\alpha}{\rho_g a_g^2} \tag{57}$$

$$a^{-2} = \rho_f\left(\frac{\alpha}{\rho_g a_g^2} + \frac{1-\alpha}{\rho_f a_f^2}\right) \quad (82);\ a^{-2} = \rho_f\frac{\alpha}{\rho_g a_g^2}; \tag{66}$$

$$a^{-2} = \rho\left(\frac{\alpha}{\rho_g a_g^2} + \frac{1-\alpha}{\rho_f a_f^2}\right) \quad (83);\ a^{-2} = \rho\frac{\alpha}{\rho_g a_g^2}. \tag{80}$$

Equation (83) is similar in its form to an equation of [10]; only the physical content of the speed of sound of the gaseous phase, determined with the help of Eq. (40), was changed. Similar equations of the type (57) and (66) are obtained in [8] for a noncomponent medium. The numerical results obtained from Eqs. (57), (66), and (80) for the very same parameters differ. This shows that it is important to take into account the structure of a flow when describing its dynamic qualities, which is in agreement with the experiment described in [1]. In this paper they measured the propagation of acoustic perturbations in a water–air flow at a pressure of 1.778 bars (1 bar = 10^5 Pa) and a temperature of 293.5°K as a function of the true volume steam content for different flow structures (see Fig. 1). The results for a homogeneous flow are in good agreement with Eq. (80). One can conclude from this that the homogeneous model (68-73) is applicable over the entire range of variations of α:

$$\alpha^* < \alpha \leqslant 1, \tag{84}$$

where

$$\alpha^* = 1 - \left[1 - 4\left(1 - \frac{\rho_g}{\rho_f}\right)\frac{\rho_g a_g^2}{\rho_f a_f^2}\right]^{-1/2} \Big/ [2(1 - \rho_g/\rho_f)]\ [5] \tag{85}$$

is the lower limit of applicability of the model obtained under the assumption of incompressibility of the liquid. Equation (85) gives very low values of α^*, lower by far than the natural volume content of air dissolved in commercial water.

The inhomogeneous model of a bubble flow gives good agreement with experiment for a speed of sound $\alpha \approx 0.5$. This value is the upper limit of applicability of the model and is in good agreement with the value $\alpha = 0.492$ indicated in [12] from geometrical concepts.

Comparing the speed of sound obtained from Eq. (57) for an inhomogeneous drop flow with the data of [11] for a projectile flow, we obtain good agreement for $\alpha > 0.1$.

The results of [13] confirm experimentally the results of [11] for projectile flow, for which a few "liquid–gas" pairs are contained per unit length of the pipe. The values obtained in [13] for the speed of sound for a large number of these pairs are identical with the results

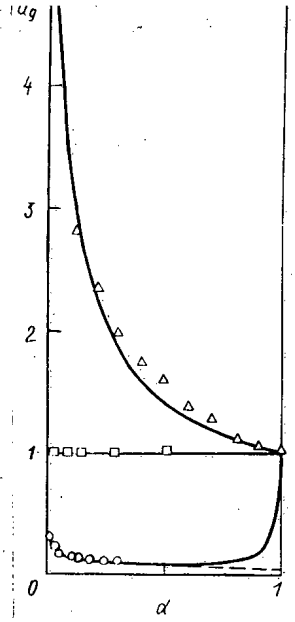

Fig. 1. A comparison of the calculated relative speed of sound in a two-phase flow with that obtained experimentally as a function of the true volume steam content for different flow structures: Δ) projectile flow ($a/a_g = 1/\alpha^{1/2}$); □) annular (stratified) flow; ○) bubble flow $[a/a_g = 1/\left(\frac{\rho}{\rho_g}\alpha\right)\alpha^{1/2}]$; and - - -) $a/a_g = 1/\left(\frac{\rho_f}{\rho_g}\alpha\right)^{1/2}$.

for a homogeneous mixture. The detected agreement offers grounds for advancing a suggestion about the similarity of the mechanism of propagation of acoustic perturbations in a projectile and a highly inhomogeneous flow with drop structure. And nevertheless the question of the applicability of the model (Eqs. 26-29, 46, 48, and 30) for projectile flow or for a highly inhomogeneous drop flow requires experimental demonstration.

As an alternative method for the description of an inhomogeneous two-component flow, one can use Eqs. (26)-(30) together with the momentum conservation equation for a two-phase flow:

$$\frac{\partial G}{\partial \tau} + \frac{\partial}{\partial z}(v_I G^2) + \frac{\partial p}{\partial z} = -Z;\ Z = \rho g \cos\varphi + R, \tag{86}$$

where

$$v_I = [S^2\alpha\rho_g + (1-\alpha)\rho_f]/\rho_S; \tag{87}$$

$$\rho_S = S\alpha\rho_g + (1-\alpha)\rho_f. \tag{88}$$

It is necessary to use an empirical correlation for taking account of phase slipping. One can select

$$\mathbf{U}^T = (\rho_L,\ T_g,\ T_f,\ p,\ \alpha,\ G) \tag{89}$$

as the vector of dependent variables. Solving Eqs. (86) by numerical means for $G_z^{\tau+\Delta\tau}$ with known values of $(p,\ v_I,\ Z)_z^{\tau}$ using some explicit or implicit method, we obtain

$$w_g = SG/\rho_S;\ w_f = G/\rho_S;$$
$$\Delta = \alpha\frac{\Delta w_g}{\Delta z} + (1-\alpha)\frac{\Delta w_f}{\Delta Z}. \tag{90-92}$$

Then one can write the system (26)-(30) as follows:

$$\begin{cases} \frac{\partial \rho_L}{\partial \tau} + w_g\frac{\partial \rho_L}{\partial z} + \Delta w\frac{\rho_L}{\alpha}\frac{\partial \alpha}{\partial z} = -\frac{\rho_L}{\alpha}\left(\frac{\mu}{\rho_f} + \Delta\right); & (93) \\ \frac{\partial T_g}{\partial \tau} + w_g\frac{\partial T_g}{\partial z} - \Delta w A_g\frac{\partial \alpha}{\partial z} = B_g + A_g\Delta; & (94) \end{cases}$$

$$\frac{\partial I_f}{\partial \tau} + w_f \frac{\partial I_f}{\partial z} - \Delta w A_f \frac{\partial \alpha}{\partial z} - \Delta w A_f \frac{\alpha}{\rho_g a_g^2} \frac{\partial p}{\partial z} = B_f + A_f \Delta; \quad (95)$$

$$\frac{\partial p}{\partial \tau} + w_g \frac{\partial p}{\partial z} + \Delta w \frac{\rho_g a_g^2}{\alpha} \frac{\partial \alpha}{\partial z} = C - \frac{\rho_g a_g^2}{\alpha} \Delta; \quad (96)$$

$$\frac{\partial \alpha}{\partial \tau} + w_f \frac{\partial \alpha}{\partial z} = -\frac{\mu}{\rho_f} + (1-\alpha) \frac{\Delta w_f}{\Delta z} \quad (97)$$

and solve it numerically by some means. If an explicit scheme is used for solution of the system (93)-(97), the constraint on the time step is not rigorous:

$$\Delta \tau < \min \left[\frac{\Delta z}{\max (|w_g|, |w_f|)} \right]_j. \quad (98)$$

Conclusion. Four models have been suggested for the description of a one-dimensional flow with a water—steam—air makeup in a system for accident localization from coolant losses, and three have been suggested with proven hyperbolic properties. The region of application of the homogeneous model and the inhomogeneous model using a correlation for phase sliding is practically the entire two-phase region. The proposed bubble-flow model is applicable up to $\alpha \leq 0.5$.

It is necessary to determine experimentally the region of application of the model of a highly inhomogeneous dispersed flow made up of air and gas, since the expression obtained for the speed of sound in this flow coincides with the speed of sound in a flow with projectile structure.

It is not difficult to obtain steady systems from the three hyperbolic systems of equations. Solving them with respect to the spatial derivatives, one can obtain an expression for the critical mass flow density.

NOTATION

A, area; a, speed of sound; c_p, specific heat at constant pressure; f_R, drag force referred to unit volume of the flow; G, density of the mass flow; g, gravitational acceleration; h, specific enthalpy; p, pressure; $\dot{q}'''$, thermal power referred to unit volume of the flow; R, gas constant; T, absolute temperature; w, velocity; $\bar{w} = (w_g = w_f)/2$; $\Delta w_j = (w_{ex} - w_j)$; z, linear coordinate; φ, angular coordinate; α, volume gas content; Δ, finite difference, ∂, partial differential; λ, eigenvalue; μ, rate of phase transitions; ρ, density; τ, time.

SUBSCRIPTS

L, air; D, steam; f, water; g, gas; ex, phase which yields mass; p, T, ρ..., const p, T, ρ...; I, impulse equation.

LITERATURE CITED

1. C. Broadus, BEACON/MOD2, A CDC-7600 Computer Program for Analyzing the Flow of Mixed Air, Steam, and Water in a Containment System, INEL, CDAP-TR-002 (1977).
2. N. Kolev, "Transient two-phase two-component flow of water—steam—air," Nucl. Sci. Eng., No. 85, 209 (1983).
3. N. Kolev, "Critical equilibrium inhomogeneous two-phase two-component water—steam—air flow," Int. J. Heat Mass Transfer, 25, No. 12, 1879 (1982).
4. N. Kolev, "Transient nonhomogeneous equilibrium water—steam—air flow," Nucl. Sci. Eng., No. 74, 265 (1982).
5. N. Kolev, "Transient inhomogeneous two-phase two-component flow composed of water—steam—air under conditions of thermodynamic nonequilibrium," Atomkernenergie/Kerntechnik, 42, No. 3, 201 (1983).
6. G. Rudinger and A. Chang, "Analysis of nonsteady two-phase flow," Phys. Fluids, 7, 1747 (1964).
7. R. Liczkowski, "Transient propagation behavior of two-phase flow equations," Presented at the 15th National Heat Transfer Conference, San Francisco, 10-13 August 1975, AIChE Paper No. 41.
8. N. Kolev, "A contribution to the theory of transient inhomogeneous two-phase flow under conditions of thermodynamic nonequilibrium," Kernenergie, 25, No. 4, 170 (1982).
9. N. Kolev, Transient Three-Phase Three-Component Nonequilibrium Nonhomogeneous Flow, NED (1984).

10. ... Two-Phase Flow, McGraw-Hill, New York (1969).
11. F. Moody, "A pressure-pulse model for two-phase critical flow and sonic velocity," J. Heat Transfer, 84 (1968).
12. G. V. Tsiklauri, V. S. Danilin, and L. I. Seleznev, Adiabatic Two-Phase Flows [in Russian], Atomizdat, Moscow (1973).
13. G. Matsui and S. Arimoto, "Propagation characteristics of a pressure wave through a gas-liquid plug-train system in a pipe," in: Proc. Joint Symp. on Design and Operation of Fluid Machinery, Colorado State University, Fort Collins, 12-14 June 1978.

BUILDUP OF RADIONUCLIDES IN NICKEL AS THE RESULT OF ELECTRON AND γ IRRADIATION

N. L. Emets, V. G. Batii,
Yu. V. Vladimirov, Yu. N. Ranyuk,
E. A. Shakun, and V. A. Yamnitskii

UDC 539.172.2

Beams of high-energy electrons and γ quanta find a wide application in activation analysis and also in the simulation of the action of fast neutrons on materials [1]. The development in targets of electron photon showers leads to the appearance in the body of the sample of high-energy γ quanta, the interaction of which with the target material mainly is similar to the interaction of neutrons [2], in particular, in the buildup of helium. The relation between the helium buildup and the amount of primary radiation defects for different parts of the sample is found to be close to that obtained during irradiation in different reactors.

At the same time, the irradiation of materials with γ quanta has its special features by comparison with neutron irradiation, first of all in the buildup of residual nuclei. It is well known [2] that the mass spectrum of the products of nuclear reactions in the case of γ irradiation is significantly broader than in the case of irradiation with neutrons. This should be taken into consideration in simulation experiments, for example, in the selection of the energy of the primary electron beam. During irradiation with a beam of electrons, radioactive nuclei will be built up as a result of reactions caused both by bremsstrahlung photons and by electrons, especially in the surface layer of the samples.

The calculated values of the formation of primary defects and the buildup of helium coincides well with those obtained in the corresponding direct experiments. However, in the region of medium energy values, a definite inadequacy is observed of experimental data about the yields of radionuclides during electron and γ irradiation of structural materials used in accelerator and reactor technology.

In the light of this, the yields of Ni and Co nuclides during the irradiation of a target of natural nickel were determined (Table 1). Their reactions of formation are shown for a given primary contribution of the interaction of photons with ^{58}Ni nuclei.

An assembly of three targets in the form of chemically pure nickel foils, with a thickness of 50 + 300 + 50 μm, was irradiated in the LUÉ-300 linear accelerator of the Khar'kov Physicotechnical Institute, Academy of Sciences of the Ukrainian SSR. The yields of nuclides from the electrodisintegration of Ni were determined from the activity of the first target, directly irradiated with the electron beam (the contribution due to photoactivation with the γ quanta generated in the target itself, did not exceed a few percent). The second target (300 μm) was used as the converter. The activity of the third target exceeded the activity of the second target by a factor of two approximately, i.e., the contribution due to electro- and photonuclear reactions was approximately identical. With this target thickness, the photons make an appreciable contribution to activation, and the electron beam is almost unattenuated which, with good accuracy, allows the yields of the photonuclear reactions to be determined. The absolute intensity of the electron beam was measured with a secondary emission delta-electron monitor.

Irradiation was carried out during 2 h in a vacuum chamber joined directly with the accelerator. The purity of the electron beam was ensured by means of a parallel transfer system. The size of the beam at the target was ~4-6 mm, with an average current of ~2 μA and an energy spread of ±0.6%. The γ-activity was measured with a Ge(Li)-detector with a volume of ~40 cm^3 and a resolution of 3.5 keV.

The independent yields σ of the Ni isotopes and the cumulative yield of ^{55}Co were determined by the formula

$$N=\frac{1}{\lambda}K\sigma(1-e^{-\lambda t_{irr}})e^{-\lambda t_{hold}}(1-e^{-\lambda t_{m}}),$$

Translated from Atomnaya Énergiya, Vol. 57, No. 4, pp. 278-279, October, 1984. Original article submitted November 23, 1983.

 0038-531X/84/5704-0742$08.50

TABLE 1. Ni and Co Nuclides, Formed during the Irradiation of Natural Nickel

Nuclide	Half-life	Transition energy, keV	Reaction	Type of yield
^{57}Ni	35,99 h	1378	(γ, n)	Independent
^{56}Ni	6,1 d	158	$(\gamma, 2n)$	Same
^{57}Co	271,65 d	122	(γ, p)	» »
^{56}Co	78,76 d	847	(γ, pn)	» »
^{55}Co	17,54 h	931	$(\gamma, p2n)$	Cumulative

TABLE 2. Yields of Radionuclides

Nuclide	E, MeV					
	100	125	150	175	200	225
^{57}Ni	11,6* / 8,9	12,1 / 9,1	10,2 / 9,2	8,0 / 9,4	10,6 / 9,4	12,0 / —
^{56}Ni	1,14 / —	1,22 / —	1,07 / 1,26	1,21 / 1,36	1,39 / —	— / —
^{57}Co	23,9 / 23,3	18,0 / 23,8	25,0 / 24,1	32,8 / 24,4	26,4 / 24,6	— / —
^{56}Co	2,48 / 0,71	0,75 / 0,88	1,05 / 0,95	0,75 / 1,13	1,39 / 1,22	2,3 / —
^{55}Co	0,25 / 0,44	0,29 / 0,54	0,39 / 0,60	0,39 / 0,72	1,34 / 0,77	0,62 / —

*The experimental value is given in the numerator and the calculated value in the denominator.

where N is the number of recorded γ transitions; λ is the radioactive decay constant of the given isotope; K is a coefficient, taking account of the detector efficiency, sample thickness, electron flux, and branching coefficients in the decay scheme; t_{irr}, t_{hold}, and t_m are the times of irradiation, holding, and measurement, respectively.

The independent yields of ^{56}Co and ^{57}Co were found by means of the equation

$$N = K\left\{\sigma_p \frac{\lambda_p\lambda_d}{\lambda_d-\lambda_p}\left[\frac{1-e^{-\lambda_p t_{irr}}}{\lambda_p^2}(1-e^{-\lambda_p t_m})e^{-\lambda_p t_{hold}}+\frac{1-e^{-\lambda_d t_{irr}}}{\lambda_d^2}(1-e^{-\lambda_d t_m})e^{-\lambda_d t_{hold}}\right]+\right.$$
$$\left.+\sigma_d\frac{1-e^{-\lambda_d t_m}}{\lambda_d}(1-e^{-\lambda_d t_m})e^{-\lambda_d t_{hold}}\right\},$$

where σ_p is the yield of the parent nuclei (^{56}Ni or ^{57}Ni); σ_d is the yield of daughter nuclei (^{56}Co or ^{57}Co), and λ_d are the corresponding radioactive constants.

Figure 1 shows the compatible theoretical and experimental values of the photonuclear (σ_Q) and the electronuclear (σ_e) reactions leading to the formation of ^{57}Co and ^{57}Ni. The yields of ^{57}Ni for energies of 40 and 80 MeV are taken from [3]. The calculated values of the yields of radioactive nuclei in the case of photospallation (solid line) were obtained with the use of programs [4, 5] for a cascade and boil-off model of the nucleus, which occurs in the composition of the IMITATOR program complex [6]. For the calculation of the yields by electrospallation of the nuclei (dashed lines), the semiempirical formula [7]

$$\frac{\sigma_Q}{\sigma_e}=\frac{\pi}{2\alpha}\left[\ln\frac{E}{0.511}-0.51\right]^{-1} \quad (1)$$

was used, where E is the energy of the electrons: α = 1/137.

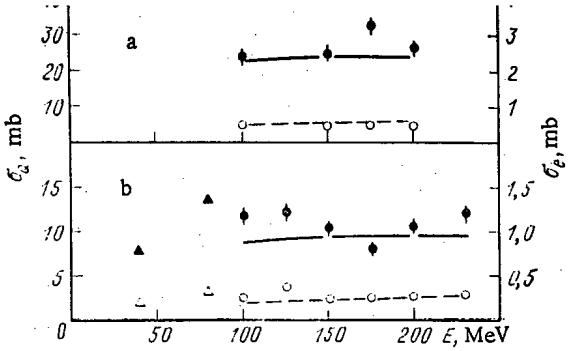

Fig. 1. Theoretical (—, - - -) and experimental profile of the formation of ^{57}Co (a) and ^{57}Ni (b) in reactions with electrons (○) and photons (●) in relation to the initial electron energies: ▲, △) experimental data from [3].

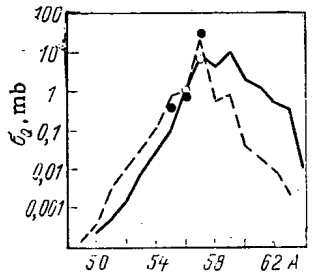

Fig. 2

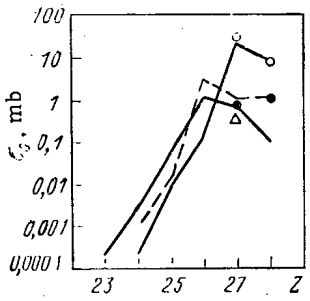

Fig. 3

Fig. 2. Experimental yields of Co (●, Z = 27) and Ni (○, Z = 28), and the calculated mass distributions of the nuclides (——, ---), with the $E_{\gamma max}$ = 175 MeV.

Fig. 3. Theoretically calculated (——, ---) and experimental charge distributions of the isotopes for $E_{\gamma max}$ = 175 MeV: △) A - 55; ●) A = 56; ○) A = 57.

It follows from Table 2 that there is satisfactory agreement between the experimental (with an error of ~10%) and theoretical yields of the nucleides Ni and Co in photon nuclear reactions.

Figure 2 shows the dependence of the yields of Ni and Co nuclides on the mass number during the irradiation of natural nickel with bremsstrahlung γ-quanta with $E_{\gamma max}$ = 175 MeV. The charge distribution of the isobar yields for A = 55, 56, and 57 (Fig. 3) indicates an appreciable excess of the yield of the (γ, p) reaction by comparison with the yield of the (γ, n) reaction, also mentioned earlier [8].

The satisfactory agreement between the experimental and theoretical data confirms the justification of the model approach for the calculation of the buildup of nuclei-residue in simulation experiments, and the feasibility of using the semiempirical formula (1) for calculating the contribution of the electronuclear reactions. From a comparison of the experimental and theoretical reaction yields for (γ, n), (γ, 2n), and (γ, pn), it follows that the IMITATOR program complex allows the yields of neutrons and other particles to be calculated, and the buildup of radionuclides to be calculated in structural materials, under the action of high-energy electrons and γ quanta.

LITERATURE CITED

1. V. F. Zelenskii et al., Problems of Nuclear Science and Technology, Series Physics of Radiation Damage and Radiation Material Behavior [in Russian], No. 1 (2) (1975), p. 8.
2. V. V. Gann et al., Problems of Nuclear Science and Technology. Series Physics of Radiation Damage and Radiation Material Behavior [in Russian], No. 2 (16), 14 (1981).

3. G. Brinkman et al., Int. J. Appl. Rad. Isotopes, 32, 13 (1981).
4. N. L. Emets et al., Preprint Kharkov Physicotechnical Institute 72-37 [in Russian], Kharkov (1972).
5. N. L. Emets and Yu. N. Ranyuk, Problems of Nuclear Science and Technology. Series Physics of Radiation Damage and Material Behavior [in Russian], No. 1(9), 31 (1979).
6. V. V. Gann, A. M. Vaisfeld, and V. A. Yamnitskii, Problems of Nuclear Science and Technology, Series Technology of Physics Experiment [in Russian], No. 1(5) (1980), p. 20.
7. V. I. Noga, Yu. N. Ranyuk, and P. V. Sorokin, Yad. Fiz., 19, 945 (1974).
8. G. V. Arustamyan et al., Yad. Fiz., 32, 1165 (1980).

CALCULATION OF THE ABSORBED DOSE OF ELECTRON BREMSSTRAHLUNG

V. I. Isaev and V. P. Kovalev

UDC 539.163:539.124

In order to estimate the radiation conditions in electron accelerator work, it is necessary to know the absorbed bremsstrahlung dose. We have derived an analytical expression for the absorbed dose whereby it can be calculated rapidly in the 10-100-MeV energy range.

The absorbed γ-radiation dose rate is determined by the expression

$$P_\gamma = B \int_0^\infty N(E)\, E_\mu(E)\, dE, \tag{1}$$

where N (E) is the γ-radiation spectrum, E is the photon energy (MeV), μ(E) is the electron conversion coefficient or the mass coefficient of actual γ-radiation energy absorption in air or in biological tissue ($cm^2 \cdot g^{-1}$), B is the normalizing factor ($B = (1.6 \cdot 10^{-6}/100)K$), $1.6 \cdot 10^{-6}$ $erg \cdot MeV^{-1}$ is the factor which converts the absorbed energy, measured in MeV units, into energy measured in erg units, 100 $erg \cdot rd^{-1}$ is the energy equivalent of 1 rd, and K is the quality factor of β radiation (1 erg = $1 \cdot 10^{-7}$ J).

The spectrum of electron bremsstrahlung is continuous and occupies the energy range from zero to E_0, where E_0 is the upper boundary value of the energy spectrum, equal to the initial value of the electron energy. For angles of up to 90°, the bremsstrahlung spectrum is defined by

$$N(E_0, T, \theta, E) = \frac{2JI(E_0, T, \theta)}{E_0 R^2}\left(\frac{1}{E} - \frac{1}{E_0}\right), \tag{2}$$

where J (E_0, T, θ) is the intensity of bremsstrahlung emitted in the given direction θ per unit solid angle ($MeV \cdot sr^{-1}$), J is the number of electrons at the target, R is the distance between the target and the point for which the dose is calculated, and T is the target thickness ($g \cdot cm^{-2}$).

The values of the coefficients of actual photon absorption in water, air, and biological tissue are close to each other. In the energy range from 1 to 100 MeV, they can be represented with an indeterminacy of a few percent by the expression

$$\mu(E) = \frac{0.15}{1+10E} + 0.015. \tag{3}$$

Substituting Eqs. (2) and (3) in expression (1), we obtain

$$P_\gamma(E_0, T, \theta)\, d\Omega = \frac{0.03BJI(E_0, T, \theta)}{E_0 R^2}(E_0/2 + \ln E_0 + 1.3)\, d\Omega. \tag{4}$$

The theoretical expression for the absorbed bremsstrahlung dose for an electron current at the target of 1 mA at a distance of 1 m from the target over a period of 1 min is given by

$$P_\gamma(E_0, T, \theta)\, d\Omega = \frac{1.8 \cdot 10^4 I(E_0, T, \theta)}{E_0 R^2}(E_0/2 + \ln E_0 + 1.3), \tag{5}$$

where the values of I(E_0, T, θ) can be borrowed from [2].

Translated from Atomnaya Énergiya, Vol. 57, No. 4, pp. 280-281, October, 1984. Original article submitted January 13, 1984.

0038-531X/84/5704-0745$08.50

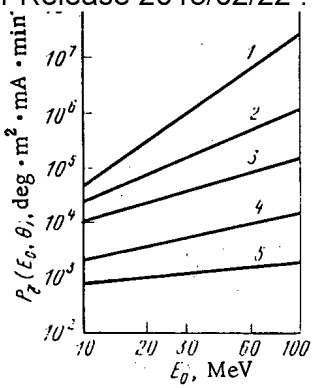

Fig. 1. Dose rate of bremsstrahlung in air from a target with the optimum thickness for the assigned direction as a function of the electron energy E_0. 1) 0°; 2) 10°; 3) 30°; 4) 90°; 5) 180°.

TABLE 1. Absorbed Dose Rate in Air (tungsten–uranium target) (rd·m²/(mA·min))

Angle, deg	10 MeV	30 MeV	60 MeV	100 MeV
	1.55 g·cm^{-2}	5.04 g·cm^{-2}	7.25 g·cm^{-2}	9.95 g·cm^{-2}
0	$4{,}24\cdot10^4$	$8{,}10\cdot10^5$	$5{,}60\cdot10^6$	$2{,}23\cdot10^7$
10	$2{,}39\cdot10^4$	$1{,}86\cdot10^5$	$5{,}25\cdot10^5$	$9{,}63\cdot10^5$
30	$9{,}16\cdot10^3$	$4{,}10\cdot10^4$	$8{,}27\cdot10^4$	$1{,}26\cdot10^5$
60	$3{,}68\cdot10^3$	$1{,}16\cdot10^4$	$2{,}41\cdot10^4$	$2{,}60\cdot10^4$
80	$2{,}00\cdot10^3$	$3{,}65\cdot10^3$	$3{,}36\cdot10^3$	$3{,}36\cdot10^3$
90	0	0	0	0
120	$6{,}00\cdot10^2$	$1{,}71\cdot10^3$	$1{,}15\cdot10^3$	--
150	$5{,}00\cdot10^2$	$1{,}44\cdot10^3$	$1{,}08\cdot10^3$	—

Table 1 provides the dose fields of bremsstrahlung for a plane-parallel plate made of heavy elements (tungsten–uranium) with infinitely large transverse dimensions.

In the forward direction, the absorbed dose rate is expressed by the equation

$$P_\gamma(E_0) = 81E_0^{2.72}. \quad (6)$$

A relationship close to the above one was described in [3]:

$$P_\gamma(E_0) = 82E_0^{2.63}.$$

The discrepancy can be explained by the inaccuracy of the approximation (40%) used in [3].

In evaluating the radiation situation at electron accelerators, it is important to know the maximum value of the dose of bremsstrahlung emitted in a given direction θ. Figure 1 shows the values of the absorbed dose rate in air of bremsstrahlung from heavy targets (tungsten–uranium), calculated by means of Eq. (4). In the forward direction, the dose rate varies in conformity with expression (6), while the dependence of the dose rate on the electron energy diminishes as the angle increases. At 90° the exponent is equal to 0.91, while at 180, it is equal to 0.41.

In certain cases, it is necessary to know the percentage composition of the dose. An expression for the percentage composition of the dose can be derived from Eq. (4) in the following manner. We use the following integration limits in this expression: E_1 for the lower limit, and E_2 for the upper limit; we have thereby assigned the required energy range. Then, by performing operations similar to those in deriving the expression for the general dose, we obtain an expression for the photon dose in the given energy range (E_1, E_2), and we divide it by the total dose value (4):

$$\delta_i = \left[\ln \frac{1+10E_2}{1+10E_1} + \frac{\Delta E}{2E_0} (2E_0 - 2 - E_2 - E_1) \right] \Big/ \left(\ln E_0 + \frac{E_0}{2} + 1.3 \right) \Big| 100. \quad (7)$$

Expression (7) characterizes the contribution (on a percentage basis) of the dose in the (E_1, E_2) photon energy range to the total dose value in the range from 0 to E_0.

LITERATURE CITED

1. Yu. A. Egorov, Fundamentals of Radiation Safety for Atomic Electric Power Plants [in Russian], Énergoatomizdat, Moscow (1982).
2. M. Berger and S. Seltzer, Phys. Rev., 2, 621 (1970).
3. V. I. Tsovbun, JINR Report 16-7104, Dubna (1983).

TRITIUM BALANCE IN THE BALTIC SEA DURING THE YEARS 1972-1982

S. M. Bakulovskii and I. Yu. Katrich

UDC 502.55(261.24):546.11*3

As a result of systematic observations of the tritium content of the waters of the Baltic Sea, in the rivers flowing into the Baltic, and in the atmospheric precipitation at points situated along its coasts [1-3], researchers have accumulated experimental data which make it possible to estimate the balance components of the tritium content of the sea and the relationships among them.

The balance equation for an arbitrary interval of time, assuming no large sources of local input of tritium into the Baltic Sea, has the following form:

$$V^i_{pr} C^i_{pr} + V^i_r C^i_r + V^i_{in} C^i_{in} + \frac{V^i_{evap} f^i}{1-f^i} C^i_{atm} = V^i_{out} C^i_{out} + \frac{V^i_{evap}}{1-f^i} C^i_{b.s},$$

where $V^i_{pr}C^i_{pr}$, $V^i_rC^i_r$, $V^i_{in}C^i_{in}$, and $V^i_{out}C^i_{out}$ are, respectively, the amounts of tritium entering the sea with the atmospheric precipitation, with the river discharges, and with the inflows into the sea and the outflows from it. $(V^i_{evap}f^i/1 - f^i)C^i_{atm}$ is the amount of tritium entering the sea as a result of the exchange of moisture between the atmospheric and the sea surface: $(V_{evap}/1 - f^i)C^i_{BS}$ is the amount of tritium leaving the sea as a result of the exchange between the atmosphere and the water surface of the sea; C^i_{BS} is the concentration of tritium in the surface water of the Baltic Sea; f^i is the relative humidity of the atmosphere near the water surface [4].

For convenience of calculation, we shall subdivide the time interval under consideration into one-year periods, and in estimating the balance components, we shall use the annual averages of the tritium concentration in the sea water, the river water, and the rain water. To simplify the calculations, we assume that the volumes of water are constant and equal to their multiyear averages. We shall also assume on the basis of [5, 6] that the annual average concentrations of tritium in the atmosphere mositure (C^i_{atm}) and the in the atmospheric precipitation (C^i_{pr}) are equal, i.e., we shall disregard the coefficient of fractionation of tritium in the phase transitions, which is equal to 1.11-1.09 in the 15-30°C range. We shall regard as equal the concentrations of tritium in the surface water of the sea, in the evaporating moisture, and in the outflow into adjacent bodies of water. As the values of the annual average concentration of tritium in the aqueous components of the balance for the Baltic Sea in 1972-1982, we used the data of [1-3, 7-9]. The tritium concentration taken for the calculations is shown in Table 1. The water-balance components are taken from [4]. Calculations of the tritium balance performed according to the equation given above showed that during the period under consideration $200 \cdot 10^{15}$ Bq of tritium entered the Baltic and $160 \cdot 10^{15}$ Bq left it.

Translated from Atomnaya Énergiya, Vol. 57, No. 4, pp. 281-282, October, 1984. Original article submitted March 26, 1984.

0038-531X/84/5704-0747$08.50

MEASUREMENT TECHNIQUES
Izmeritel'naya Tekhnika
Vol. 27, 1984 (12 issues) $520

MECHANICS OF COMPOSITE MATERIALS
Mekhanika Kompozitnykh Materialov
Vol. 20, 1984 (6 issues) $430

METAL SCIENCE AND HEAT TREATMENT
Metallovedenie i Termicheskaya Obrabotka Metallov
Vol. 26, 1984 (12 issues) $540

METALLURGIST
Metallurg
Vol. 28, 1984 (12 issues) $555

PROBLEMS OF INFORMATION TRANSMISSION
Problemy Peredachi Informatsii
Vol. 20, 1984 (4 issues) $420

PROGRAMMING AND COMPUTER SOFTWARE
Programmirovanie
Vol. 10, 1984 (6 issues) $175

PROTECTION OF METALS
Zashchita Metallov
Vol. 20, 1984 (6 issues) $480

RADIOPHYSICS AND QUANTUM ELECTRONICS
Izvestiya Vysshikh Uchebnykh Zavedenii, Radiofizika
Vol. 27, 1984 (12 issues) $520

REFRACTORIES
Ogneupory
Vol. 25, 1984 (12 issues) $480

SIBERIAN MATHEMATICAL JOURNAL
Sibirskii Matematicheskii Zhurnal
Vol. 25, 1984 (6 issues) $625

SOIL MECHANICS AND FOUNDATION ENGINEERING
Osnovaniya, Fundamenty i Mekhanika Gruntov
Vol. 21, 1984 (6 issues) $500

SOLAR SYSTEM RESEARCH
Astronomicheskii Vestnik
Vol. 18, 1984 (6 issues) $365

SOVIET APPLIED MECHANICS
Prikladnaya Mekhanika
Vol. 20, 1984 (12 issues) $520

SOVIET ATOMIC ENERGY
Atomnaya Énergiya
Vols. 56-57, 1984 (12 issues) $560

SOVIET JOURNAL OF GLASS PHYSICS AND CHEMISTRY
Fizika i Khimiya Stekla
Vol. 10, 1984 (6 issues) $235

SOVIET JOURNAL OF NONDESTRUCTIVE TESTING
Defektoskopiya
Vol. 20, 1984 (12 issues) $615

SOVIET MATERIALS SCIENCE
Fiziko-khimicheskaya Mekhanika Materialov
Vol. 20, 1984 (6 issues) $445

SOVIET MICROELECTRONICS
Mikroélektronika
Vol. 13, 1984 (6 issues) $255

SOVIET MINING SCIENCE
Fiziko-tekhnicheskie Problemy Razrabotki Poleznykh Iskopaemykh
Vol. 20, 1984 (6 issues) $540

SOVIET PHYSICS JOURNAL
Izvestiya Vysshikh Uchebnykh Zavedenii, Fizika
Vol. 27, 1984 (12 issues) $520

SOVIET POWDER METALLURGY AND METAL CERAMICS
Poroshkovaya Metallurgiya
Vol. 23, 1984 (12 issues) $555

STRENGTH OF MATERIALS
Problemy Prochnosti
Vol. 16, 1984 (12 issues) $625

THEORETICAL AND MATHEMATICAL PHYSICS
Teoreticheskaya i Matematicheskaya Fizika
Vol. 58-61, 1984 (12 issues) $500

UKRAINIAN MATHEMATICAL JOURNAL
Ukrainskii Matematicheskii Zhurnal
Vol. 36, 1984 (6 issues) $500

Send for Your Free Examination Copy

Plenum Publishing Corporation, 233 Spring St., New York, N.Y. 10013
In United Kingdom: 88/90 Middlesex St., London E1 7EZ, England
Prices slightly higher outside the U.S. Prices subject to change without notice.

RUSSIAN JOURNALS IN THE PHYSICAL AND MATHEMATICAL SCIENCES

AVAILABLE IN ENGLISH TRANSLATION

ALGEBRA AND LOGIC
Algebra i Logika
Vol. 23, 1984 (6 issues) $360

ASTROPHYSICS
Astrofizika
Vol. 20, 1984 (4 issues) $420

AUTOMATION AND REMOTE CONTROL
Avtomatika i Telemekhanika
Vol. 45, 1984 (24 issues) $625

COMBUSTION, EXPLOSION, AND SHOCK WAVES
Fizika Goreniya i Vzryva
Vol. 20, 1984 (6 issues) $445

COSMIC RESEARCH
Kosmicheskie Issledovaniya
Vol. 22, 1984 (6 issues) $545

CYBERNETICS
Kibernetika
Vol. 20, 1984 (6 issues) $445

DIFFERENTIAL EQUATIONS
Differentsial'nye Uravneniya
Vol. 20, 1984 (12 issues) $505

DOKLADY BIOPHYSICS
Doklady Akademii Nauk SSSR
Vols. 274-279, 1984 (2 issues) $145

FLUID DYNAMICS
Izvestiya Akademii Nauk SSSR, Mekhanika Zhidkosti i Gaza
Vol. 19, 1984 (6 issues) $500

FUNCTIONAL ANALYSIS AND ITS APPLICATIONS
Funktsional'nyi Analiz i Ego Prilozheniya
Vol. 18, 1984 (4 issues) $410

GLASS AND CERAMICS
Steklo i Keramika
Vol. 41, 1984 (6 issues) $590

HIGH TEMPERATURE
Teplofizika Vysokikh Temperatur
Vol. 22, 1984 (6 issues) $520

HYDROTECHNICAL CONSTRUCTION
Gidrotekhnicheskoe Stroitel'stvo
Vol. 18, 1984 (12 issues) $385

INDUSTRIAL LABORATORY
Zavodskaya Laboratoriya
Vol. 50, 1984 (12 issues) $520

INSTRUMENTS AND EXPERIMENTAL TECHNIQUES
Pribory i Tekhnika Eksperimenta
Vol. 27, 1984 (12 issues) $590

JOURNAL OF APPLIED MECHANICS AND TECHNICAL PHYSICS
Zhurnal Prikladnoi Mekhaniki i Tekhnicheskoi Fiziki
Vol. 25, 1984 (6 issues) $540

JOURNAL OF APPLIED SPECTROSCOPY
Zhurnal Prikladnoi Spektroskopii
Vols. 40-41, 1984 (12 issues) $540

JOURNAL OF ENGINEERING PHYSICS
Inzhenerno-fizicheskii Zhurnal
Vols. 46-47, 1984 (12 issues) $540

JOURNAL OF SOVIET LASER RESEARCH
A translation of articles based on the best Soviet research in the field of lasers
Vol. 5, 1984 (6 issues) $180

JOURNAL OF SOVIET MATHEMATICS
A translation of Itogi Nauki i Tekhniki and *Zapiski Nauchnykh Seminarov Leningradskogo Otdeleniya Matematicheskogo Instituta im. V. A. Steklova AN SSSR*
Vols. 24-27, 1984 (24 issues) $1035

LITHOLOGY AND MINERAL RESOURCES
Litologiya i Poleznye Iskopaemye
Vol. 19, 1984 (6 issues) $540

LITHUANIAN MATHEMATICAL JOURNAL
Litovskii Matematicheskii Sbornik
Vol. 24, 1984 (4 issues) $255

MAGNETOHYDRODYNAMICS
Magnitnaya Gidrodinamika
Vol. 20, 1984 (4 issues) $415

MATHEMATICAL NOTES
Matematicheskie Zametki
Vols. 35-36, 1984 (12 issues) $520

continued on inside back cover